Biophysical, Cellular, and Animal Models of Dystrophin Missense Mutations

A DISSERTATION
SUBMITTED TO THE FACULTY OF THE GRADUATE SCHOOL
OF THE UNIVERSITY OF MINNESOTA
BY

Dana Marie Talsness

IN PARTIAL FULFILLMENT OF THE REQUIREMENTS
FOR THE DEGREE OF
DOCTOR OF PHILOSOPHY

Advisor, James M. Ervasti

December, 2014

© Dana Marie Talsness, 2014

Acknowledgements

First I would like to thank my graduate advisor, Jim Ervasti. He took me into his lab when I was an orphaned graduate student, and he has mentored and supported me ever since. I will forever be grateful to him for teaching me how to be a scientist.

I would also like to thank all of the members of the Ervasti laboratory throughout my years here: Ben Perrin, Chris Chamberlain, Joe Belanto, Davin Henderson, Michelle Jaeger, Jackie McCourt, Ali O'Rourke, J.T. Olthoff, Tung Nguyen, Xiaobai Patrinostro, Chris Scherber, and Paul Chatterton. These people have made it a pleasure to come into work everyday, and they have all contributed hands-on effort to my projects or helpful conversations about science.

Dawn Lowe is a long time collaborator with the Ervasti lab and I would like to thank her for her help with the eccentric contraction protocol and all of her muscle physiology knowledge.

Thank you to my committee, Mary Porter, Harry Orr, David Largaespada, and Lihsia Chen, for their support of my graduate career throughout the years.

I need to thank our program administrator, Sue Knoblauch. If it were not for her, no graduate student would ever sign up for classes on time, have a student seminar, pass their credit for student seminar, or even be recruited to the program in the first place.

I would like to thank all of the graduate students in my year: Joe Belanto, Keli Holzapfel, Chris Braden, Frazer Heinis, Brent Rivard, Spencer Lubben, Jung Kim, Adrienne Watson, and Nick Baltes. We formed a special bond at Itasca, and their friendship and support ever since has helped me to get through grad school.

I would have never made it to grad school in the first place if it were not for my parents, Andy and Ruth Strandjord. I would like to thank them for all of their emotional, spiritual, and physical support throughout the years. My parents, along with my sisters Laurie and Kirsten, have been my foundation in life.

Finally I would like to thank my husband, Jeff Talsness. I am so lucky to have found someone who supports me in my higher education endeavors, even though it means nights spent staring at my computer and weekends spent in the lab. Thank you for all of your encouragement and your calm voice of reason.

Dedication

This dissertation is dedicated to my grandparents, Rolf and Henrietta Strandjord and Robert and Margaret Boyd.

Abstract

The 427kDa protein dystrophin is expressed in skeletal muscle where it localizes to the costamere and physically links the interior of muscle fibers to the extracellular matrix. Mutations in the *DMD* gene encoding dystrophin lead to a severe muscular dystrophy known as Duchenne (DMD) or a mild form known as Becker (BMD). Currently, there is no cure for DMD or BMD, but there are several therapies being investigated that target specific types of mutations found in the *DMD* gene. Nonsense mutations almost always lead to a complete lack of dystrophin protein, with stop codon read-through drugs being studied for personalized treatments. Out-of-frame deletions and insertions also cause nearly a complete lack of dystrophin, for which exon-skipping is currently being investigated. Missense mutations in dystrophin, however, cause a wide range of phenotypic severity in patients, the molecular and cellular consequences of such mutations are not well understood, and there are no therapies currently targeting this genotype. Here, we report on three separate model systems of missense mutations in dystrophin: an *in vitro* biochemical model, a myoblast cell culture model, and an *in vivo* animal model. Together, they provide evidence that different missense mutations cause variable degrees of thermal instability, which leads to proportionally decreased dystrophin expression, and subsequently causes dystrophic phenotypes. In addition, our initial studies of small molecule treatments show that it is possible to increase the levels of mutant dystrophin, and may lead to personalized therapeutics for patients with missense mutations.

Table of Contents

Acknowledgements…… i

Dedication…… ii

Abstract……..…… iii

Table of Contents…… iv

List of Tables…… vi

List of Figures……... vii

Chapter 1: Introduction…… 1

Muscle and the Dystrophin-Glycoprotein Complex…… 2

Dystrophin…… 4

Duchenne Muscular Dystrophy…… 8

Amino Acid Substitutions in Dystrophin…… 10

Current Therapies for Duchenne Muscular Dystrophy…… 15

Questions Addressed by this Thesis…….. 18

Figures……... 20

Chapter 2: A Biophysical Model of Missense Mutations in Dystrophin…... 24

Summary……... 25

Introduction…… 26

Materials and Methods…… 29

Results…… 34

Discussion…….. 41

Figures…… 45

Chapter 3: A Cell Culture Model of Missense Mutations in Dystrophin..... 54

Summary..... 55

Introduction..... 56

Materials and Methods..... 62

Results..... 67

Discussion..... 76

Figures..... 79

Chapter 4: A Mouse Model of Missense Mutations in Dystrophin..... 86

Summary..... 87

Introduction..... 88

Materials and Methods..... 92

Results..... 98

Discussion.....103

Figures..... 107

Chapter 5: Conclusions and Discussion..... 115

Thesis Findings..... 116

Personalized Therapeutics for Missense Mutations in Dystrophin..... 119

Applications to Other Mutations and Therapies..... 122

Continuing Study..... 124

References.....127

List of Tables

Table 2.1: Selected amino acid substitutions for analysis

Table 4.1: Summary of *ex vivo* EDL parameters

List of Figures

Figure 1.1: Dystrophin Glycoprotein Complex (DGC)

Figure 1.2: Schematic representation of dystrophin protein domains

Figure 1.3: Gower's Maneuver

Figure 1.4: Distribution of dystrophin missense mutations

Figure 2.1: Expression construct and experimental concept

Figure 2.2: Solubility and expression levels of missense mutations in Dp260

Figure 2.3: Secondary structure and stability of missense mutations in Dp260

Figure 2.4: Average size and polydispersity of missense mutations in Dp260

Figure 2.5: Solubility and expression levels of missense mutations in full-length Dp427

Figure 2.6: Secondary structure and stability, tertiary stability, and average size of missense mutations in Dp427

Figure 3.1: Expression construct and experimental concept

Figure 3.2: Expression levels of transgenic dystrophin in myoblast cell lines

Figure 3.3: Differentiation of stable transgenic cell lines

Figure 3.4: Effect of missense mutations on heat shock pathway in cells

Figure 3.5: Small molecule therapeutics screen to increase dystrophin levels

Figure 3.6: Effect of positive hits from therapeutics screen on total dystrophin protein levels and ubiquitination

Figure 3.7: Effect of positive hits from therapeutic screen on the heat shock pathway

Figure 4.1: Expression construct and experimental concept

Figure 4.2: RNA and protein expression levels in transgenic mouse lines

Figure 4.3: Expression levels and localization of components in the Dystrophin Glycoprotein Complex

Figure 4.4: Fiber morphology and permeability

Figure 4.5: Physiology of transgenic mouse models

Figure 4.6: Effect of missense mutations on the heat shock pathway of the mice

Chapter 1

Introduction

Muscle and the Dystrophin-Glycoprotein Complex

Skeletal muscle is composed of a bundle of fascicles each surrounded by the perimysium connective tissue, and each fascicle is composed of a bundle of muscle fibers, or myofibers. Myofibers are the cellular unit, each surrounded by a plasma membrane, or sarcolemma. An individual myofiber is formed during development by the fusion of several embryonic myoblast cells, giving it an elongated shape with multiple nuclei. When a myofiber is viewed microscopically, it appears striated with alternating light and dark bands known as I and A bands respectively due to the protein patterns of the bundled myofibrils within a myofiber. The dark A bands are composed mostly of myosin and the light I bands of actin filaments. In the center of each I band is a thin dark Z line to which the actin filaments are anchored. Between two Z discs, the actin and myosin interact to form a functional contractile unit know as the sarcomere.

Localized at the Z disc and extending from the bundle of myofibrils out to the sarcolemma is a cluster of proteins known as the costamere (Ervasti, 2003), which couples the force generated by the sarcomeres to the plasma membrane of the cell, as a highly specialized type of focal adhesion. A sub-complex within the costamere, known as the dystrophin-glycoprotein complex (DGC), physically links the cytoplasmic actin to the extracellular matrix (Figure 1.1). The DGC was first discovered when it was found that the protein of interest, dystrophin, could be enriched by wheat germ agglutinin chromatography, and then the complex further purified into 10 constitutive proteins (Ervasti et al., 1990). The major

components of the DGC are dystrophin, α- and β-dystroglycan, sarcospan, the sarcoglycans, dystrobrevin, and the syntrophins (Figure 1.1) (Ervasti, 2007).

It is clear that the dystrophin glycoprotein complex is necessary for myofiber integrity given that mutations in many of the subunits cause various forms of muscular dystrophy (Rahimov and Kunkel, 2013). Mutations that lead to a loss of function in dystrophin cause Duchenne and Becker muscular dystrophy, which is the major focus of this thesis. α- and β-dystroglycan are encoded by a single gene and then post-translationally cleaved. Mutations in the glycosyltransferases that glycosylate α-dystroglycan lead to several forms of congenital muscular dystrophy (Michele et al., 2002). Additionally, mutations in the dystroglycan gene itself lead to limb girdle muscular dystrophy (Hara et al., 2011). Autosomal recessive mutations that occur in any of the 4 sarcoglycans also leads to limb girdle muscular dystrophy (Ozawa et al., 2005). Knock-out of α-dystrobrevin has been shown to cause progressive myopathy (Grady et al., 1999). Together these lines of evidence show that an intact DGC is essential to muscle fiber integrity and tissue function.

Dystrophin

DNA

The gene encoding dystrophin, known as *DMD*, is located on the short arm of the X chromosome and is the largest in the human genome at 2.4Mb of DNA (Koenig et al., 1987). It is comprised of 79 exons (Roberts et al., 1993), far above the genomic average of 8.8 exons per gene (Sakharkar et al., 2004). The introns for dystrophin average over 30kb, again above the genomic average with <10% of all introns being more than 11kb in length. There are also several alternate promoter regions which express dystrophin in non-muscle tissues of the body including brain (Nudel et al., 1989; Górecki et al., 1992), retina (Pillers et al., 1993), peripheral nerves (Byers et al., 1993), liver, lung, and kidney (Bar et al., 1990). The high number of exons, the large length of the introns, and the multiple promoters all contribute to the enormity of the *DMD* locus.

RNA

Due to the length of the *DMD* gene, transcription and splicing takes up to 16 hours in the cell (Tennyson et al., 1995). This study was in fact one of the first lines of evidence that splicing in vertebrates occurs co-transcriptionally. All of the exons together with the 5' and 3' UTRs generate a 14kb dystrophin transcript. The dystrophin mRNA has a half life of 15.6 ± 2.8 hours, and at steady-state levels there are approximately 5-10 copies per nucleus in adult muscle tissue, making dystrophin a low-copy transcript (Tennyson et al., 1996). In addition to the dystrophin mRNA, the *DMD* locus also encodes several long non-coding

RNAs (lncRNA) within the intronic regions (Bovolenta et al., 2012). These lncRNAs are localized to the nucleus and were shown to specifically target the promoter regions for the *DMD* gene itself and to down-regulate transcription. In this way, it appears that the gene encoding dystrophin has its own negative feedback, ensuring proper expression levels.

Protein

Dystrophin protein is a 427kDa structural protein composed of an N-terminal globular domain, a long central rod region, a cysteine-rich globular domain, and an intrinsically disordered C-terminal tail (CT) (Figure 1.2) (Koenig et al., 1988). The central rod region is composed of 24 spectrin-like repeats (SLR), each a triple helical structure (Muthu et al., 2012), with four hinge domains interspersed, allowing for some flexibility of the protein (Koenig and Kunkel, 1990). The N-terminus (NT) (crystalized in Norwood et al. 2000) is composed of tandem calponin homology (CH) domains, which together bind filamentous actin and are designated actin binding domain 1 (ABD1). A second actin-binding domain (ABD2) was discovered in the central rod region (SLR11-17), suggesting dystrophin binds laterally along filamentous actin (Rybakova et al., 1996).

The structure of the cysteine rich (CR) region can be subdivided into several common motifs: There is a WW domain, so named for two conserved tryptophan residues, which recognizes proline-rich regions of binding-partner proteins (Bork and Sudol, 1994). Then, there are two EF-hand domains, a structural element found in calcium binding proteins (Koenig et al., 1988). And

finally there is a ZZ domain, where cysteine residues coordinate Zn^{2+} ions in a conserved zinc finger motif (Ponting et al., 1996). Together the WW, EF-hand, and ZZ motifs form a region that binds to β–dystroglycan (Hnia et al., 2007), and so the CR domain is also referred to as the dystroglycan-binding domain (DgBD). The specific residues that interact between dystrophin and β-dystroglycan have been reported in a crystal structure : H3076, T3081, Y3072, and W3083 (Huang et al., 2000). β–dystroglycan is a transmembrane protein and a component of the complex that binds the extracellular basal lamina (Ervasti and Campbell, 1991). The interactions of dystrophin with both actin filaments and microtubules and then β–dystroglycan effectively links the cytoskeleton to the extra-cellular matrix and localizes dystrophin to the sarcolemma of muscle cells (Zubrzycka-Gaarn et al., 1988).

While full-length dystrophin is an extremely large protein, transcription from unique promoter regions result in multiple small isoforms of dystrophin, each a different length C-terminal fragment (Blake et al., 2002). After full-length dystrophin (Dp427), the largest isoform is Dp260 (named for its molecular weight) which is expressed in the retina (D'Souza et al., 1995). While it has a unique N-terminus, it is identical from SLR 10 to the C-terminus of full-length dystrophin and so mimics full-length dystrophin in all of its C-terminal functions such as binding to β–dystroglycan. Dp140 is expressed in the central nervous system and in the kidney (Lidov et al., 1995), and Dp116 in the peripheral nerves (Byers et al., 1993). Another notable isoform, Dp71, has been shown to be

expressed in neurons and contains no spectrin-like repeats, but only the CR and CT domains (Lederfein et al., 1992). While many isoforms of dystrophin have been identified in cells other than muscle, the functions of these proteins are not well studied. It is interesting to note, however, that mutations within these most C-terminal domains would affect each of the dystrophin isoforms.

Duchenne Muscular Dystrophy

Since *DMD* is the largest gene in the genome, it is statistically more prone to *de novo* mutation; and because it is encoded on the X-chromosome, males only have one chance for a functional copy. Therefore the incidence of dystrophinopathies is approximately 1 in 4000 live male births (Mendell et al., 2012), making it the most common muscular dystrophy. Males who unfortunately harbor a disease-causing mutation in their single copy of the *DMD* gene develop a muscular dystrophy either with severe symptoms referred to as Duchenne (DMD) (OMIM: **310200**) or milder symptoms referred to as Becker (BMD) (OMIM: **300376**) (Hoffman et al., 1987a). Generally, patients with milder symptoms have in-frame deletions resulting in an internally-truncated dystrophin protein (Monaco et al., 1988), while more severely-affected patients have out-of-frame deletions or nonsense mutations resulting in a lack of dystrophin expression (Koenig et al., 1989).

The clinical symptoms of DMD were first described in the 1830-1860's by a few physicians, but the one that became associated with the disease was Duchenne (Duchenne, 1861). Symptoms onset at approximately 5 years of age and include elevated serum creatine kinase, muscle weakness, decreased ability to perform physical activities, calf muscle hypertrophy, and often mild cognitive impairment. One of the earliest clinical signs described was the Gower's maneuver which is a common mechanism the boys use to raise themselves up to standing that is necessary because of their weak leg muscles (Figure 1.3)

(Gowers, 1886). Muscle degeneration is progressive and boys are often wheel chair bound in their teenage years. Fatality occurs in the second or third decade of life, often due to cardiomyopathy or respiratory failure (Rall and Grimm, 2012). Support of a ventilator extends life expectancy by a few years, and corticosteroids have been shown to alleviate some symptoms through poorly understood mechanisms (Angelini, 2007).

The causative mutations for patients with Duchenne/Becker muscular dystrophy span the entire spectrum of possible mutations. In 2006 it was calculated that 72% of reported cases were caused by intragenic deletions (Aartsma-Rus et al., 2006). The majority of these deletions occur in exons 45-53, making this region a “hot spot”. Duplications were found to occur in 7% of patients, including single- and multi-exon duplications; the most common one reported is a single duplication of exon 2 (White et al., 2006). Up to 30% of reported cases are caused by single point mutations. The majority of these are nonsense mutations, leading to a premature stop-codon and the severe symptoms of Duchenne muscular dystrophy. The remaining mutations are missense mutations, causing a single amino acid change in the protein and a wide spectrum of symptoms ranging from Duchenne to Becker diagnoses. While missense mutations are rare, they offer insight into the structure and function of dystrophin, and they have the potential for alternate therapeutic interventions.

Amino Acid Substitutions in Dystrophin

The full-length muscle isoform of human dystrophin is comprised of 3685 amino acids, and there are several incidences of substitutions that differ from the reference sequence. The Leiden Muscular Dystrophy Pages (www.dmd.nl) (Aartsma-Rus et al., 2006) is a database of all dystrophin mutations found in DMD/BMD patients. We compared all of the reported unique missense mutations to all amino acid substitutions found in the general population recorded in the Single Nucleotide Polymorphism (SNP) database (http://www.ncbi.nlm.nih.gov/projects/SNP/). The distribution of these unique amino acid changes across the primary sequence of dystrophin is different depending on whether the substitutions associate with disease or are present in the population (Figure 1.4). The distribution of missense mutations (shown in red) has noticeable peaks in the NT and CT domains, while there are no obvious hotspots for missense mutations in the large SLR domain. In comparison, SNP substitutions (shown in green) appear with higher frequency throughout the SLR domain. When analyzed as a function of dystrophin structural domain, there was a significant difference in the proportion of substitutions that cause disease between the NT and SLR (z-score=7.02, $p<0.0001$) and between the CT and SLR (z-score=4.97, $p<0.0001$). There was no difference between proportions in the NT and CT. These data suggest that if an amino acid change occurs in the NT or CT it is more likely to cause disease than if it had occurred in the SLR domain.

This thesis will largely focus on two missense mutations that were discovered in patients with Duchenne/Becker muscular dystrophy, L54R and L172H; and one amino acid substitution that is found in a small percentage of the population and is not associated with disease, I232M. All three amino acid changes are located within the N-terminal ABD1, for a more equivalent comparison between the molecular effects of each.

The first missense mutation discovered in dystrophin was L54R (Prior et al., 1993). Previous to this study, patients presenting with muscular dystrophy symptoms were screened by multiplex PCR, the clinical standard at the time. This technique, however, is only able to detect large deletions or insertions and a set of 105 DMD patients remained with undefined mutations. Through the use of heteroduplex PCR (White et al., 1992) they were able to detect a single T to G transversion in exon 3 of one patient resulting in a leucine to arginine amino acid change in dystrophin. It was hypothesized that this was a severely deleterious substitution given that this leucine is conserved in mouse and chicken dystrophin, and that it changes a non-polar, hydrophobic amino acid into a basic, positively charged one. Indeed the patient was only 8 years old at the time of molecular diagnosis and presented with severe muscle weakness and exhibited the Gower's maneuver. Western blot analysis from muscle biopsy showed a large decrease in full-length dystrophin protein compared to an unaffected control. Immunofluorescent staining of muscle sections showed dystrophin properly localized to the sarcolemma, but at reduced intensity. Missense mutation L54R

clearly represents a substitution that causes the severe symptoms of Duchenne muscular dystrophy.

With the advancement of sequencing technology, a group was able to amplify dystrophin cDNA from a set of 18 muscular dystrophy patients with unknown genetic causes and then sequence each sample and align it to the reference sequence (Hamed et al., 2005). Several novel mutations were discovered including a T to A nucleotide change in exon 6 causing the L172H substitution. This leucine is also conserved across mouse, dog, and chicken; and histidine is, similarly to L54R, a change to a basic, positively-charged amino acid. The L172H mutation, however, was found in a mildly-affected patient who presented with symptoms at 42 years of age. Muscle biopsy revealed decreased levels of full-length dystrophin by western blot and correct localization by immunofluorescent staining. L172H serves as a good representative of missense mutations that cause the mild symptoms of Becker muscular dystrophy. Together, L54R and L172H, can potentially help us to distinguish between the molecular mechanisms of substitutions that cause severe symptoms and those that cause mild.

In addition to missense mutations that cause disease, there are several benign amino acid changes expressed by small portions of the population within the N-terminal ABD1 of dystrophin. After the completion of the human genome reference sequence in 2003, several efforts were started to find the variants that existed in the population, including the International HapMap Consortium and the

1000 Genomes Project (Pennisi, 2010; Buchanan et al., 2012). Between these two major projects over 10 million single nucleotide polymorphism (SNPs) have been discovered. From the deposited data in the SNP database (ncbi.nlm.nih.gov/snp), the protein coding region of dystrophin contains over 450 nucleotide variants, approximately half of which are non-synonymous. One of these is amino acid substitution I232M, validated by multiple, independent submissions to the database (rs145668843). It is not unreasonable that this substitution does not cause disease given that both isoleucine and methionine are hydrophobic, non-polar amino acids. In this thesis I232M serves as an amino acid substitution control in addition to the "WT" reference sequence control for dystrophin.

Previous work from our lab analyzed the biochemical and biophysical consequences of several missense mutations found in the N-terminal ABD1, including L54R and L172H (Henderson et al., 2010). It was hypothesized that mutations in this domain could decrease the actin-binding affinity of dystrophin, so mutations were engineered into full-length mouse dystrophin cDNA and protein purified from a baculovirus expression system. Cosedimentation assays with filamentous actin revealed that mutations K18N and L54R significantly decreased the binding affinity, but only by 4-fold from a Kd of 0.223μM to Kd's of 0.76μM and 0.85μM respectively. The four other missense mutations (including L172H) had no effect on actin affinity. Biophysical analysis of the full-length proteins, however, revealed that each of the mutations rendered dystrophin more

insoluble, more likely to self-pellet by ultracentrifugation, and less stable during thermal denaturation. Protein instability is a likely mechanism of disease in dystrophin missense patients, but the cellular and physiological consequences of these mutations has not yet been examined.

Current Therapies for Duchenne Muscular Dystrophy

Gene therapy

Gene replacement of dystrophin has been a difficult task given that the cDNA is approximately 14kb. Therefore studies have focused on creating functional mini- and micro- versions of dystrophin which are small enough to be delivered systemically by adeno-associated virus (AAV) (Watchko et al., 2002; Gregorevic et al., 2004). Administration of these viral vectors in *mdx* mice leads to micro-dystrophin expression and reduced CK activity. Progression of this therapy into human patients has been complicated by possible immune responses to the foreign dystrophin protein. A study administering mini-dystrophin in rAAV found that there was a CD4+ T cell response to the transgene, decreasing the efficacy of this treatment (Mendell et al., 2010). Future studies aim to develop better vectors and more specific promoters in order to decrease immune response.

Protein therapy

Due to the immune response seen in gene replacement therapies, several studies have examined the possibility using the homolog of dystrophin, utrophin as a protein replacement therapy. Utrophin is structurally similar to dystrophin and is found at the sarcolemma during fetal development but in adult muscle is restricted to the myotendinous and neuromuscular junctions. It has been shown that utrophin can functionally replace dystrophin in *mdx* mice (Miura and Jasmin, 2006). Increasing utrophin levels can be achieved by either up-regulating

endogenous transcription and translation (Chakkalakal et al., 2008; Moorwood et al., 2013) or delivering exogenous utrophin protein (Sonnemann et al., 2009). Such therapies would avoid an immune response since utrophin is normally expressed in fetal muscle and in adult muscle junctions. There is, however, increasing evidence that utrophin does not replace all of the functions of dystrophin including nNOS and microtubule binding (Li et al., 2010a; Belanto et al., 2014).

Exon skipping

One of the emerging therapies targeting the endogenous *DMD* transcript is exon-skipping. In this method oligonucleotides with a morpholino backbone are synthesized with antisense sequence to a region of dystrophin pre-mRNA (Alter et al., 2006). The antisense oligonucleotide (AON) binds to the nascent transcript causing the splicing machinery to skip over the targeted exon. This therapy is most applicable to patients with out-of-frame deletions or duplications, where exon-skipping leads to restoration of the reading frame. Clinical trials of an AON targeted to exon 51 have demonstrated restored dystrophin protein and improved physiological activity (Goemans et al., 2011). Exon-skipping obviously leads to small deletions in the protein product and therefore research is ongoing to determine the best non-native junctions possible.

Nonsense read-through

Many DMD patients harbor a nonsense mutation, as discussed above. It was discovered that the antibiotic gentamicin binds to 18S rRNA causing

ribosomes to sometimes “read-through” a stop codon, inserting a random amino acid instead (Palmer et al., 1979). *In vitro* and *in vivo* administration of gentamicin to the nonsense mutation mouse model (*mdx*) lead to dystrophin expression and proper localization (Barton-Davis et al., 1999). Subsequent studies have brought gentamicin to the clinic with mixed results (Malik et al., 2010). The next generation read-through drug, Ataluren, is not an antibiotic and has been shown to effectively read-through all three stop codons at low dosages (Peltz et al., 2013). Ataluren has shown positive results in nonsense models of cystic fibrosis, dysferlin-deficient myopathy, Hurler syndrome, and Duchenne muscular dystrophy in the *mdx* mouse; this drug is currently in phase 3 clinical trials for boys with DMD due to nonsense mutations (clinicaltrials.gov/show/NCT01826487). This is one of the first examples of personalized medicine that is not targeting a disease but rather a specific molecular cause. It is interesting to note that this treatment leads to a phenotypic missense mutation. As of yet there are no personalized medicine approaches that are being explored for DMD patients with missense mutations.

Questions Addressed by this Thesis

Previous work in our lab has demonstrated that missense mutations in the N-terminal ABD1 domain cause protein instability *in vitro* (Henderson et al., 2010). And other groups have studied the *in vitro* effects of missense mutations in other domains of dystrophin, but in small fragment peptides (Legardinier et al. 2009; Acsadi et al. 2012). Given that WT full-length dystrophin is stable and unfolds in one cooperative transition and that some isolated fragments of WT dystrophin are not even stable enough to be studied *in vitro,* we aimed to study missense mutations in all the major domains in a full-length construct to answer the question: **Do missense mutations in every domain of dystrophin have the same propensity to cause protein instability *in vitro*?**

The biophysical characterization of mutations L54R and L172H showed that each caused protein instability. Protein instability can have several different consequences when expressed in the cellular environment including protein aggregation, protein mislocalization, or protein degradation (Liu et al., 2009; Lee et al., 2011). It is currently unknown what happens to full-length mutant dystrophin protein in a cell. Therefore we generated a cell culture model in order to potentially distinguish between the severe symptoms associated with L54R and the mild symptoms with L172H, to serve as a screening platform for small molecular therapeutics, and most importantly to answer the question: **What are the cellular consequences for the dystrophin protein when harboring missense mutations L54R and L172H?**

Dystrophin is a structural protein and therefore its full activity cannot be measured in a cell culture model, but rather only *in vivo* through physiological assays. We wanted to see if the molecular phenotypes of the cell culture model would translate to an animal model, so we generated two transgenic mouse lines. These lines will also demonstrate the tissue and whole body consequences of the missense mutations, serve as models for new potential therapeutics, and answer the question: **Can transgenic mice harboring missense mutations L54R and L172H faithfully recapitulate the severe and mild phenotypes of the patients which they are modeling?**

Figures

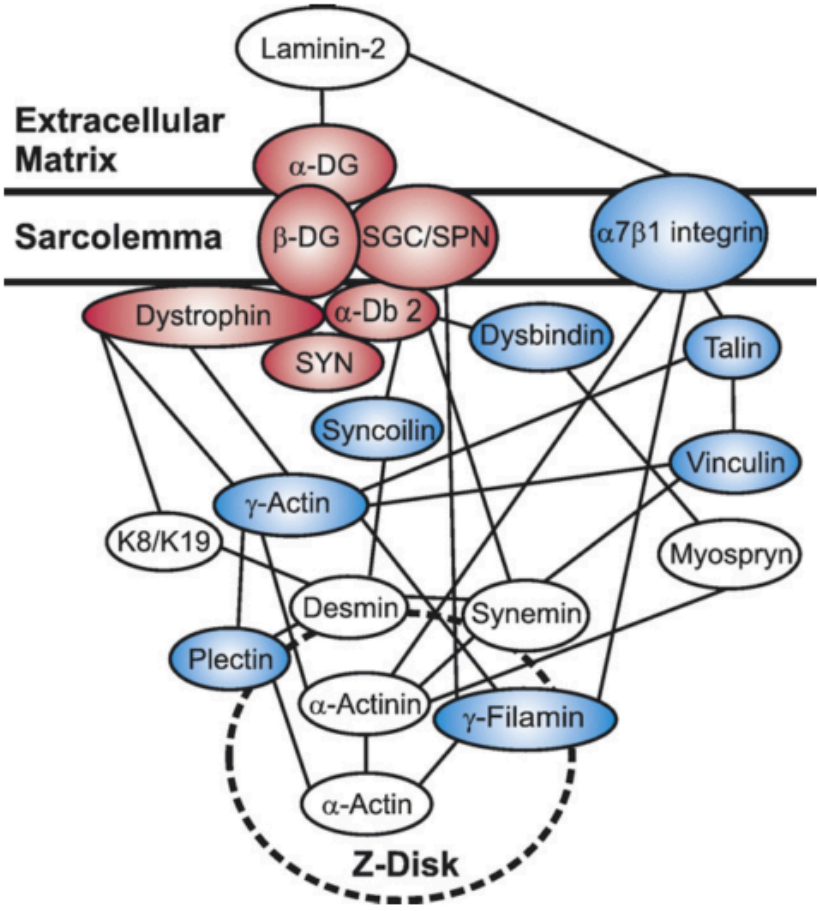

Figure 1.1: Dystrophin Glycoprotein Complex (DGC). The core DGC components are shown in red: dystrophin, α- and β-dystroglycan, syntrophin, dystrobrevin, the sarcoglycans and sarcospan. Shown in blue and white are other structural components of the costamere, those in blue are found upregulated in dystrophin deficient muscle. Figure from Ervasti 2007.

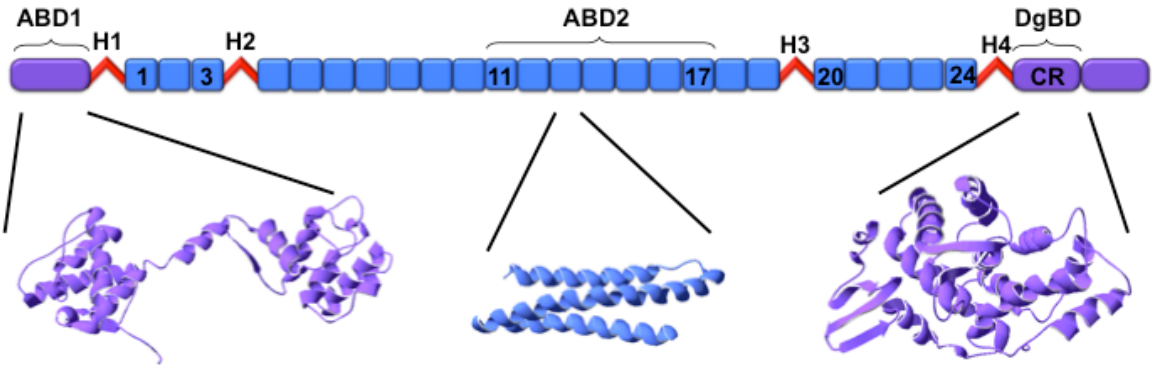

Figure 1.2: Schematic representation of dystrophin protein domains. ABD1 = actin binding domain 1, ABD2 = actin binding domain 2, H1-4 = hinges, DgBD = dystroglycan binding domain. Below are the 3 crystal structures that have been generated for dystrophin. Crystal structure of the ABD1 = 1DXX (Norwood et al., 2000). Crystal structure of one of the spectrin repeats = 3UUL (Muthu et al., 2012). Crystal structure of the CR DgBD = 1EG4 (Huang et al., 2000).

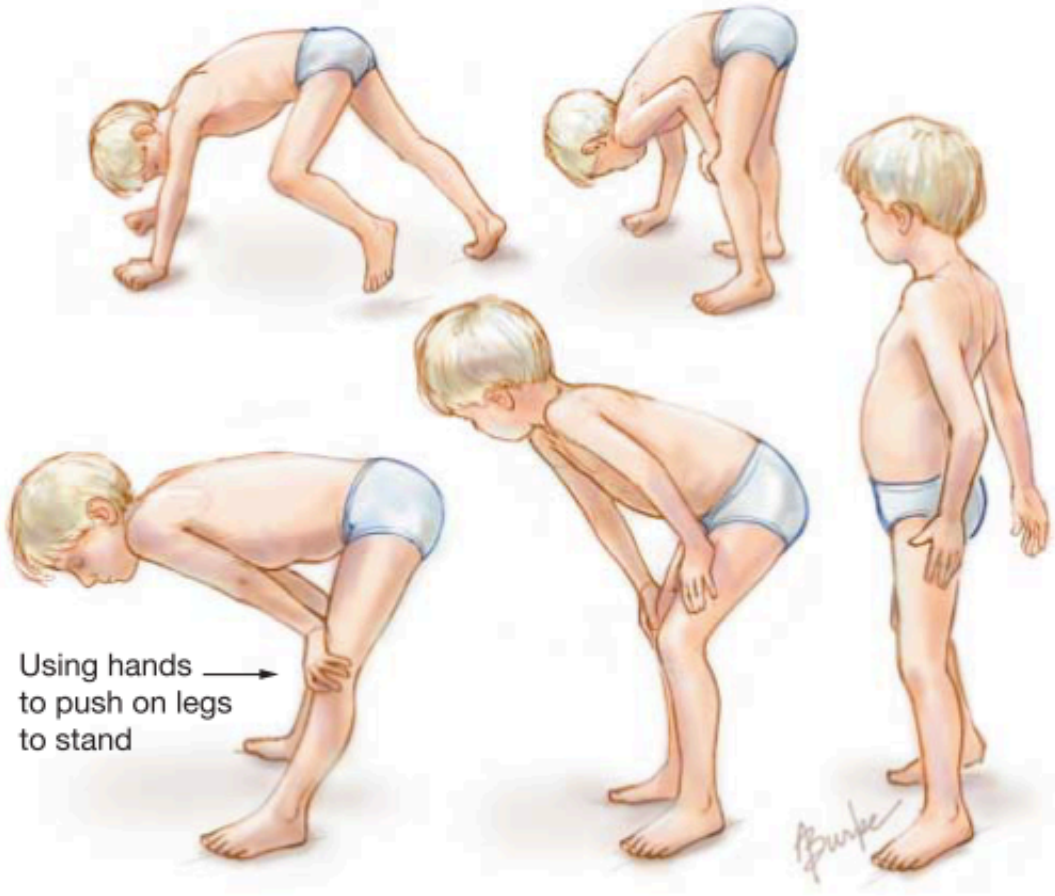

Figure 1.3: Gower's Maneuver. Technique young boys with Duchenne muscular dystrophy use to raise themselves to standing, first described by (Gowers, 1886). Image illustrated by Alison Burke (Punnoose et al., 2011).

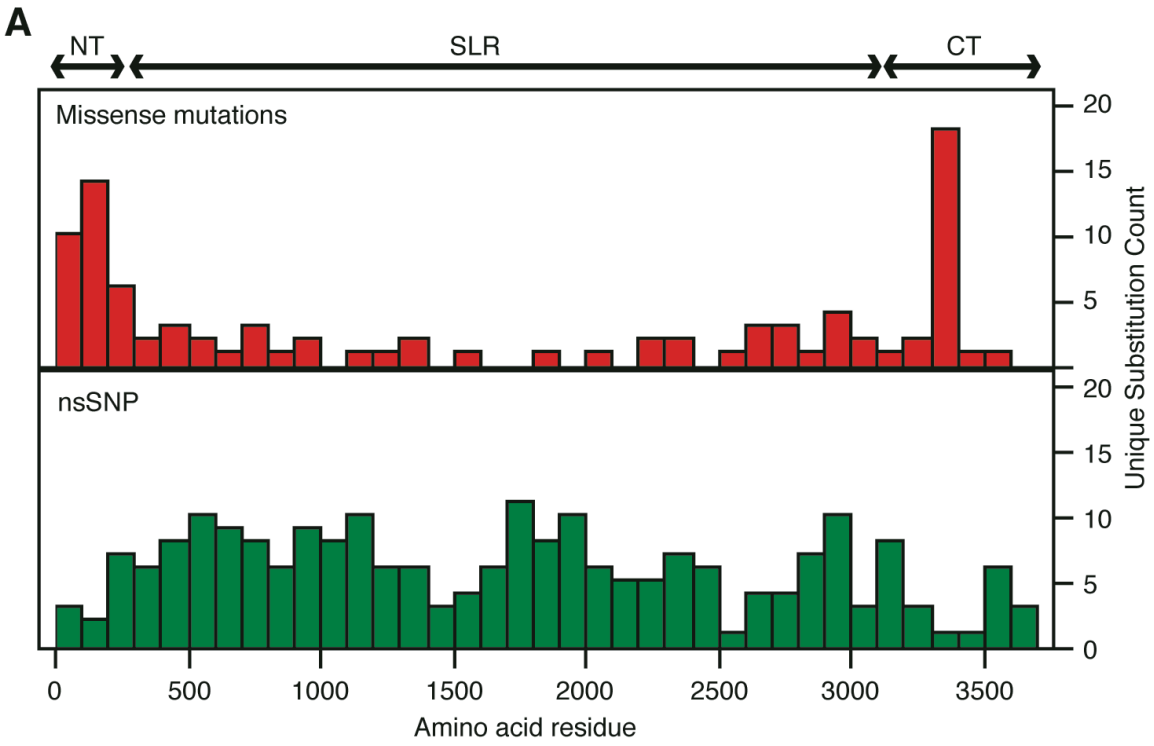

Figure 1.4: Distribution of dystrophin missense mutations (**A**) Total documented amino acid substitutions are shown as they are distributed along the primary sequence of dystrophin. The top graph in red represents all unique missense mutations found in patients with DMD/BMD (Leiden pages). The bottom graph in green represents unique, non-synonymous SNPs found in the population (dbSNP). NT: Amino Terminus (a.a. 1-252), SLR: Spectrin Like Repeats (also known as central rod region) (a.a. 253-3112), CT: Carboxy Terminus (a.a. 3113-3685).

Chapter 2

A Biophysical Model of Missense Mutations in Dystrophin

Initial sub-cloning of full-length mouse dystrophin into Gateway vectors was performed collaboratively with Joseph Belanto. All subsequent cloning, protein purification, and biophysical analyses were performed by Dana Talsness.

Summary

Duchenne and Becker Muscular Dystrophies (DBMD) are debilitating disorders affecting males with a mutation in their single copy of the dystrophin gene, and a growing number of DBMD cases have been linked to missense mutations. While many of these missense mutations are localized in the amino terminal (NT) actin-binding domain (ABD1), previous studies have shown these to affect protein thermal stability rather than cause a substantive loss in actin binding activity. To determine whether missense mutations in other dystrophin domains also cause protein instability, we characterized an array of disease-associated amino acid substitutions by *in vitro* expression in recombinant Dp260, or full-length dystrophin (Dp427). Biochemical analyses of mutations within the spectrin like repeats (SLR) of the central rod domain showed no perturbations in solubility or stability. Mutations in the carboxy terminal (CT) domain, however, partitioned into two groups: those without effect and those that significantly impaired protein solubility and expression levels. Spectroscopic analyses of the soluble dystrophin fraction revealed that the stability of the secondary structure could be affected by mutations in both the NT and CT domains, while the stability of the tertiary structure was affected only by mutations in the NT. These findings suggest that disease-causing missense mutations differentially affect the stability and solubility of dystrophin dependent on the domain in which they reside.

Introduction

The majority of missense mutations that have been studied at the protein level using biophysical methods are located in the amino terminal (NT) actin-binding domain 1 (ABD1) (Henderson et al., 2010; Singh et al., 2010). While none of the ABD1 mutations studied were found to dramatically reduce the actin-binding activity of dystrophin *in vitro*, all caused protein instability as evidenced by decreased solubility and non-cooperative melting transitions (Henderson et al., 2010), and also plaque-like aggregation when expressed in NT-fragment peptides (Singh et al., 2010). Consistent with these findings, a recent clinical study reported a DMD patient encoding L53R in the NT who had reduced sarcolemmal dystrophin immunoreactivity in the muscle biopsy (Juan-Mateu et al., 2013), likely due to a decrease in protein stability similar to the previously biophysically characterized mutations in the NT domain.

Clinical studies have also identified DBMD patients with amino acid substitutions within the 24 spectrin-like repeats (SLR) of the central rod domain that result in mild to severe disease. Two mildly affected siblings encoding L427P in SLR1 were recently reported, and subsequent biochemical analyses of the mutant SLR1 peptide demonstrated misfolding *in vitro* (Acsadi et al., 2012). Other patients have been found with two proximate missense mutations (Juan-Mateu et al., 2013; Legardinier et al., 2009), and one study concluded that both mutations were necessary to cause protein instability in the SLR peptide (Legardinier et al., 2009). It remains unclear whether mutations in the SLR

domain are likely to cause instability or not. This lack of understanding is partially due to previous studies expressing mutations in peptide fragments, and behaviors of even WT SLRs have been shown to vary dramatically when studied in isolation (Mirza et al., 2010). While these studies suggest the molecular consequences of individual missense mutations, comparing mutations within the SLR requires expression in the context of full-length dystrophin isoforms.

DBMD patients with missense mutations in the carboxy-terminal (CT) domain often display severe symptoms including a DMD patient encoding C3340Y (Lenk et al., 1996), and another encoding D3335H (Goldberg et al., 1998). The CT domain of dystrophin consists of a cysteine-rich region that binds beta-dystroglycan (Suzuki et al., 1994), and an unstructured “tail” region that binds to syntrophins (Ahn and Kunkel, 1995). Previous studies of CT missense mutations have been limited to assessing their effects on beta-dystroglycan binding *in vitro* or localization in heterologous cells, both using isolated recombinant domains (Ishikawa-Sakurai et al., 2004; Draviam et al., 2006). A recent report revealed the first missense mutation to definitively lack beta-dystroglycan binding *in vivo* (Vulin et al., 2014). Yet, other missense mutations do not appear to ablate dystroglycan binding, and it is not known how they affect the biophysical stability of full-length dystrophin protein.

To better understand the biophysical consequences of amino acid substitutions distributed throughout the three principal domains of dystrophin (NT, SLR, CT), we generated a biophysical model of an array of disease-

associated missense mutations and non-disease nsSNP in full-length purified dystrophin. Of the five disease-associated substitutions and three nsSNPs analyzed in the SLR of the central rod region, none appeared to markedly decrease protein solubility or stability. Analysis of six disease-associated substitutions and one nsSNP within the CT domain also revealed some mutations without effect on protein stability or solubility. Yet other CT mutations showed significantly decreased solubility and expression level. Biophysical analyses of mutants in full-length dystrophin (Dp427) revealed that while both NT and CT mutations can decrease solubility and expression, only NT mutations drastically alter the tertiary folding and stability of soluble protein. Our results demonstrate that domain location influences the biophysical consequences of disease-causing missense mutations in dystrophin *in vitro*.

Materials and Methods

In silico Amino Acid Substitution Analysis

Supplemental Table 1 summarizes all data obtained for *in silico* analysis. The list of non-synonymous SNPs for the human DMD gene was obtained from the SNP database on the National Center for Bioinformatics webpage (http://www.ncbi.nlm.nih.gov/snp). The list of disease-associated missense mutations were obtained from the Leiden Muscular Dystrophy pages (http://www.dmd.nl/), and any that overlapped with known SNPs were considered not associated with disease and were discarded. Unique amino acid substitutions were plotted as a distribution across the primary amino acid sequence. Statistical analysis of the proportion of amino acid substitutions (n) that cause disease (x) for the three domains NT: Amino Terminus (a.a. 1-252), SLR: Spectrin Like Repeats (also known as central rod region) (a.a. 253-3112), CT: Carboxy Terminus (a.a. 3113-3685) were calculated. NT: n=36, x=26, p=0.7222. SLR: n=230, x=41, p=0.1782. CT: n=44, x=23, p=0.5227. H_0: $p_1=p_2$. z-score comparisons between the three proportions were calculated and significance determined at a level of $\alpha=0.05$.

Cloning

The Dp260 and Dp427 mouse dystrophin cDNA constructs (**NM_007868.5**) were cloned into the entry vector pENTR™/D-TOPO® (Life Technologies) according to manufacturer's instructions. Individual nucleotide changes corresponding to human amino acid changes were made with the following site directed

mutagenesis reaction: 39.5µl dH_2O, 5µl Pfu buffer, 200µM dNTPs, 125ng of Fwd mutation primer, 125ng Rev mutation primer, 1µl template plasmid, 1µl PfuUltra II Fusion HotStart polymerase (Agilent). Reaction was cycled with the protocol: 92° for 2 min, 35 cycles of [92° for 1 min, 50° for 1 min, 68° for 10 min], 68° for 15 min. Nucleotide changes were verified by Sanger sequencing.

Protein expression and purification

Construct cassettes were recombined from entry vector into the Baculovirus destination vector pDEST™8 using Life Technology's Gateway® LR Clonase® (Hartley, 2000). These plasmids were transformed into DH10Bac competent *E.coli*, so that the expression insert could transpose into the Bacmid DNA. Bacmid DNA was purified according to manufacturer's protocol and transfected into Sf9 insect cells with the transfection reagent Cellfectin® II (Life Technologies). All culturing of insect cells was performed in the serum-free media Sf-900™ II SFM (Life Technologies) at a concentration of 1×10^6 cells/mL. A maximum titer of virus was produced by successive infections. The P2 baculovirus stocks were used in excess volumes to infect 250mL cultures for 72-hour expressions of recombinant protein such that variable multiplicities of infection (MOI) were negligible. After the 72 hours of protein expression, insect cells were pelleted and re-suspended in a solution of Phosphate Buffered Saline (PBS) [8mM NaH_2PO_4, 42mM Na_2HPO_4, 150mM NaCl] and protease inhibitors [100nM Aprotonin, 10mg/ml E-64, 100µM Leupeptin, 1mM PMSF, 1µg/ml Pepstatin], and then lysed by sonication for 30 seconds 3 times at 30% power.

The lysate was applied to an anti-FLAG M2 agarose column (Sigma Aldrich) and washed with >10 volumes of PBS + protease inhibitor solution. Bound protein was eluted with buffer containing 100μg/ml FLAG peptide. The purified protein was dialyzed overnight in 2L of PBS and concentrated using an Amicon Centrifugal Filter unit (UFC801024). Purity was assessed by Coomassie staining of an SDS-PAGE separation and concentration determined by A_{280}.

Solubility Quantification

Sf9 insect cells were infected with high titer Baculovirus encoding the protein of interest and incubated for 48 hours (Dp260) or 72 hours (Dp427). Cells were then collected and lysed in a solution of PBS (with protease inhibitors as above) + 1% Triton X-100 for 30 minutes. Samples were centrifuged at >20,000 x *g* for 10 minutes. Supernatant was collected as the soluble fraction and the insoluble pellet resuspended in the same volume of a solution of 2M Urea, 1% SDS and incubated at 50°C for 30 minutes. All samples were boiled at 95° for 5 minutes and equal volumes loaded onto a 3-12% polyacrylamide gel. Samples were electrophoresed at 150V for 1 hour, then transferred to PVDF membrane at 100V/0.7Amp for 1 hour. Membranes were blocked in 5% non-fat milk in phosphate buffered saline 0.1% Tween solution for 1 hour. FLAG-Dystrophin fusion protein was detected by M2 α-FLAG primary antibody (Sigma) at 1:1000 in blocking buffer, then secondary antibody anti-mouse IgG Dylight® 800 (Cell Signaling) at 1:10,000 in blocking buffer. Secondary antibody signal was visualized on Licor's Odyssey® Infrared Imaging System and band density

calculated with Odyssey Software v2.1.

Circular Dichroism (CD)

Purified protein was prepared at a concentration of 0.5mg/ml for Dp260 and 0.3mg/ml for Dp427 in PBS. Samples were centrifuged at >20,000 x *g* for 10 minutes to pellet dust. Absorption spectra were acquired with a Jasco J-815 spectropolarimeter, at 20°C as controlled by a Peltier device, from 200 to 260nm wavelength. Spectra were then acquired at 1° intervals from 20-90° and the characteristic alpha-helical wavelength (θ_{222}) recorded. Values of ellipticity were normalized from 0 to 1 for each sample and plotted against temperature, then fit by regression analysis in Sigma Plot (Systat Software, Inc.) using an equation for a two state or three state unfolding model.(Legardinier et al., 2009)

Differential Scanning Fluorimetry (DSF)

Method described by Niesen et al.(Niesen et al., 2007) Purified protein at a concentration of 0.5mg/ml for Dp260 and 0.3mg/ml for Dp427 in PBS was incubated with the fluorescent dye SYPRO® Orange (Life Technologies™ #S6650) at a concentration of 1:1000. When bound to hydrophobic regions of protein, the dye fluoresces with an emission of 610nm wavelength. Emission was measured with a BioRad iQ light cycler as temperature was increased from 20° to 90°. Relative Fluorescent Units were measured and standardized to show a 0.0 to 1.0 fraction of unfolded protein and plotted against temperature. Curves were fit by regression analysis in Sigma Plot (Systat Software, Inc.) using an equation for a two state unfolding model.(Legardinier et al., 2009) Samples were

measured in technical triplicate.

Dynamic Light Scattering (DLS)

Purified protein was diluted to a concentration of 0.1mg/ml for Dp260 or 0.05mg/mL for Dp427 in PBS. Samples were centrifuged at >20,000 x *g* for 10 minutes to pellet dust. Light scattering was measured by the Malvern Instrument Zetasizer μV for 100uL of sample in a disposable cuvette. Scattering intensity was measured 13 times over 10-second intervals, and each interval correlated as a function of time. From the correlogram, a diffusion coefficient was extracted and used to calculate particle size with the Stokes-Einstein equation. Malvern Zetasizer software reports the hydrodynamic radius of the particle as a Z-average in nm and the polydispersity Index (PdI) of the solution on a scale or 0 to 1 where 0 is perfectly uniform in size.

Results

Biophysical characterization of missense mutations in the CT and SLR domains of Dp260

Several DBMD and SNP amino acid changes in the SLR and CT domains were selected for biophysical characterization in recombinant Dp260 protein, which offers the context of an endogenous protein yet is logistically easier than full-length dystrophin (Table 2.1). Proteins were engineered in a baculovirus system and expressed in Sf9 insect cells with an amino-terminal FLAG epitope (Figure 2.1). To determine the solubility of each, cells were fractionated into soluble (S) and insoluble (I) portions (Figure 2.2A) and the percentage of soluble protein was quantified (Figure 2.2B). The WT Dp260 itself was only ~50% soluble, most likely due to overexpression in the baculovirus system, yet provides a standard against which to measure the substituted proteins. None of the amino acid changes in the SLR domain caused a decrease in solubility of the protein relative to WT Dp260. In the CT domain however, D3335Y caused a significant reduction in the percent soluble protein ($p<0.01$), and A3311P, C3313F, and C3340Y caused an even more dramatic decrease ($p<0.0005$). Total protein expression levels (S + I) normalized to WT (Figure 2.2C) confirmed a highly significant reduction of C3207R expression ($p<0.01$) that was apparent from the raw data (Figure 2.2A).

Each of the substituted proteins were then expressed on a larger scale in the insect cells and purified by FLAG-affinity chromatography. Total purified

protein is shown with equal loading (by A_{280}) for SDS-PAGE separation and Coomassie staining (Figure 2.2D). Purification results confirm solubility and total protein quantifications; C3313F is visibly reduced in the purification sample and C3207R and C3340Y are not observable at all by Coomassie stain. These results indicate that several of the amino acid substitutions in the CT domain of Dp260 decrease the solubility and purifiable fraction. While not all proteins are visible by Coomassie, subsequent analyses indicate that each is present in the respective purification samples.

Because many of the SLR and CT mutations were comparable to WT Dp260 in terms of solubility and expression, we investigated whether any of the purified proteins exhibited altered secondary structure as analyzed by circular dichroism (CD) spectroscopy. Absorption spectra (Figure 2.3A) for each protein were characteristic of a highly alpha-helical peptide with minima at 208 and 222nm. The magnitude of absorption is visibly reduced for C3207R and C3340Y, indicative of the lower percentage content in the purification sample as was seen in Figure 2.2. Yet each of these cysteine mutants maintains the alpha-helical secondary structure. As a negative control, uninfected Sf9 lysate was purified in a similar manner and the elution measured by CD; no absorption spectrum was observed (data not shown). To determine the thermal stability of the secondary structure, the 222nm minimum was monitored over a temperature course (Figure 2.3B). The WT Dp260 protein was observed to exhibit two unfolding transitions (T_m's = 52.7°C, 74.8°C), consistent with previous reports

(Henderson et al., 2011; Mirza et al., 2010). While some of the substituted SLR (P3011S and E3032K) and CT domain proteins (A3311P, C3313F, and R3673K) exhibited two-transition unfolding similar to WT, several others exhibited single-transition unfolding (Figure 2.3B). Thus, there was no obvious relationship between thermal stability and disease association for substitutions in the SLR or CT.

We also monitored the unfolding of each substituted protein by differential scanning fluorimetry (DSF), which measures the tertiary structure of a protein as assessed by hydrophobic residue exposure (Niesen et al., 2007). Monitoring DSF signal as a function of temperature revealed a single-transition unfolding for WT Dp260 protein with a T_m of 43.31°C (data not shown). This melting inflection point is lower than that calculated for the CD melt, as is expected because tertiary structure is lost before secondary structure during thermal denaturation. All amino acid substitutions in the SLR and CT (both disease-associated and SNP) had a similar transition with similar T_m. These data indicate that mutations in the SLR and CT domains have no effect on the tertiary stability of the Dp260 protein.

Lastly we analyzed the purified Dp260 proteins by Dynamic Light Scattering (DLS). Because DLS calculations of molecular weight depend on the assumption of spherical shape, absolute values of hydrodynamic radius (z-average) were not used to calculate molecular weight of rod-shaped Dp260, but rather were used for relative comparisons. DLS for WT Dp71, Dp260, and

Dp427 reported z-average values of 16.76±0.11, 24.76±0.11, and 40.86±1.05nm respectively (data not shown). DLS of all amino acid substituted Dp260 proteins reveals some heterogeneity in size, yet all are comparable to WT (Figure 2.4A). While WT protein served as a negative control of aggregation, our equivalent positive control was WT protein boiled for 5 minutes and then brought back to room temperature. Various concentrations of protein were boiled and each had z-averages between 150-200nm (data not shown). None of the amino acid changes caused this magnitude of radius, as would be expected in a plaque-type aggregation. The polydispersity index (PdI) can also be measured by DLS on a scale from 0 to 1. WT Dp260 has a PdI within quality control standards, as do each of the substituted proteins (Figure 2.4B) (ISO standards document 13321). The amino acid changes C3207R, C3313F, and C3340Y have a visibly increased PdI, which we believe is due to these proteins comprising a lower percentage of the purified sample as seen in Figure 2.2D, rather than indicating protein aggregation. The size and polydispersity were measured by DLS at several different concentrations and for time courses (data not shown); none of the substituted proteins were significantly different than WT. Together these data indicated that the soluble Dp260 protein purified from cells is not prone to plaque-like aggregation.

Biophysical characterization of missense mutations in the NT, SLR, and CT domains of Dp427

Results from the Dp260 constructs were obscured by the nature of WT

Dp260 (particularly in regards to CD melt transitions), and we wanted to directly compare amino acid substitutions in the SLR and CT domains with previously characterized substitutions in the NT domain. Therefore we engineered two disease-associated substitutions and one nsSNP for each of the three domains into full-length dystrophin, Dp427 (Table 2.1). Constructs were again expressed in insect cells via the baculovirus system. Cell lysates were fractioned into (S) and insoluble (I) portions and Dp427 levels analyzed (Figure 2.5A). Quantification of the percent soluble protein showed no significant decreases in any of the amino acid substituted proteins compared to WT, although L54R appears to trend towards a decrease (Figure 2.5B). C3207R appears to be highly soluble, but this calculation should not be taken too literally as it is obviously the result of dividing by values near zero. Quantification of the total expressed protein relative to WT (Figure 2.5C), revealed a significant decrease for L54R ($p<0.05$); and as expected from the raw data (Figure 2.5A), a highly significant decrease for C3207R ($p<0.0001$). Expression of protein in insect cells was then scaled up for purification, and total purified protein is shown with equal loading (by A_{280}) for SDS-PAGE separation and Coomassie staining (Figure 2.5D). Dp427 C3207R represented a smaller percentage component of the purified sample confirming total expression levels in Figure 2.5C. Also as expected from results in Dp260, none of the substitutions in the SLR domain affected protein solubility or purification ability.

Purified protein samples were measured by circular dichroism (CD) to

determine global secondary structure (Figure 2.6A). The absorption spectrum of Dp427 WT was characteristic of a highly alpha helical protein with minima at 208 and 222nm and each of the substituted proteins showed similar spectra. The absorption at 222nm was observed over a temperature course to determine thermal stability of the secondary structure (Figure 2.6B). Dp427 WT showed a single-step unfolding (T_m = 48.59°). In the NT domain, L54R displayed a more linear unfolding transition indicative of a less stable or heterogeneous folded state and consistent with previous reports (Henderson et al., 2010). Both SNP and missense mutations in the SLR domain gave similar melt curves to WT. In the CT domain, C3207R is seen above the WT curve at low temperatures and below the WT curve at high temperatures; again this less cooperative transition indicates less stability in the secondary structure of this mutant.

The differences in CD melt transitions are subtle, so we also examined the stability of these full-length Dp427 constructs by Differential Scanning Fluorimetry (DSF) which measures the tertiary state of the protein (Figure 2.6C). Dp427 WT gave a melting temperature of 43.36°C. Both the SNPs and missense mutations in the SLR and CT domains gave this same unfolding curve, indicating there were no perturbations in the tertiary stability of these proteins. Yet, large differences are noticeable in the NT domain. Importantly, the SNP I232M shows a similar melt curve to WT, while L172H is shifted slightly left (T_m = 42.08°C) indicating a decrease in protein stability. And L54R is far left-shifted (T_m = 40.03°C) indicating either a large tertiary instability or an already partially

unfolded state of the protein at initiation of the experiment. These data indicate a unique disturbance in global folded state caused only by missense mutations located in the NT domain of Dp427.

To determine the potential aggregation state of the protein we analyzed each by Dynamic Light Scattering (DLS). The z-average relative size of Dp427 WT was determined to be 40.86±1.05nm and each of the substituted proteins gave similar measurements (Figure 2.6D). None were the orders of magnitude larger indicative of amyloid-like aggregations. The polydispersity of each purified protein was similar to WT and within quality control standards (Figure 2.6E). Again the dispersity indicates that these amino acid substitutions did not cause aggregation in full-length Dp427. Even the NT mutations that caused global misfolding (Figure 2.6C) did not appear to cause aggregation by this highly quantitative method.

Discussion

Here we report on the effect of several disease-causing missense mutations found in DBMD patients spanning the three major domains within full-length dystrophin protein. Firstly, it was observed that all mutations tested in the SLR domain had no effect on solubility, stability of secondary or tertiary structure, or aggregation state of purified Dp260 or Dp427 protein. Secondly, it was found that missense mutations in both the NT and CT can cause subtle effects on the solubility and stability of dystrophin. And finally, no missense mutation tested caused plaque-like aggregation of the purified protein under the conditions tested. It seems that the principle effect of missense mutations in full-length protein is insolubility in the cellular context, and that after purification only subtle biophysical perturbations are measurable.

Several previous biophysical studies of dystrophin missense mutations have been performed on isolated recombinant domains (Singh et al., 2010; Acsadi et al., 2012; Legardinier et al., 2009; Ishikawa-Sakurai et al., 2004; Draviam et al., 2006), but it has been demonstrated that even the WT amino acid sequence of some individual SLRs are not stable enough for biophysical characterization (Mirza et al., 2010). Therefore, introduction of a missense mutation into a stability-compromised peptide fragment may exaggerate the effect of the mutation on protein stability. Our data and that of others suggest that such context-dependent effects of mutation are evident in naturally occurring isoforms of dystrophin. For example, the C3313F mutant version of Dp71 only

expressed to a small fraction of the level observed for WT Dp71 and was almost completely insoluble when expressed in insect cells, HEK293 cells, or mouse skeletal muscle (Vulin et al., 2014), while we observed that increasing amounts of this mutant were recovered when expressed in Dp260, or Dp427. The C3313F mutant demonstrates that the effects of some missense mutations on dystrophin folding and stability are highly context-dependent.

Although the effects we observed in Dp260 and Dp427 are subtle, it appears that mutations in the two termini of the dystrophin protein are more destabilizing than those in the SLRs of the central rod domain. The different susceptibilities of the three major domains is likely a result of their inherent structures and functions. In the NT, mutations can cause a disturbance in the tertiary structure as revealed by DSF. This dependence on domain location may be due to the nature of the protein folding process in which chaperones begin to fold a nascent peptide as it is translated from amino- to carboxy-terminus (Kramer et al., 2009; Zhang and Ignatova, 2011). A mutation that is encountered early in the folding process may be more globally destabilizing. In the SLR, none of the mutations tested had an effect on solubility and expression of the protein or on biophysical stability. The ability of a spectrin repeat to acquire a mutation and maintain structure and stability is not unexpected based on the sequence variability seen between individual spectrin-like repeats in dystrophin and between spectrin repeats in other members of the large family of spectrin-like proteins (Pascual et al., 1997; Djinovic-Carugo et al., 2002). In the CT domain,

the cysteines which appear to be necessary for proper solubility and expression are critical for Zn^{2+} binding and subsequent structure (Ponting et al., 1996; Hnia et al., 2007). The three major domains of dystrophin therefore appear to be differentially affected by disease-causing missense mutations.

In our system, even the missense mutations associated with severe dystrophy in patients (L54R, C3313F) had relatively small biophysical effects *in vitro* so it follows that missense mutations associated with milder dystrophy may show no difference from WT protein *in vitro*. Clearly, such missense mutations must affect some aspect of dystrophin structure or function. For instance, they may alter the activity of dystrophin for one of its binding-partners as seen for loss of beta-dystroglycan binding by Dp71 mutant D3335H (Vulin et al., 2014), as well as syntrophin (Ahn and Kunkel, 1995), dystrobrevin (Sadoulet-Puccio et al., 1997), nNOS (Brenman et al., 1995), phospholipids (DeWolf et al., 1997; Legardinier et al., 2008), intermediate filaments (Stone et al., 2005; Bhosle et al., 2006), or microtubules (Prins et al., 2009). Another possibility is that nucleotide changes predicted to effect amino acid substitutions may actually perturb transcript splicing (Xing and Lee, 2006; López-Bigas et al., 2005). The 79 exons of the dystrophin gene raise the probability that nucleotide substitution may affect splicing, which would not be observable in our experimental design. Finally, the possibility remains that some of the amino acid changes found in DBMD patients are not the causative mutation. The abundance of documented polymorphisms in dbSNP demonstrates that a variety of substitutions can occur and not cause

disease.

In order to move towards a more personalized medicine approach where the most effective therapy can be developed for DBMD patients with missense mutations, it will be necessary to fully understand how each missense mutation affects dystrophin structure and function. Our results reinforce the importance of evaluating missense mutations in the context of full-length dystrophin, and likely in the context of a mammalian cellular system or model organism.

domain	a.a. Δ	designation	reference
N-terminal Domain (NT)	L54R	DMD	Prior et al.(Prior et al., 1993)
	L172H	BMD	Hamed et al.(Hamed et al., 2005)
	I232M	SNP	rs145668843
Spectrin-Like Repeats, (SLR)	A1872V	DMD	LMDP 00001
	R2155W	SNP	rs1800273
	L2267F	DMD	LMDP 00017
	A2682S	DMD	LMDP 00001
	D2740G	BMD	Flanigan, et al.(Flanigan et al., 2009)
	Q2937R	SNP	rs1800280
	P3011S	DMD	LMDP 00003
	E3032K	SNP	rs72466562
C-terminal Domain (CT)	D3187G	DMD	Taylor et al.(Taylor et al., 2007)
	C3207R	DMD	Taylor et al.(Taylor et al., 2007)
	A3311P	BMD	LMDP 00198
	C3313F	DMD	Flanigan et al.(Flanigan et al., 2003)
	D3335Y	DMD/BMD	Flanigan et al.(Flanigan et al., 2009)
	C3340Y	DMD	Lenk et al.(Lenk et al., 1996)
	R3673K	SNP	rs1795743

Table 2.1: Selected amino acid substitutions for analysis in Dp260 and full-length Dp427. Designation of amino acid change is listed by disease on the Leiden Muscular Dystrophy Pages (DMD=Duchenne Muscular Dystrophy, BMD=Becker Muscular Dystrophy) or as a SNP on dbSNP (NCBI). SNPs are referenced by their rs ID number (marked in green), and disease-associated changes by their original publication or Leiden Muscular Dystrophy Pages (LMDP) database submitter ID (red).

Figures

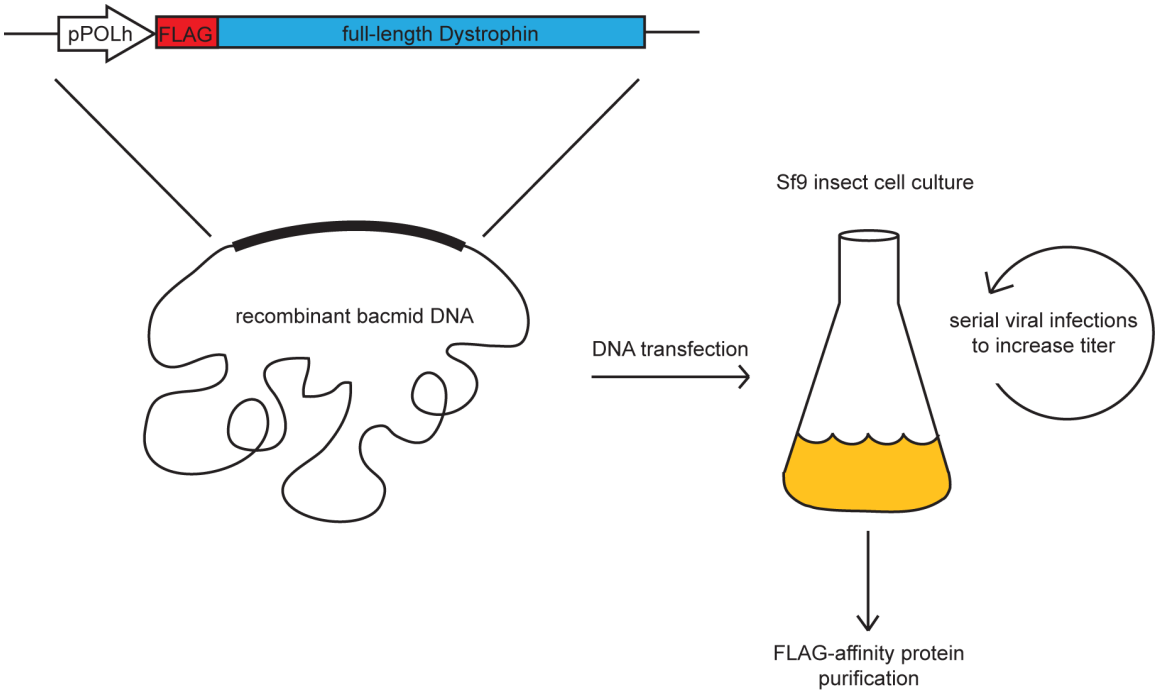

Figure 2.1: Expression construct and experimental concept

Full-length, mouse dystrophin DNA was subcloned with an N-terminal FLAG epitope tag under a polyhedron promoter (pPOLh). This cassette was recombined into the baculovirus genome, or Bacmid DNA. Bacmid DNA was transfected into Sf9 insect cells by lipid-mediated methods. Virus was expressed from the Bacmid DNA while dystrophin protein was expressed from the polyhedron promoter; serial infections were performed to maximize viral titer. The final viral titer was used to infect a large culture of insect cells which was then lysed and dystrophin protein purified by FLAG affinity chromatography.

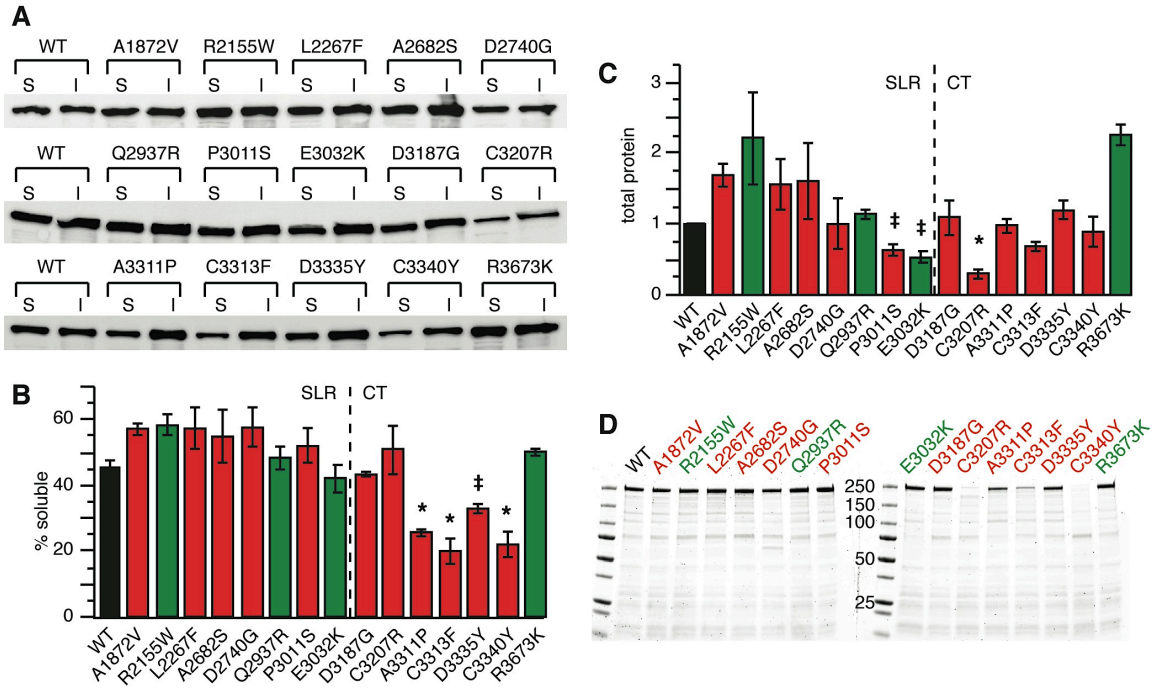

Figure 2.2: Solubility and expression levels of missense mutations in Dp260 **(A)** Representative immunoblot analysis of soluble fraction (S) and insoluble fraction (I) from Sf9 cell lysates infected with baculovirus expressing the Dp260 isoform of dystrophin with indicated amino acid change. **(B)** Quantification of percent solubility by calculating soluble band values divided by soluble and insoluble band totals from immunoblots depicted in (A). n=3. Red = disease associated, green = SNP, significantly decreased from WT (‡ $p<0.01$), (* $p<0.0005$). **(C)** Quantification of the total protein expressed in soluble and insoluble band values normalized to WT total on each blot. n=3. Significantly decreased (‡ $p<0.05$) (* $p<0.01$) **(D)** Coomassie-stained acrylamide gel of total purified protein. Purified protein was concentrated and then measured by A_{280}. 10µg of each sample was loaded.

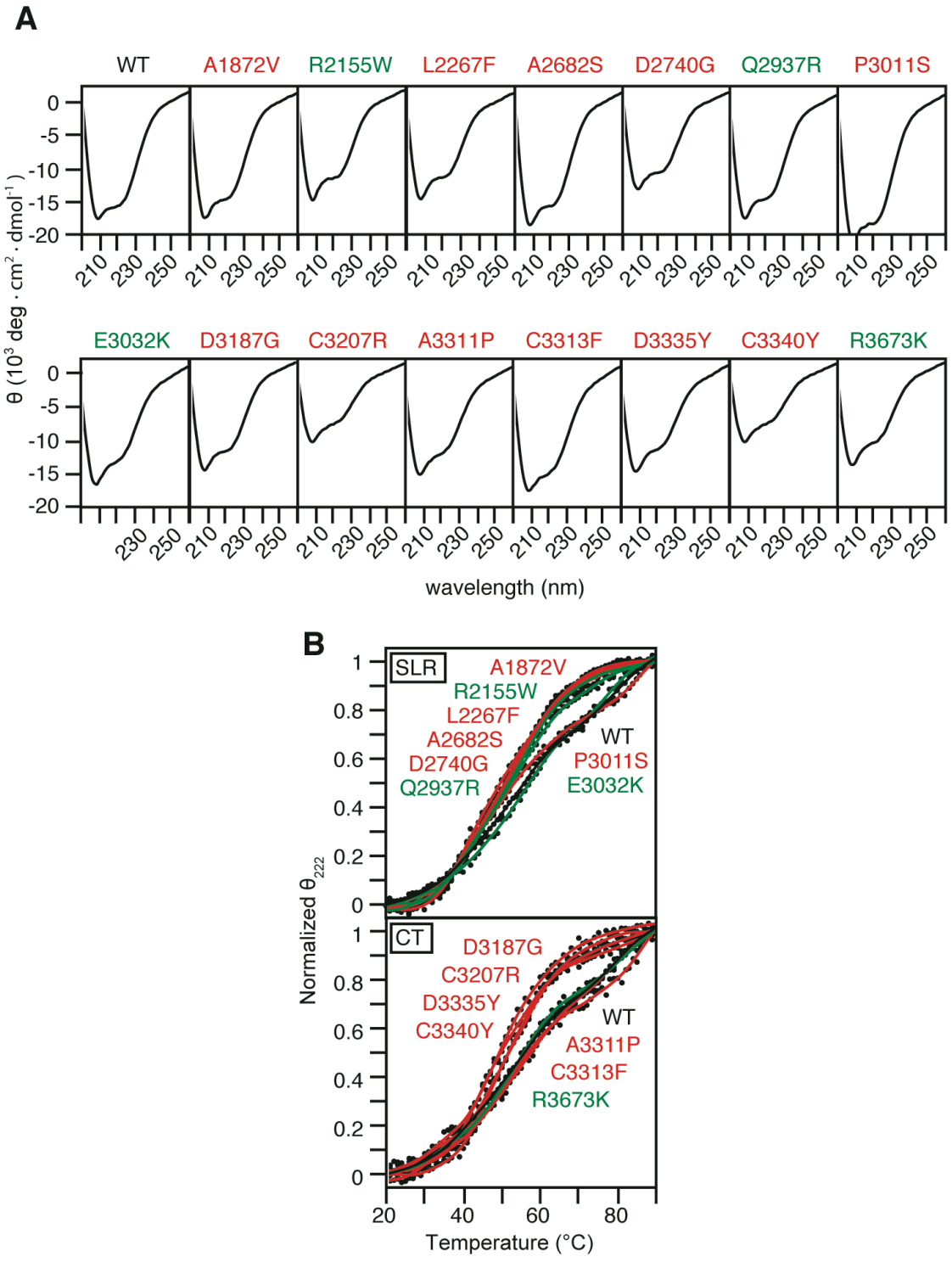

Figure 2.3: Secondary structure and stability of missense mutations in Dp260 (A) Circular Dichroism absorption spectra of each Dp260 purified protein.

All spectra display molar ellipticity minima at 208 and 222nm indicative of a highly alpha-helical protein. **(B)** Circular Dichroism melt curves obtained by monitoring absorption values at 222nm over temperature gradient of 20-90°. Values are normalized from 0-1 fraction unfolded. SLR = Spectrin Like Repeat Domain, CT = Carboxy Terminal Domain, green = SNP, red = missense mutation. Curves partitioned into a single transition unfolding (upper curves) or a two transition unfolding (lower curves).

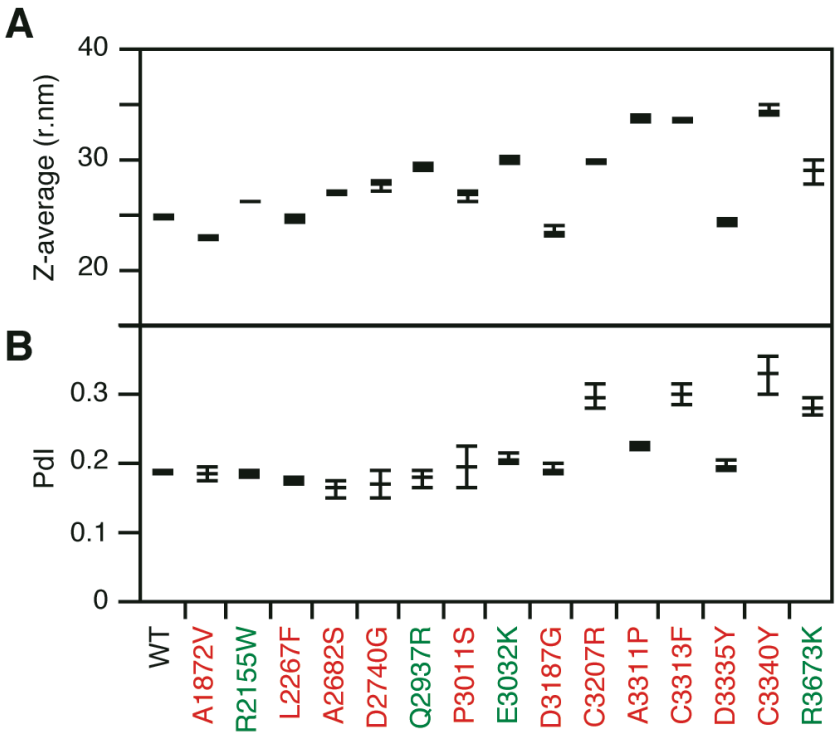

Figure 2.4: Average size and polydispersity of missense mutations in Dp260 **(A)** Z-average radius for each Dp260 isoform protein measured by Dynamic Light Scattering. Mean value and standard deviation bars are shown for a technical triplicate, units in nm of hydrodynamic radius. None show an increase in particle size by an order of magnitude above WT protein. **(B)** Polydispersity Index measured on a scale from 0 to 1, where 0 indicates complete monodispersity and 1 a completely heterogeneous mixture. WT protein has a PdI within quality control standards. Green = SNP, red = missense mutation.

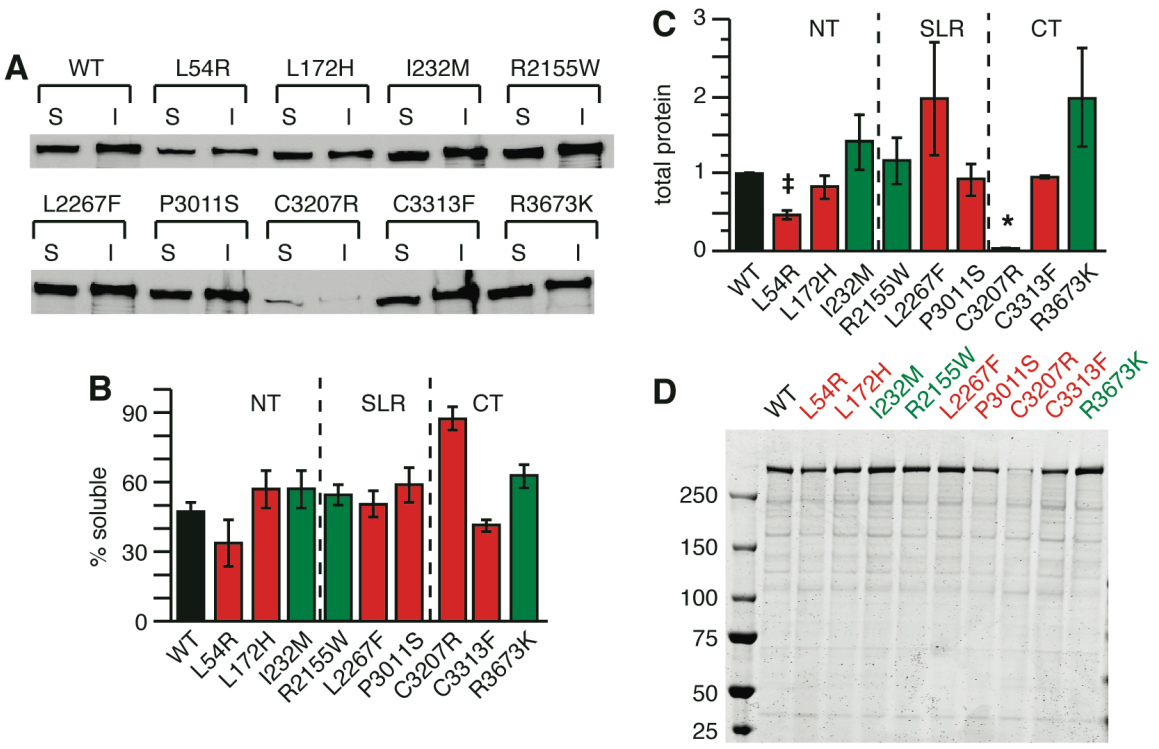

Figure 2.5: Solubility and expression levels of missense mutations in full-length Dp427 **(A)** Representative immunoblot analysis of soluble fraction (S) and insoluble fraction (I) from Sf9 cell lysates infected with baculovirus expressing the full-length isoform of dystrophin with indicated amino acid change. **(B)** Quantification of percent solubility by calculating soluble band values divided by soluble and insoluble band totals from immunoblots depicted in (A). n=3. Red = disease associated, green = SNP, none were significantly different than WT. **(C)** Quantification of the total protein expressed in soluble and insoluble band values normalized to WT total on each blot. n=3. Significantly decreased (‡ $p<0.05$) (* $p<0.0001$) **(D)** Coomassie-stained acrylamide gel of total purified protein. Protein was concentrated and then measured by A_{280}. 6µg of each sample was loaded.

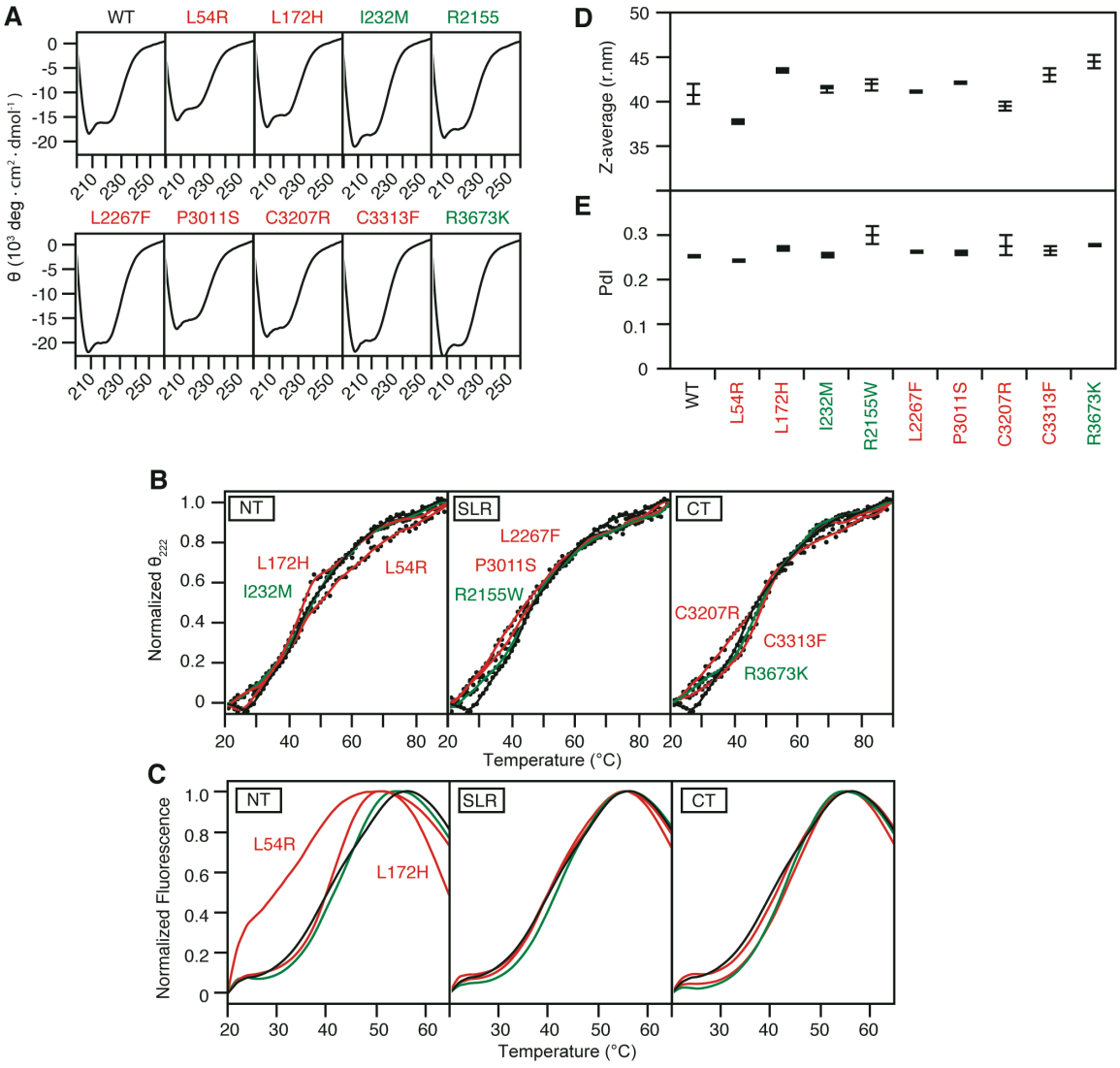

Figure 2.6: Secondary structure and stability, tertiary stability, and average size of missense mutations in Dp427 **(A)** Circular Dichroism absorption spectra of each Dp427 purified protein. All spectra display molar ellipticity minima at 208 and 222nm indicative of a highly alpha-helical protein. **(B)** Circular Dichroism melt curves obtained by monitoring absorption values at 222nm over temperature gradient of 20-90°. Values are normalized from 0-1 fraction unfolded. NT = Amino Terminal, SLR = Spectrin Like Repeat Domain, CT = Carboxy Terminal Domain, green = SNP, red = missense mutation. Unlike

the Dp260 isoform, WT unfolds with a single transition, making it distinguishable from proteins with a more linear unfolding (L54R and C3207R). **(C)** Differential Scanning Flourimetry monitored at 610nm over a temperature range of 20-90°. Fluorescent values are normalized from 0-1 fraction unfolded. NT = Amino Terminal Domain, SLR= Spectrin Like Repeat Domain, CT = Carboxy Terminal Domain. WT protein shown in black, disease associated missense mutations in red, and SNPs in green. All amino acid changes align with WT in the SLR and CT. L54R and L172H in the NT, however, show a left shift indicating instability or a partial unfolded state at ambient temperature. **(D)** Calculated z-average for each full-length Dystrophin protein measure by Dynamic Light Scattering. Mean value and standard deviation bars are shown for a technical triplicate, units in nm of hydrodynamic radius. Z-average values are relatively larger than those for Dp260 as is expected. None show an increase in particle size by an order of magnitude above WT protein. **(E)** Polydispersity Index measured on a scale from 0 to 1, where 0 indicates complete monodispersity and 1 a completely heterogeneous mixture. WT protein has a PdI within quality control standards, and all other proteins have a similar value.

Chapter 3

A Cell Culture Model of Missense Mutations in Dystrophin

Flow cytometry analysis was performed with the assistance of the University of Minnesota flow core technicians. All other cloning, cell culture, and analyses were performed by Dana Talsness.

Summary

Duchenne and Becker muscular dystrophies are genetic disorders that cause muscle weakness and atrophy primarily in male patients with a mutation in their gene encoding the protein dystrophin. In several cases the causative mutation is a single nucleotide change, or missense mutation, which results in an amino acid substitution in the protein. A previous study characterized a set of missense mutations found in the amino terminal, first actin-binding domain of dystrophin and found each caused protein misfolding and thermal instability *in vitro*. To determine the cellular consequences of *in vitro* instability, we generated four transgenic C2C12 myoblast cell lines expressing full-length dystrophin with coding sequence for WT, missense mutations L54R or L172H, or single nucleotide polymorphism I232M. Quantitative RT-PCR and western blot analysis revealed that full-length dystrophin protein levels were decreased for both mutants relative to respective transcript levels when compared to WT. In addition, it was possible to increase mutant dystrophin levels with several different small molecule therapeutics aimed at increasing osmotic stability, up-regulating the heat shock pathway, or inhibiting the proteasome. The C2C12 myoblast models indicate that mutant dystrophin is targeted to the proteasome for degradation and represent a system for potential discovery of personalized therapeutics.

Introduction

Given that dystrophin is a structural protein without enzymatic activity and given the *in vitro* evidence in Chapter 2, it is likely that missense mutations would lead to protein instability in the cell as seen by either aggregation or degradation of the protein. The cell has several pathways for dealing with unstable proteins including the heat shock pathway. The heat shock pathway was first discovered as a set of proteins that were up-regulated in response to a transient increase in temperature of the cell (Ritossa, 1962; Ashburner and Bonner, 1979). Further investigation has revealed these proteins are molecular chaperones which aid in the initial folding of proteins as well as the refolding of misfolded proteins, collectively known as the heat shock proteins (HSPs), and transcribed by the heat shock factors (HSFs) (Bozaykut et al., 2014). There are several families of HSPs including the high molecular weight, ATP-dependent HSPs: Hsp90, Hsp70, and Hsp40; as well as the small, ATP-independent HSPs such as Hsp27.

Hsp90s are responsible for binding to recently folded proteins and maintaining them in a folded state. When not bound to a client protein, Hsp90s bind to and inhibit the transcription factor HSF1, thereby acting as a negative regulator of the heat shock pathway (Akerfelt et al., 2010). Additionally it has been shown that the phosphorylation of Hsp90s can affect their affinities for client proteins (Bozaykut et al., 2014). Hsp70s facilitate both de novo folding and refolding of misfolded proteins in the cell utilizing an ATP/ADP dependent cycle of binding and unbinding to substrates (Mayer and Bukau, 2005). Their functions

are ubiquitous and necessary for protein quality control in the cell. Hsp40s recognize unfolded protein and transfers them to Hsp70, thereby acting as a co-chaperone (Summers et al., 2009). Hsp27s can form large oligomers and generally function to prevent aggregation of misfolded proteins (Bozaykut et al., 2014). Phosphorylation of Hsp27s favors small oligomers and decreases its ability to prevent aggregation (Lanneau et al., 2010). Together, all of the HSPs work to properly fold proteins. When a protein is considered beyond repair (by unknown mechanisms) the same Hsp40 and Hsp70 chaperones that attempted refolding will then facilitate the entrance of the protein into the ubiquitin proteasome system (Shiber and Ravid, 2014).

The cell has multiple methods for eliminating proteins that are not properly folded by the translational chaperones and the heat shock pathway, including the ubiquitin proteasome system (UPS). The UPS utilizes a cascade of conjugation to ubiquitin, a small 76 amino acid protein used as a post-translational modification. Ubiquitin is highly conserved in all eukaryotes and expressed in every cell, hence the name. In the first step of the UPS cascade one of eight E1 activating enzymes utilizes energy from ATP to form a thioester bond to ubiquitin (Schulman and Harper, 2009). Ubiquitin is then passed to a pathway specific E2 conjugating enzyme; there are approximately 40 known E2 ligases (Ye and Rape, 2009). They determine both ubiquitin chain elongation and type of ubiquitin linkage on the protein substrate. The E2 conjugating enzyme then binds to an E3 ligase of which there are over 600 (Deshaies and Joazeiro, 2009).

Each E3 ligase has specific protein substrates to which it binds. When the E3 binds to an E2 complexed with ubiquitin, the ubiquitin is transferred from E2 to the substrate. Therefore in the ubiquitin cascade, the E3 ligase provides the ultimate specificity of the system. When 4 ubiquitins have been transferred to a substrate, in a K48-linked chain, the protein is targeted for degradation by the proteasome (Thrower et al., 2000).

The proteasome is made of two major subcomplexes: the 20S core which contains the proteolytic sites and the 19S regulatory unit that caps either one or both ends of the 20S core (reviewed in Glickman & Ciechanover 2002). Altogether this protein complex is about 2.5MDa (26S). The 19S regulatory unit is composed of at least 18 subunits and functions to recognize ubiquitinated substrates and mediate their transfer into the 20S core. The 20S complex is a hollow core made of 4 stacked rings from top to bottom α, β, β, α. The β rings each contain three proteolytic sites facing the interior of the cylinder which have caspase-, trypsin-, and chymotrypsin-like activity respectively (Weathington and Mallampalli, 2014). Through these three protease-like activities, the 20S core is able to effectively degrade all protein substrates. The proteasome utilizes ATP hydrolysis to cleave proteins into 3-23 amino acid peptides which can then be further degraded by proteases in the cell (Kisselev et al., 1998), effectively eliminating and recycling the targeted protein.

There are several examples of missense mutations in proteins other than dystrophin being studied in cell culture models. One such example is a study of

missense mutations in the gene EPM2A encoding the protein laforin which cause Lafora's Disease (Liu et al., 2009). They expressed EPM2A with several different missense mutations in both HEK293 and NIH3T3 cell lines and found that all mutations caused a decrease in the soluble protein levels of laforin. Another group analyzed missense mutations in the protein SIMPLE that cause Charcot-Marie-Tooth Disease (Lee et al., 2011). SIMPLE is a membrane bound protein and missense mutations caused both mislocalization and aggregation of the protein when expressed in HeLa cells. Recently there was a study of missense mutations in the protein B3GNT1, a type II transmembrane protein which localizes to the Golgi and causes Walker-Warburg Syndrome (Buysse et al., 2013). When mutant B3GNT1 was expressed in PC3 cells, it localized correctly to the Golgi, but it impaired the glycosyltransferase enzymatic activity of the protein. These cell culture models have shown that missense mutations can lead to disease through various mechanisms.

There are relatively few successes to study recombinant dystrophin in cell culture models. The short isoform Dp71 has been transiently expressed in HEK293 and C2C12 cell lines in order to study the effect of alternate splicing on localization (González et al., 2000). Studies have transfected cells with AAV constructs containing small, truncated versions of dystrophin to prove the constructs would express before using them in animal transfection experiments (Fabb et al., 2002). A micro-dystrophin construct (144 kDa) was transiently transfected into primary mouse myoblasts and C2C12 cells and was shown to

localize to the plasma membrane of cells upon differentiation to myotubes (Draviam et al., 2006). Another study transiently transfected HEK293 cells with several Dp71-like constructs: WT and three missense mutations located in the ZZ domain of the cysteine rich region (Vulin et al., 2014). It was found that two of the missense mutations (C3313Y and C3340Y) dramatically decreased the levels of soluble Dp71 protein expressed in the cells, while one mutation (D3335H) expressed at WT levels. Mutation D3335H was determined to have decreased binding affinity to β-dystroglycan. To date there have been no cell line models stably expressing transgenic, full-length dystrophin.

One of the best candidate cell lines to use for expressing full-length dystrophin is the C2C12 line. C2C12 is a mouse myoblast cell line, first immortalized as a control population in order to study dystrophic cells (Yaffe and Saxel, 1977). Karyotype analysis of C2C12 cells reveals tetraploidy with an average of 80 chromosomes per genome (Chang et al., 2007). The cells are female in origin with four X-chromosomes, two of which are inactivated (Casas-Delucchi et al., 2011); this is important to note given that the mouse DMD gene is encoded on the X-chromosome similar to humans. C2C12 cells can be cultured indefinitely as myoblasts with splitting at subconfluency, or they can be differentiated into terminal myotubes with reduced serum media. Microarray analyses comparing C2C12 cells before and after differentiation into myotubes reveal over 1500 transcript expression changes including several transcription factors and genes responsible for chromatin remodeling (Delgado et al., 2003).

LC-MS proteomic analysis of differentiating C2C12 showed similar changes in proteins linked to cell adhesion, intracellular signaling, gene expression, metabolism, and muscle contraction. Overall C2C12 cells serve as an easy to use and well-studied skeletal muscle cell culture system.

To determine the cellular fate of dystrophin proteins harboring missense mutations, we engineered two candidate mutations, L54R and L172H into full length dystrophin and expressed them in C2C12 mouse myoblast cells with the use of the PiggyBac transposon system. In this model system we demonstrated that mutant dystrophin is misfolded and degraded by the proteasome to a degree that is proportional to the severity of disease seen in the patients harboring these mutations. Our results reveal the cellular consequences of a protein that is unstable *in vitro* as well as potential avenues of therapeutic treatment.

Materials and Methods

Cloning

Full-length mouse dystrophin cDNA (WT, and all missense mutations) was subcloned into the Gateway system Entry vector as described in Chapter 2. The mammalian expression vector PiggyBac-CMV-MCS-EF1-Puro (System Biosciences) was purchased and then a destination cassette was subcloned into the MCS in order to adapt it to the Gateway® system. The dystrophin cDNA was recombined from the entry vector into the newly made PiggyBac™ destination vector using Life Technology's Gateway® LR Clonase® (Hartley, 2000).

Cell transfection and stable line selection

The PiggyBac destination vector with inserted dystrophin cDNA along with the Super PiggyBac Transposase vector (System Biosciences PB200PA-1) was electroporated into C2C12 cells (ATCC CRL-1772) using a Nucleofector™ 2b (Lonza) device with the accompanying C2C12 kit (Amaxa VCA-1003). After electroporation cells were cultured for 48 hours. Then cells were split 1:15 into media containing 2ug/mL puromycin and cultured for 2 weeks until colonies of cells were visible to the naked eye. Individual colonies were selected, cultured, and then screened for similar levels of transgene insertion by gDNA qPCR described below.

Cell culture and differentiation

C2C12 (ATCC CRL-1772) transgenic cell lines were cultured in Dulbecco's Modified Eagle Medium (Gibco) supplemented with 10% Fetal Bovine Serum

(Gibco), 1% penicillin/streptomycin cocktail (Hyclone 15290), and 0.1% fungizone (Gibco); and grown at 37°C, 5% CO_2. Cells were always grown to 80% confluency and then either split for further subculturing or used for an analysis. C2C12 lines were differentiated by growing cells to 80% confluency and then changing the media to DMEM supplemented with 2% Horse Serum (Gibco) and penicillin/streptomycin and fungizone. Differentiation media was changed every other day until full differentiation was reached 7 days after initiation.

gDNA qPCR

Cells were collected and gDNA was isolated with GenElute™Mammalian Genomic DNA Miniprep kit (Sigma-Aldrich G1N70). The DNA was then amplified by primers within the CMV promoter region of the transgene: forward [GGCCTCCAAGGCCACTAGTAT] and reverse [TCCACGCCCATTGATGTACT] using SsoAdvanced™ Universal SYBR® Green Supermix (Biorad 172-5270). All measurements were relative to the reference gene ADH: forward [GCACTGCGGGAAAAGTAAGG] and reverse [TAGCAGGTCAAGCTGTGCTC]. Measurements were collected with the C1000 Touch Thermal Cycler (Biorad) and analyzed with the CFX Manager software (Biorad).

RT-qPCR

Cells were collected and RNA isolated with Aurum™ Total RNA Mini Kit (Biorad 732-6820). Total RNA was reverse transcribed into cDNA using the iScript™ Advanced cDNA Synthesis Kit (Biorad 170-8843). cDNA was amplified with primers within the GFP sequence in order to detect on transgenic dystrophin

transcript: Forward [TCCGCCATGCCCGAAGGCTA] and Reverse [CCGTTCACCAGGGTGTCGCC] using SsoAdvanced™ Universal SYBR® Green Supermix (Biorad 172-5270). All measurements were relative to reference transcript Hprt: Forward [CCCTGGTTAAGCAGTACAGCCCC] and Reverse [GGCCTGTATCCAACACTTCGAGAGG]. Measurements were collected with the C1000 Touch Thermal Cycler (Biorad) and analyzed with the CFX Manager software (Biorad).

Western blot analysis

Cells were collected and lysed with RIPA buffer [10 mM Tris-Cl (pH 8.0), 1 mM EDTA, 0.5 mM EGTA, 1% Triton X-100, 0.1% sodium deoxycholate, 0.1% SDS, 140 mM NaCl] with added protease inhibitors [100nM Aprotonin, 10mg/ml E-64, 100μM Leupeptin, 1mM PMSF, 1μg/ml Pepstatin] proportional to mass of cell pellet. Equal volumes of lysate were then separated by electrophoresed at 150V for 1 hour, then transferred to PVDF membrane at 100V/0.7Amp for 1 hour. Membranes were blocked in either [5% non-fat milk in phosphate buffered saline 0.1% Tween solution] or [5% Bovine Serum Albumin in tri buffered saline 0.1% Tween solution] depending on the primary antibody for 1 hour. Primary antibodies used were anti-GFP (Cell Signaling 2956) at 1:1000, anti-pan actin C4 ( ) at 1:5000, anti-Desmin D93F5 (Cell Signaling 5332) at 1:1000, anti-Hsp40 C64B4 (Cell Signaling 4871) at 1:1000, anti-Hsp70 (Cell Signaling 4872) at 1:1000, anti-Hsp90 (abcam 19021) at 1:1000, anti-Phosph-Hsp90α (Cell Signaling 3488) at 1:1000, anti-Phospho-Hsp27 (Cell Signaling 9709) at 1:1000,

and anti-Ubiquitin P4D1 (Cell Signaling 3936) at 1:1000. Blots were ten incubated in secondary antibodies anti-mouse or anti-rabbit IgG Dylight® 800 (Cell Signaling) at 1:10,000 in blocking buffer. Secondary antibody signal was visualized on Licor's Odyssey® Infrared Imaging System and band density calculated with Odyssey Software v2.1.

Small molecule treatments

Trehalose (Sigma Aldrich T0167) was prepared as a stock solution at 100mM in H_2O; cells were treated at working concentrations for 24 hours. TMAO [Trimethylamine N-oxide] (Acros Organics 421890250) was prepared as a stock solution at 1M in H_2O; cells were treated at working concentrations for 24 hours. Betaine (Alfa Aesar B24397) was prepared immediately before use at 400mM in cell culture media; cells were treated with working concentrations for 24 hours. Celastrol (Sigma Aldrich C0869) was prepared as a stock solution at 10mM in DMSO; cells were treated at working concentrations in equal volumes of DMSO for 18 hours. BGP-15 (Sigma Aldrich B4813) was prepared as a stock solution at 10mM in H_2O; cells were treated at working concentrations in equal volumes of H_2O for 18 hours. Gedunin (Santa Cruz 203867) was prepared as a stock solution at 10mM in DMSO; cells were treated at working concentrations in equal volumes of DMSO for 18 hours. MG-132 (American Peptide 81-5-15) was prepared as a stock solution at 1mM in DMSO; cells were treated at working concentrations in equal volumes of DMSO for 18 hours. MG-262 (A.G. Scientific Z-1003) was prepared as a stock solution at 100μM in DMSO; cells were treated

at working concentrations in equal volumes of DMSO for 18 hours. Bortezomib (Cell Signaling 2204) was prepared as a stock solution at 10mM in DMSO; cells were treated at working concentrations in equal volumes of DMSO for 18 hours. Epoxomicin (Sigma Aldrich E3652) was prepared as a stock solution at 1mM in DMSO; cells were treated at working concentrations in equal volumes of DMSO for 18 hours.

Flow Cytometry

Cells were dislodged from the cell culture plate with TrypLE Express™ (Gibco) and resuspended in Phosphate Buffered Saline (Gibco) supplemented with 1%FBS. Cells were incubated with SYTOX® Red Dead Cell Stain (Invitrogen S34859) per the manufacturer's instructions. Measurements were taken at the University of Minnesota's Flow Core facility on an Accuri C6 Flow cytometer (BD Biosciences). Cells were gated for forward and side scatter, against positive SYTOX® staining, and measured for GFP fluorescence. All analysis was performed on FloJo v7.6 software.

Statistics

All statistical calculation were performed with JMP® statistics software. Data are presented as mean ± standard error of the mean in bar graphs. To determine significance for all data with three or more groups, one-way ANOVA analysis was performed with $\alpha=0.05$. Upon significance of the ANOVA, the Tukey post hoc test was performed with all pairs of data at $\alpha=0.05$.

Results

In order to understand the cellular consequences of missense mutations in dystrophin, stably-expressing transgenic mouse myoblast C2C12 cell lines were generated with the PiggyBac™ transposon system (Figure 3.1). Two disease-causing missense mutations were investigated: L54R representing severely affected Duchenne patients and L172H representing mildly affected Becker patients. In addition to a WT dystrophin transgenic line, a single nucleotide polymorphism (SNP) found in the population, I232M, was generated as a control. In the range of 3-5 clonal colonies were generated for each genotype and screened for equivalent levels of transposon integration.

The selected myoblast cell lines expressing full-length dystrophin were analyzed for genomic transgene levels by qPCR (Figure 3.2A). As expected the non-transgenic C2C12 line had no incorporation of transgene and each of the other lines showed similar levels. The L172H line was found to have statistically higher incorporation of transgene, approximately 2-fold that of the WT line. A 2-fold difference is small compared to the orders of magnitude range that was measured during the screening process for stable lines. It was determined that the myoblast lines generated were sufficient to act as a model of different missense mutations in dystrophin given that quantitation corrected for differences in apparent genome copy number. The transcript levels expressed from the transgenes were then measured by RT-qPCR (Figure 3.2B). As expected based on gDNA analysis, L172H and now I232M had statistically higher levels of

dystrophin mRNA.

Each cell line was then analyzed for full-length GFP-dystrophin fusion protein (455 kDa) by Western blot analysis (Figure 3.2C). It was observed that the two disease-causing mutations, L54R and L172H, showed decreased protein expression. Quantification of three separate lysates revealed both missense mutations significantly decreased the steady-state level of dystrophin while the SNP I232M increased it significantly. Due to the differences in transgene and transcript levels (Figure 3.2A&B) inherent to transgenic models, the protein levels were normalized relative to their respective transcript level (Figure 3.2E). The steady-state ratio of protein:mRNA for L54R was only 13% of WT protein and L172H expressed 46% of WT protein while I232M was comparable to WT. These data indicate that the severity of disease found in patients inversely correlates with the level of mutant dystrophin protein.

A benefit of utilizing the C2C12 myoblast cell line is its facile differentiation into myotubes. We wanted to determine whether differentiation into myotubes had any affect on the steady-state levels of the transgenic dystrophin due to increased presence of normal binding partners or any other myotube specific mechanism. Myoblast cells were switched to a low serum media and analyzed at days 0, 3, and 7 post-differentiation initiation. Transcript analysis of desmin, a marker of differentiation (Figure 3.3A), revealed an apparent increase from day 0 to day 7 for each of the lines analyzed. There was no difference in degree of differentiation between non-transgenic, WT, or mutant. Transcript analysis of the

GFP-dystrophin transgene (Figure 3.3B) showed there was no stabilization of the transcript upon differentiation for either WT or mutant dystrophin.

Western blot analysis of desmin protein (Figure 3.3C) confirmed the RT-qPCR analysis. Abundance of desmin protein (Figure 3.3D) increased from day 0 to day 7 for each of the cell lines analyzed. For both WT and L54R there were statistically significant increases in desmin protein from day 0 to day 7, indicating that a mutation in dystrophin apparently had no effect on the ability of the C2C12 cells line to differentiate. The GFP-dystrophin fusion protein was also measured by Western blot analysis (Figure 3.3C) and three separate differentiations quantified (Figure 3.3E). The WT dystrophin line saw an apparent increase in protein levels, but it was not statistically significant. Most importantly, despite a trend of increasing L54R transcript (Figure 3.3B) upon differentiation, there was no increase in protein (Figure 3.3E). These results indicate that the mutant protein was not stabilized upon differentiation of myoblasts into myotubes.

Given that previous studies have shown L54R and L172H are thermally unstable *in vitro* (Henderson et al. 2010, Chapter 2) and that there is less steady-state levels of protein with these mutations (Figure 3.2), we hypothesized that L54R and L172H mutant dystrophins are misfolded in C2C12 myoblasts. The heat shock system of the cell is known to up-regulate heat shock proteins in response to misfolded protein. Therefore we assessed by western blot analysis whether expression of mutant dystrophin caused an increase in heat shock protein expression (Figure 3.4A). Quantification revealed that there were few

significant increases of the various heat shock proteins in the lines expressing mutant dystrophin compared to WT dystrophin. (Figure 3.4B). There was a significant increase in Hsp40 and a significant decrease in phosphorylated Hsp27 measured in the L172H line. Given that L172H is the mutation associated with mild muscular dystrophy symptoms, the apparent changes are likely stochastic. Cell culture experiments in which the whole culture is actually shocked with heat show rapid and dramatic increases in the heat shock pathway proteins (Ashburner and Bonner, 1979), which is not unexpected given that a majority of the proteome is now misfolded. By comparison, only one protein out of the whole proteome is potentially misfolded in our cell line models, therefore it is not surprising that we did not see a large increase in heat shock protein levels. In fact the lack of up-regulation offers a possible avenue of therapeutics that could force up-regulation of the heat shock pathway and lead to stabilization of the dystrophin protein.

We screened three categories of small molecules with promise of increasing mutant dystrophin levels by various mechanisms. The first category of small molecules screened was osmolytes (Figure 3.5A), which are thought to populate the interior of the cell at high concentrations enhancing thermodynamic stability of proteins (Kumar, 2009; Arakawa et al., 2006). The osmolyte trehalose is commonly synthesized by bacteria and yeast under thermodynamic stress, has been found to alleviate symptoms in models of protein misfolding (Castillo et al., 2013; Tanaka et al., 2004), and is even sold in nutrition supplement stores.

When applied to the mutant L54R line at the highest concentration of 500mM cells did not survive. At lower concentrations there was no apparent increase in dystrophin protein levels. Another osmolyte, TMAO [Trimethylamine N-oxide], is found in salt water animals such as sharks and rays to stabilize proteins against the osmotic pressure (Yancey et al., 1982) and was applied to the mutant dystrophin cell line. Like trehalose, very high concentrations killed the cells and lower concentrations had no effect on protein levels. Lastly betaine was screened for effect; betaine is an osmolyte found in the kidney of mammals (Burg, 1995). At the highest dose of 400mM there was a visible increase in mutant dystrophin protein, which is a proof of principle result that osmolytes can stabilize full-length dystrophin protein. The extremely high doses required, however, make this a null option for therapeutic treatment.

The second class of small molecules screened was the heat shock activators (Figure 3.5B). The first compound, celastrol, is a natural product isolated from the plant family Celastraceae which activates the conserved heat shock factor 1 (HSF1) which in turn transcribes several downstream components of the heat shock pathway (Trott et al., 2008; Westerheide et al., 2004). At tolerated doses up to 1μM there was no increase in mutant dystrophin protein. Another heat shock activator, BGP-15, specifically induces one of the heat shock proteins, HSP72, and has been shown to alleviate symptoms in models of both diabetes and muscular dystrophy (Chung et al., 2008; Gehrig et al., 2012). Unfortunately we saw no direct molecular effect on dystrophin protein levels at

tolerated doses up to 50μM. The third heat shock activator screened was gedunin, a product isolated from the tree species *Azadirachta indica* which binds to and inhibits Hsp90 thereby releasing bound HSF1 for transcriptional activity (Brandt et al., 2008; Neef et al., 2011). Concentrations between 10 and 80μM were found to have a dose-response relationship with dystrophin protein. These data indicate that it is possible to pharmacologically activate the heat shock system of the cell which then facilitates the chaperone-mediated stabilization of mutant dystrophin.

Lastly proteasome inhibitors were screened in an attempt to find more small molecules that can increase the levels of mutant dystrophin protein (Figure 3.5C). Both the classic proteasome inhibitor MG132 and its derivative MG262 had a robust effect on the mutant dystrophin in a dose-response relationship, indicating that 1) the proteasome is at least one of the mechanisms by which mutant dystrophin is degraded in the cell and 2) proteasome inhibitors are a viable option for molecular correction of Duchenne muscular dystrophy caused by missense mutations. Several proteasome inhibitors are currently in clinical trials for treatment of multiple myeloma including bortezomib and derivatives of epoxomycin both of which we also screened. Bortezomib is a member of the boronic acid class of proteasome inhibitors and inhibits the chymotrypsin-like site of the proteasome (Kisselev et al., 2012). Recently, a study demonstrated its *in vivo* ability to increase levels of missense mutated dysferlin (Azakir et al., 2014). Bortezomib showed a strong dose-response effect on missense mutated

dystrophin as well (Figure 3.4C). Epoxomycin is an epoxyketone and also targets the chymotrypsin-like site of the proteasome (Kisselev et al., 2012); its derivative, carfilzomib, is currently in clinical trials for multiple types of cancers. Epoxomycin also had a robust effect on the level of dystrophin protein in our cell culture model.

To investigate further the effects of three positive hits from the screen (gedunin, bortezomib, and epoxomicin), both L54R and L172H cells were treated in parallel with each of the small molecules at a submaximal dose determined in the screen (Figure 3.6). Western blot analysis of the full-length GFP-dystrophin fusion protein (Figure 3.6A) shows marked increases in the L54R for all three small molecules. The line L172H without treatment has a higher level of mutant dystrophin protein, yet an increase is still visible for both bortezomib and epoxomicin. When the proteasome is inhibited there is an accumulation of ubiquitinated proteins that are being targeted to the proteasome for degradation, therefore we blotted for ubiquitin in each of the small molecule treatments (Figure 3.6A bottom panel). Not surprisingly the two proteasome inhibitors show a large increase in ubiquitination across the proteome. The heat shock activator gedunin had a similar effect on ubiquitination in the cell, emphasizing the close connection between the heat shock pathway and the ubiquitin-proteasome pathway, and corroborating previous studies that have found Hsp90 inhibition increases the ubiquitination state of the proteome (Basak et al., 2008).

The transgenic myoblast models were designed with a GFP-dystrophin

fusion construct in the anticipation that they will be used in the future for high-throughput screens, monitoring GFP fluorescence by flow cytometry. The functionality of this approach was validated (Figure 3.6B). The non-transgenic C2C12 cells were used as a negative control to gate for positive GFP fluorescence. The WT Dystrophin cell line showed a positive population shift for GFP fluorescence compared to non-transgenic cells which correlates with the Western blot analysis in Figure 3.2C. It is important to note that the fluorescent signal is much lower than that seen in cells expressing GFP alone; GFP fused to a 427 kDa protein gives a low yet still detectable signal. The two missense lines were then treated with submaximal doses of the three effective small molecules and GFP fluorescence measured by flow cytometry. As expected the L54R cell line when untreated had very low fluorescent signals with only 2.39% of cells above the threshold of detectable signal relative to non-transgenic. Upon treatment with gedunin, bortezomib, or epoxomicin 86.6%, 91.2%, and 82.9% of cells had positive GFP signal respectively, again corresponding to Western blot results (Figure 3.5 and Figure 3.6A). The L172H line without treatment had approximately the same percentage of positive GFP cells (28.8%) as the WT, but with a lower average intensity. Upon treatment with the three small molecules, cells positive for the GFP-dystrophin protein increased to 80.7%, 95.6%, and 84.2%. Figure 3.6C shows the same data in a histogram of percent maximal signal for each treatment group. It is clear that each of the three small molecule treatments detectably increases GFP fluorescent signal. These results both

confirm the findings by western blot analysis and validate flow cytometry as a method for high throughput screening of these cell models.

In addition to monitoring the ubiquitination state of the cell after treatment with the three small molecules, we wanted to see their effect on the heat shock pathway of the cells (Figure 3.7). Both the L54R and L172H cell lines were treated with submaximal doses of gedunin, bortezomib, and epoxomicin and then blotted for the same heat shock proteins as in Figure 3.4. There were significant increases in the heat shock proteins Hsp70, Hsp90P, and Hsp27P compared to the untreated control cells. An increase in HSPs would be expected from both the heat shock activator, gedunin, and the proteasome inhibitors given that when the proteasome is no longer functioning, there will be more misfolded protein present in the cell and therefore it is likely to see an increase in the heat shock pathway. The largest increases in the heat shock proteins were seen with the small molecule epoxomicin likely because it was simply the most potent of the three at their respective given dosages.

Discussion

We report here the generation of a myoblast cell culture model stably expressing full-length dystrophin protein variants of WT, L54R, L172H, and I232M. The missense mutation associated with the severe symptoms of Duchenne Muscular Dystrophy, L54R, had steady-state levels of dystrophin protein at less than 10% of WT levels; while the missense mutation associated with the mild symptoms of Becker Muscular Dystrophy, L172H, expressed at approximately 40% of WT. The data suggest that the severity of disease is inversely correlated with the level of dystrophin protein in the cell.

In Chapter 2 and in a previous publication (Henderson et al., 2010) we demonstrated that these mutations cause thermal instability of dystrophin protein. It is now apparent that this instability *in vitro* leads to a degradation of the protein by the proteasome in the cellular environment. Proteins are targeted to the proteasome for different reasons: either they have served their function and now need to be removed such as the cyclins during the cell cycle, or they are misfolded beyond the repair of the heat shock pathway. For a given WT protein, it is estimated that up to 30% of the translated protein is sent to the proteasome due to lack of native folding (Wang et al., 2013). When a protein is mutated, however, that percentage increases to a point that causes an insufficiency in the cell. Our two candidate mutations have shown that the more destabilizing the amino acid change, the more misfolding and degradation there will be for the dystrophin protein and consequently more severe symptoms in patients.

In our proof-of-concept screen to increase the levels of dystrophin there was at least one positive hit from each of the three categories: osmolytes, heat shock activators, and proteasome inhibitors. The osmolyte betaine was able to increase mutant dystrophin protein at very high concentrations. It is not surprising that the one osmolyte that is naturally found in mammals was the only one to have effect, but the extreme dosage that would be required makes any type of potential therapy with this small molecule less feasible. The heat shock activator gedunin had a positive effect on dystrophin protein levels at moderate concentrations. Even though it did not inhibit the proteasome, it still increased levels of ubiquitination in the cell, which further speaks to how closely related the heat shock pathway and the ubiquitin proteasome system are. The efficacy of gedunin supports that heat shock activators may be useful to treat DMD patients with missense mutations and a broader screen may identify heat shock activators that are effective at lower doses that may be better tolerated by patients.

When the L54R line was treated with any one of a number of proteasome inhibitors, protein levels were restored to WT levels indicating that the majority of the mutant protein is being degraded by the proteasome, differentiating it from mutations that cause aggregation of proteins like those found in Alzheimer's and Huntington's. In protein degradation diseases there is often a gain-of-function toxic effect caused by the aggregates and therefore treatment is two-fold: removing the aggregate and replacing with a functional protein. The L54R and L172H mutant dystrophins expressed in myoblasts are degraded by the

proteasome and therefore treatment is potentially one-fold: stop the degradation of the mutant protein. Further work will be needed to determine if the protein inhibited from being degraded is fully or partially functional, as the functionality of dystrophin is not measurable in a cell culture system.

In summary, our new C2C12 cell models suggest the molecular mechanism of decreased dystrophin expression in patients with two different missense mutations. In addition, we have generated an efficient model system for large scale screens of other small molecule libraries as well as siRNA knock-down libraries.

Figures

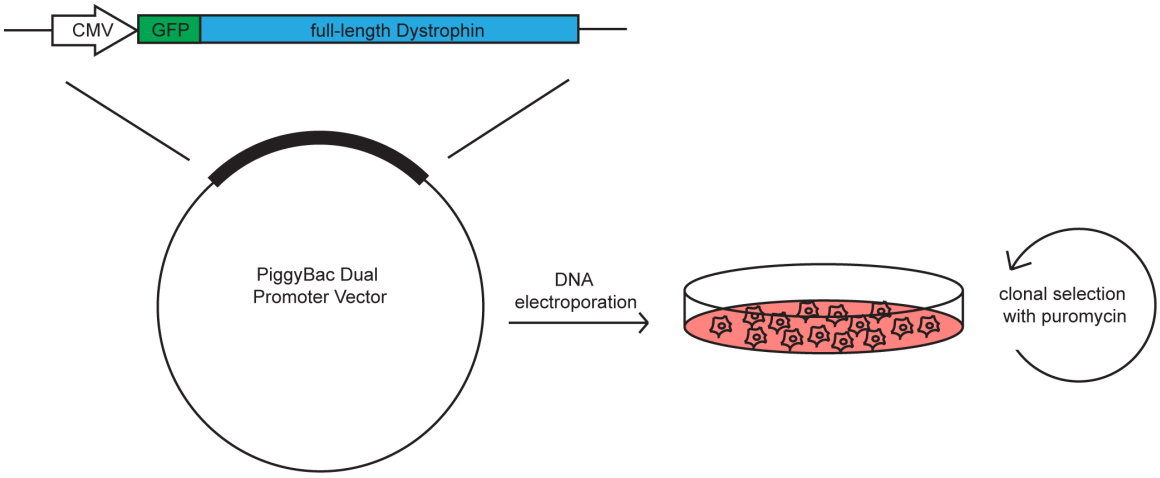

Figure 3.1: Expression construct and experimental concept

Full-length, mouse dystrophin cDNA was subcloned with an N-terminal GFP protein under a CMV promoter. This expression cassette was a part of the PiggyBac vector which also expressed a puromycin resistance gene under a EF1α promoter. The PiggyBac transposon vector with dystrophin insert was co-transfected with the PiggyBac transposase vector by electroporation into C2C12 cells. After 48 hours, cells were selected for transposon insertion into the genome with puromycin. Clonal lines were screened for similar levels of transgene incorporation.

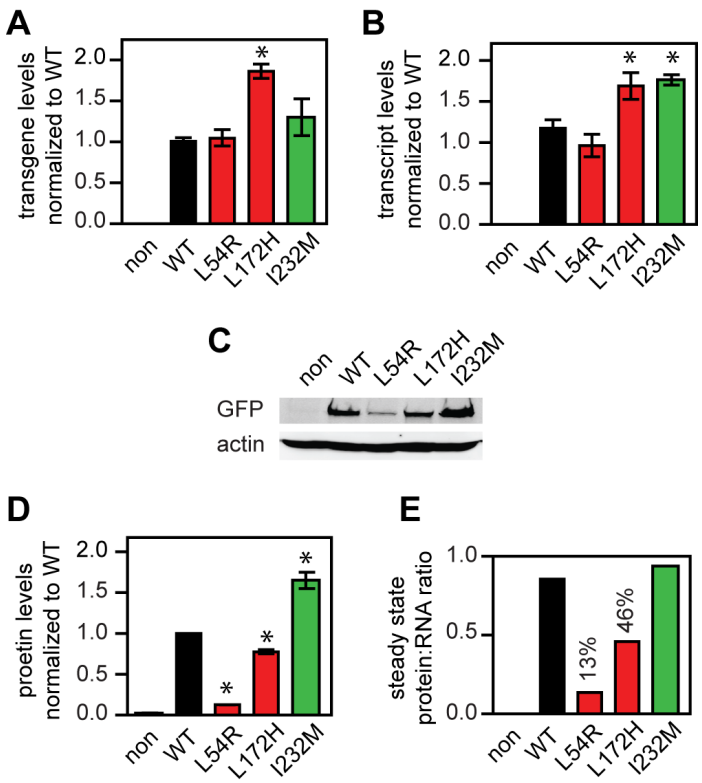

Figure 3.2: Expression levels of transgenic dystrophin in myoblast cell lines. (A) qPCR analysis of genomic DNA. Sequence amplified within CMV promoter to measure degree of transgene insertion into genome. n=3 separate sample collections and gDNA isolations. Measurements relative to reference gene ADH and normalized to a WT sample. ANOVA $F<0.0001$, $*p<0.05$ compared to WT. **(B)** RT-qPCR of total RNA. Sequence amplified within GFP sequence to measure levels of transgenic transcript. n=3 separate sample collection, RNA isolation, and reverse transcription. Measurements relative to reference transcript Hprt and normalized to a WT sample. ANOVA $F<0.0001$, $*p<0.05$ compared to WT. **(C)** Representative Western blot of cell lysate. Blot was probed with GFP primary antibodies to detect the transgenic GFP-Dystrophin fusion protein (455 kDa). **(D)** Quantification of n=3 separate cell lyses and Western blot analyses. Measurements normalized to WT sample on each blot. ANOVA $F<0.0001$, $*p<0.05$ compared to WT. **(E)** The ratio of the normalized protein levels to the normalized transcript levels.

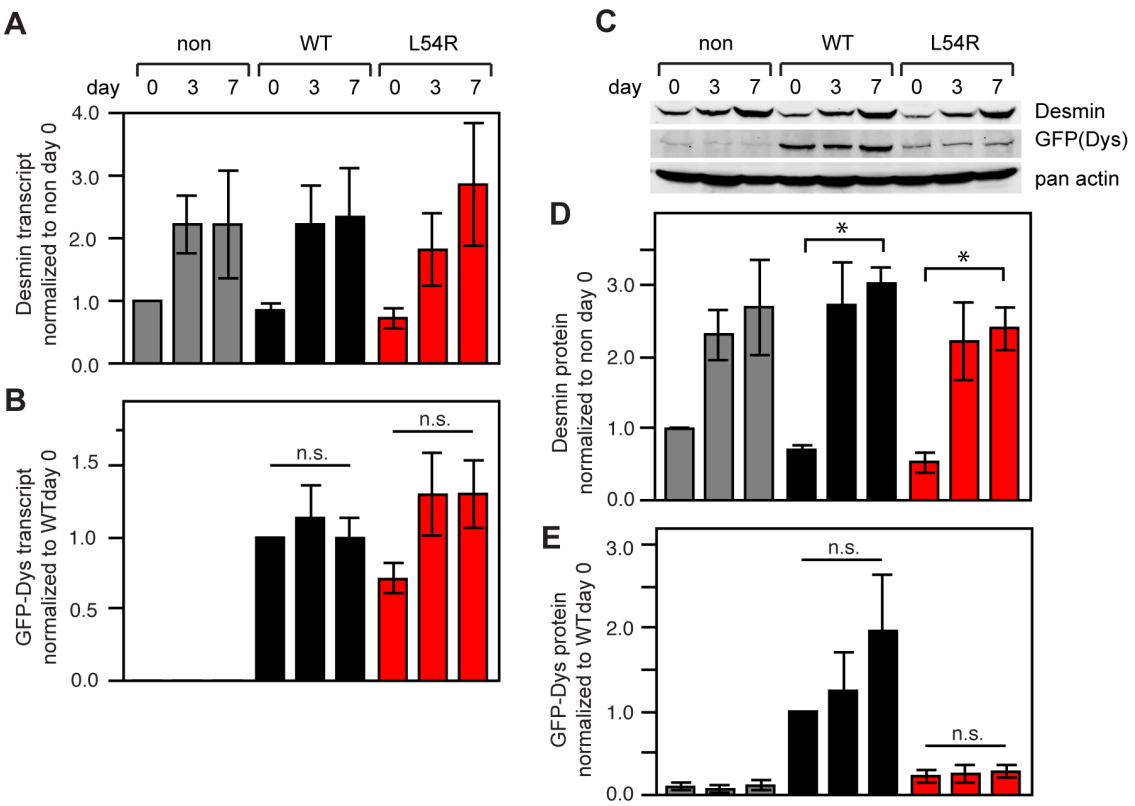

Figure 3.3: Differentiation of stable transgenic cell lines. (A&B) RT-qPCR analysis of cell lines differentiated for 0, 3, and 7 days in reduced-serum media. All measurements are relative to reference transcript Hprt. n=3 separate sets of differentiation, RNA isolation, reverse transcription, and analysis. **(A)** Desmin measurements were normalized to the non-transgenic C2C12 line, day 0. No significant differences by ANOVA. **(B)** Transgenic dystrophin measurements were normalized to the WT line, day 0. ANOVA $F<0.0001$, WT and L54R statistically different than all non-trangenic samples. not significant within one sample type. **(C-E)** Western blot analysis of cell lines differentiated for 0, 3, and 7 days. n=3 separate sets of differentiation, cell lysis, and Western blot analysis. **(C)** Representative western blots of desmin and transgenic dystrophin expression. **(D)** Quantification of n=3 for Desmin protein. ANOVA $F<0.001$, $p<0.05$. **(E)** Quantification of n=3 for GFP-Dystrophin protein. ANOVA $F<0.001$, WT and L54R statistically different than all non-transgenic samples. n.s.= not significant within one sample type.

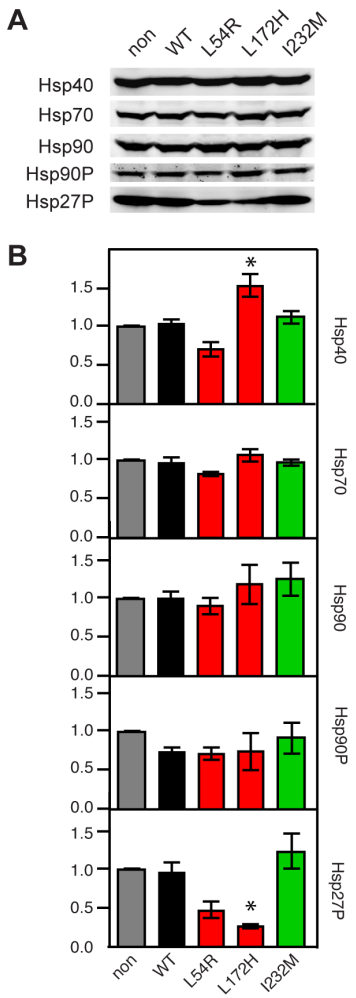

Figure 3.4: Effect of missense mutations on heat shock pathway in cells. **(A)** Representative western blots for heat shock proteins in the 5 cell lines. **(B)** Quantification of n=3 separate cell lysis and Western blot analysis, all values normalized to non-transgenic sample. For Hsp70, Hsp90, and Hsp90P, ANOVA was not significant. For Hsp40, ANOVA $F<0.01$, $*p<0.05$ compared to WT. For Hsp27P, ANOVA $F<0.01$, $*p<0.05$ compared to WT.

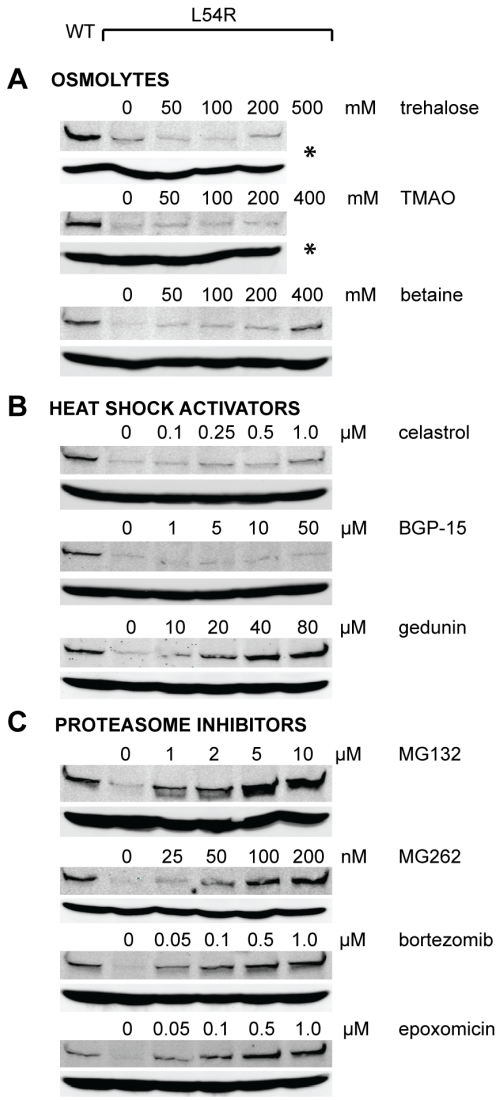

Figure 3.5: Small molecule therapeutics screen to increase dystrophin protein levels **(A)** Western blot analysis of osmolyte dosage treatments. Cells were treated with varying concentrations of a given osmolyte (all in equal volumes of vehicle) for 24 hours. Lysates were separated by electrophoresis and blotted with GFP antibody to detect the GFP-dystrophin fusion protein. C4 antibody to detect pan actin was used as a loading control. * These cells did not survive the given dosage. **(B)** Western blot analysis of 18-hour heat shock activator dosage treatments. Blots generated the same as A. **(C)** Western blot analysis of 18-hour proteasome inhibitor dosage treatments. Blots generated the same as A.

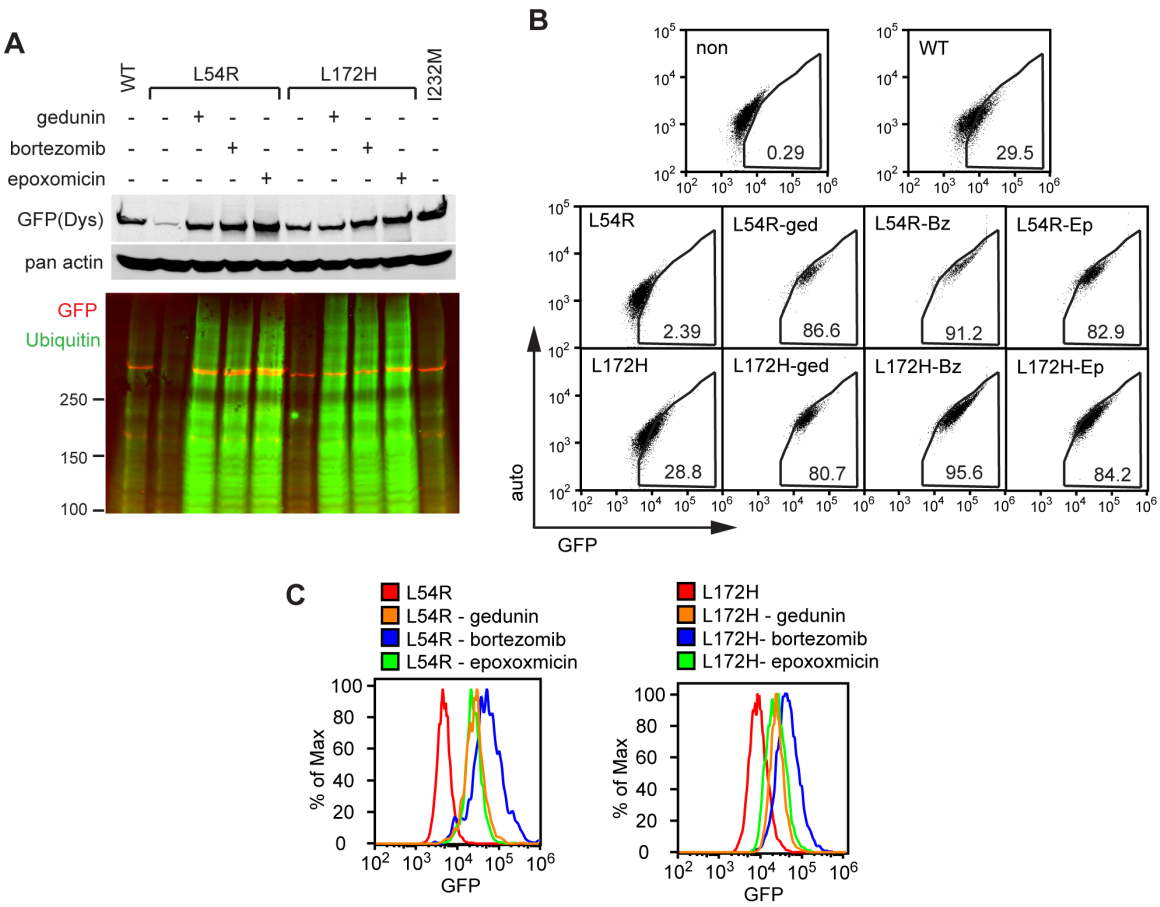

Figure 3.6: Effect of positive hits from therapeutics screen on total dystrophin protein levels and ubiquitination **(A)** Cells were treated with 40μM gedunin, 0.5μM bortezomib, or 0.5μM epoxomicin for 18 hours. Cell lysates were separated by electrophoresis and blotted with GFP to detect the fusion protein, C4 to detect actin as a control, or ubiquitin antibody. **(B)** Flow Cytometry of live cells. Cells were removed from culture and resuspended in PBS. Cells were analyzed for GFP fluorescence while gated for forward and side scatter, and dead cells with the dye Sytox Red. Fluorescence levels of GFP were measured versus auto-fluorescence. Percentages represent the number of cells that had GFP signal above negative control. **(C)** Flow Cytometry data in B displayed as histograms plots of the percentage of maximum cells with a given GFP fluorescent signal.

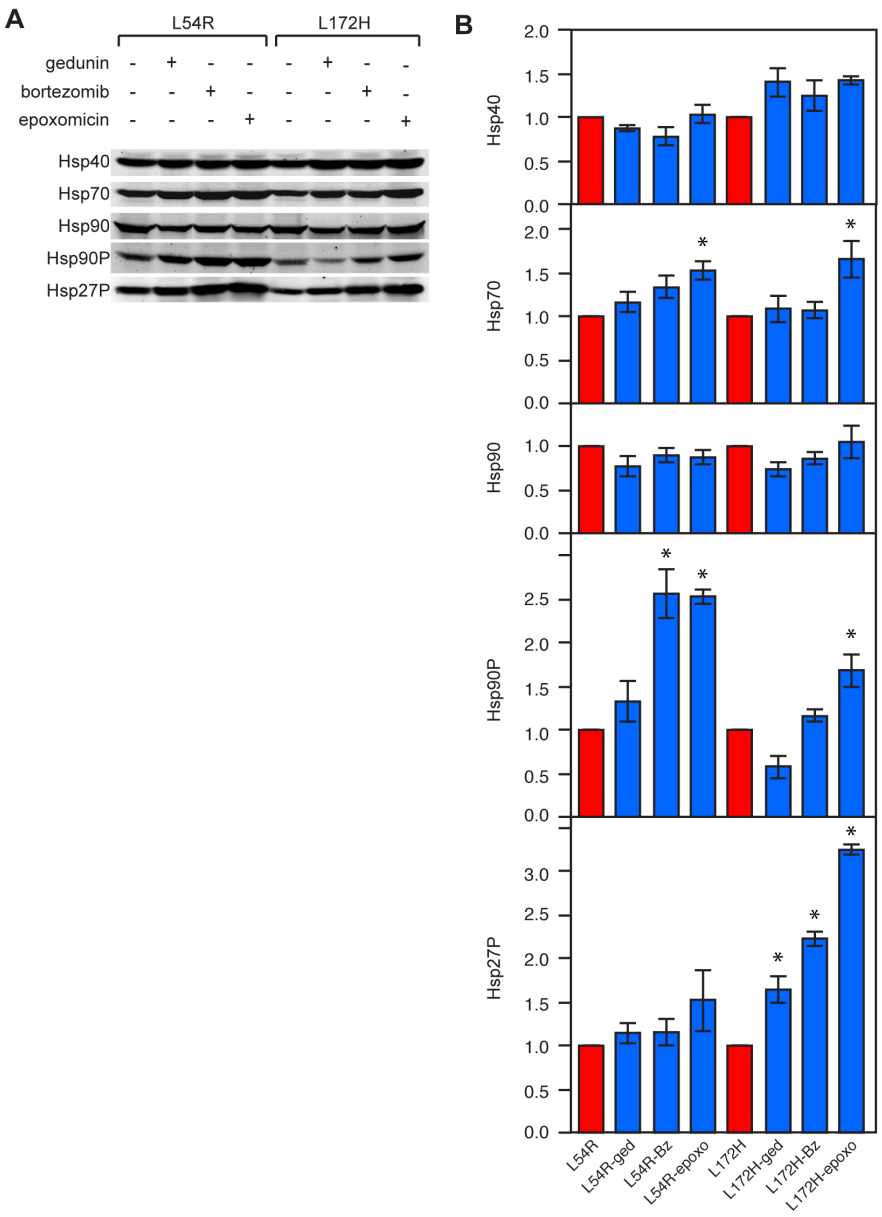

Figure 3.7: Effect of positive hits from therapeutic screen on the heat shock pathway. (A) Cells were treated with 40μM gedunin, 0.5μM bortezomib, or 0.5μM epoxomicin for 18 hours. Lysates were analyzed by Western blot analysis for heat shock proteins. **(B)** Quantification of n=3 separate treatments, cell lysis, and western blot analysis represented in A. Hsp40 and Hsp90 for both L54R and L172H, and Hsp27P for L54R, ANOVA was not significant. For all other measurements, ANOVA $F<0.05$, ∗ $p<0.05$ compared to untreated control.

Chapter 4

A Mouse Model of Missense Mutations in Dystrophin

Immunofluorescent microscopy was performed by John Olthoff. Physiology assays for grip strength, whole body tension, activity after exercise, and serum CK activity were performed by Paul Chatterton while he was blinded to genotype. Eccentric contraction analysis was performed collaboratively with Dawn Lowe. All other cloning, mouse-line development, and analyses were performed by Dana Talsness.

Summary

Mutations in the *DMD* gene encoding for the protein dystrophin lead to Duchenne and Becker muscular dystrophy. Several cases are reportedly caused by a missense mutation, which leads to a single amino acid substitution in the 427 kDa dystrophin protein. Two candidate missense mutations in the amino terminal first actin binding domain represent the spectrum of phenotypic severity seen in patients: L54R was found in a patient with the severe symptoms of Duchenne and L172H in a patient with the mild symptoms of Becker. When previously studied *in vitro*, each mutation caused thermal instability of the full-length protein. Here we report the generation of two transgenic mouse models expressing full-length dystrophin with L54R or L172H mutations on a dystrophin-null background. Mutant protein levels were found to inversely correlate with the severity of disease first reported in the represented patients. Histological analyses indicate that the L54R transgenic mouse line is just as severely affected as the dystrophin-null, while L172H has a more mild phenotype. Physiological analyses indicate that both transgenic lines display symptoms of muscular dystrophy. Together, the new mouse models of missense mutations in dystrophin indicate the major cause of disease is the decreased abundance of dystrophin protein and will serve for future studies of therapeutics targeted towards missense genotypes.

Introduction

The most widely used animal model of Duchenne Muscular Dystrophy is the *mdx* mouse, a naturally occurring model due to a spontaneous mutation that was first discovered in a colony of C57BL/10 mice (Bulfield, 1984). The *mdx* mouse presented with increased serum kinase levels and the phenotype segregated with the X-chromosome in a recessive manner. Shortly thereafter it was discovered that the *mdx* mouse lacked the dystrophin protein seen in WT mice (Hoffman et al., 1987b) and had reduced levels of full-length dystrophin mRNA (Chamberlain et al., 1988). These two molecular symptoms were very quickly ascribed to a nonsense mutation in exon 23 of the DMD gene (Sicinski et al., 1989), which definitively proved the *mdx* mouse was a genetic model for Duchenne Muscular Dystrophy.

The *mdx* mouse has been well characterized since its discovery. In the same study that discovered the proteins of the dystrophin-glycoprotein complex (DGC) it was shown that they were decreased in the *mdx* mouse (Ervasti et al., 1990). Histological analyses have revealed smaller fiber size and increased central nucleation at 7 weeks of age compared to WT (Briguet et al., 2004), caused by the necrosis and then regeneration of muscle fibers (McGeachie et al., 1993). Physiological analyses show that *mdx* mice have mild symptoms compared to human DMD patients, but are distinguishable from WT mice for the parameters of forelimb grip strength, whole body tension, and force drop after eccentric contractions (Connolly et al., 2001; Carlson and Makiejus, 1990; Moens

et al., 1993), and these symptoms are ameliorated when dystrophin is transgenically over-expressed (Cox et al., 1993). There are several hypotheses for their mild phenotype including up-regulation of the autosomal homolog utrophin, longer chromosome telomeres for increased regenerative capacity, and the simple fact that mice are quadrupedal and therefore less stress is put on limb muscles. Despite its mild pathophysiology, the *mdx* mouse is a perfect genetic model of DMD patients with nonsense mutations; it has served and will continue to serve as a valuable tool for muscular dystrophy research.

A naturally occurring mutation that segregated with the X-chromosome was also found in a golden retriever dog that lacked protein expression of dystrophin (Cooper et al., 1988). The causative mutation was later found to be a single nucleotide change in the 3' splice site of intron 6 which results in out-of-frame exclusion of exon 7 (Sharp et al., 1992). The dogs are visibly dystrophic with abnormality of gait at nine to twelve weeks of age and moderate kyphosis by 6 months of age (Valentine et al., 1988). They develop muscle atrophy and subsequently have elevated serum CK levels. The muscles of the GRMD dog are weaker and more susceptible to contraction-induced injury than a WT dog (Nguyen et al., 2002). Overall the pathophysiology of the dogs more closely model the human DMD patients including decreased lifespan often as a result of cardiac or respiratory failure (reviewed in Kornegay et al. 2012). While the GRMD dog more closely models human patients with loss-of-protein mutations in dystrophin there are obvious drawbacks such as the relative cost of housing a

large animal with a longer lifespan.

Just within the last year the first animal model with a missense mutation in dystrophin was reported (Hollinger et al., 2013). A line of pigs was discovered in Iowa that had a point mutation in exon 41 resulting in a full-length dystrophin protein with the amino acid change R1958W. Phenotypically the R1958W pigs appear to most closely model mildly-affected BMD patients. Western blot analysis revealed that dystrophin protein was expressed at only 30% of WT levels in diaphragm, psoas, and longissimus muscles, but localized correctly to the plasma membrane as assessed by immunofluorescent staining. There was also decreased abundance of several DGC protein components consistent with DMD in humans. Histologically there were necrotic lesions in the muscle and serum CK levels were 5-fold that of WT littermate controls. While the R1958W pig will likely be a valuable tool in muscular dystrophy research and therapy development, there currently is no animal model that harbors a missense mutation specifically seen in any patients with Duchenne or Becker muscular dystrophy.

Here we report on the generation of two new mouse models expressing missense mutant dystrophins. One mouse represents a severely affected DMD patient with mutation L54R while the other represents a more mildly affected patient with mutation L172H. Molecular analysis of the two lines revealed that disease severity correlates with decreased levels of dystrophin protein which, corroborates results obtained with C2C12 cell lines modeling the same mutations

(Chapter 3). Histological and physiological analyses further support the use of these two mouse lines as models of patients with Duchenne and Becker muscular dystrophy.

Materials and Methods

Cloning and mouse generation

Full-length mouse dystrophin cDNA (with missense mutations L54R and L172H) was subcloned into the Gateway system Entry vector as described in Chapter 2. The cDNA was then recombined into a vector containing the human skeletal alpha-actin (HSA) promoter and Vp1 intron that had been adapted to the Gateway system. The expression cassette was cut out of the vector with restriction enzymes and sent to the University of Cincinnati Transgenic Mouse Core (L54R) or The Scripps Research Institute Mouse Genetics Core (L172H) for pronuclear injection into fertilized eggs. Injected eggs were transplanted into pseudopregnant mice. Progeny were screened for the transgene by genomic PCR. Transgenic mice were crossed onto the *mdx* background (mL54R and mL172H), and transgenic male progeny were analyzed. All analyses were performed on mice 10-14 weeks of age.

RT-qPCR

Tissue was pulverized with mortar and pestle in liquid nitrogen. RNA was isolated with the Aurum Total RNA Fatty and Fibrous Tissue (BioRad 732-6870). Total RNA was reverse transcribed into cDNA using the iScript™ Advanced cDNA Synthesis Kit (Biorad 170-8843). cDNA was amplified using SsoAdvanced™ Universal SYBR® Green Supermix (Biorad 172-5270). Primers for endogenous mouse dystrophin: Forward [TGGCAGATGATTTGGGCAGA] and Reverse [CCATGCGGGAATCAGGAGTT]. Primers for transgenic mouse

dystrophin: Forward [ACAATGTAGAAGGGTGGGCG] and Reverse [GCGTAGAATCGAGACGCGAGG]. Primers for intragenic mouse dystrophin: Forward [GCGCCAACACAAAGGACGCC] and Reverse [GCTTCAGCCTGGGGCTGCTC]. All measurements were relative to reference transcript Hprt: Forward [CCCTGGTTAAGCAGTACAGCCCC] and Reverse [GGCCTGTATCCAACACTTCGAGAGG]. Measurements were collected with the C1000 Touch Thermal Cycler (Biorad) and analyzed with the CFX Manager software (Biorad).

Western blot analysis

Tissue was pulverized with mortar and pestle in liquid nitrogen. Tissue was then lysed with 1% SDS solution with added protease inhibitors [100nM Aprotonin, 10mg/ml E-64, 100μM Leupeptin, 1mM PMSF, 1μg/ml Pepstatin] proportional to mass of the tissue pellet. Protein concentration was measured by A_{280} absorbance. Equal concentrations of lysate were then separated by electrophoresed at 150V for 1 hour, then transferred to PVDF membrane at 100V/0.7Amp for 1 hour. Membranes were blocked in either [5% non-fat milk in phosphate buffered saline 0.1% Tween solution] or [5% Bovine Serum Albumin in tris buffered saline 0.1% Tween solution] depending on the primary antibody for 1 hour. Primary antibodies used were anti-Dys1 (Leica) at 1:100, anti-Dys2 (Leica) at 1:100, anti-utrophin (Santa Cruz 8A4) at 1:100, anti-α-dystroglycan (Millipore 05-593) at 1:1000, anti-β-dystroglycan (vector labs VP-B205) at 1:100, anti-dystrobrevin (BD labs 610766) at 1:1000, anti-syntrophin (abcam 11425) at

1:1000, anti-pan actin C4 (Seven Hills Bioreagent LMAB-C4) at 1:5000, anti-Desmin D93F5 (Cell Signaling 5332) at 1:1000, anti-Hsp40 C64B4 (Cell Signaling 4871) at 1:1000, anti-Hsp70 (Cell Signaling 4872) at 1:1000, anti-Hsp90 (abcam 19021) at 1:1000, anti-Phosph-Hsp90α (Cell Signaling 3488) at 1:1000, anti-Phospho-Hsp27 (Cell Signaling 9709) at 1:1000, and anti-Ubiquitin P4D1 (Cell Signaling 3936) at 1:1000. Blots were then incubated in secondary antibodies anti-mouse or anti-rabbit IgG Dylight® 800 (Cell Signaling) at 1:10,000 in blocking buffer. Secondary antibody signal was visualized on Licor's Odyssey® Infrared Imaging System and band density calculated with Odyssey Software v2.1.

Immunofluorescent analysis

Quadriceps and gastrocnemius muscles were dissected, frozen in melting isopentane, and embedded in optimum cutting temperature (OCT) compound submerged in liquid nitrogen. Transverse sections of 10 μm were cut on a Leica CM3050 cryostat, air dried, and then fixed in 4% paraformaldehyde for 10 minutes. Sections were washed with PBS (150mM NaCl, 8 mM NaH_2PO_4, 42 mM Na_2HPO_4) before being blocked with 5% goat serum/0.1% Triton X-100 for 30 minutes. A secondary block in Rodent Block M (Biocare Medical) was also performed for 30 minutes. The sections were then incubated with primary antibodies overnight at 4°C. Primary antibody dilutions were: NCL-Dys1 (1:20) (Leica), NCL-Dys2 (1:20) (Leica), Rb2 (1:20), Utrophin (1:50) (Santa Cruz), α-Dystroglycan (1:50) (Millipore), β-Dystroglycan (1:50) (Vector Labs), Dystrobrevin

(BD Biosciences), nNOS (1:50) (Invitrogen), and Laminin (1:1000) (Sigma). Sections were then washed with PBS and incubated with Alexa Fluor 488- or Alexa Fluor 568-conjugated secondary antibodies (1:500 dilutions) for 30 minutes at 37°C. Sections were washed with PBS and coverslips were applied with a drop of Prolong Gold antifade reagent with DAPI (Molecular Probes). Images were collected on a Deltavision PersonalDV microscope equipped with a 20x/0,75 objective (Applied Precision) and viewed with GIMP (GNU Image Manipulation Program) software.

Histology and CNF count

Cryosections were cut from the same blocks prepared for immunofluorescence at 10μm thickness. Sections were stained with hematoxylin and eosin-phloxine and imaged on Leica DM5500 microscope at 200x total magnification. A total of at least 250 fibers were imaged from each muscle of each mouse and then centrally nucleated fibers (CNF) counted as a percentage of the total.

Serum CK analysis

Serum samples of the mice were collected by cheek bleed. The samples were diluted 1:20 and then serum creatine kinase (CK) activity analyzed using CK DT slides (Ortho-Clinical Diagnostics) and a Kodak Ektachem DT 60 Analyzer. CK activity is reported as U/L.

Forelimb grip strength

Mice were gripped at the base of their tail and positioned to grab the DFE series digital force gauge (Chatillon) with grip bar attachment. Once the mouse was

gripping the bar with both hands, the mouse was slowly with consistent force pulled perpendicularly away from the grip bar. Five trails were run per mouse and the average force was calculated.

Whole body tension

Mice were placed between parallel barriers, allowing only for forward movement. A slipknot suture was used to attach the base of the mouse tail to a fixed range force transducer (BioaPac Systems). The tail of the mouse was then lightly pinched and the subsequent force evoked was measured. Five minute traces were collected and the top 5 peaks were averaged for each mouse and then normalized to body weight. Protocol adapted from (Carlson and Makiejus, 1990).

Activity after exercise

Mice were acclimatized to the treadmill for 3 consecutive days, for 5 minutes at 0m/min followed by 5 minutes at 9m/min at 0° decline. On the fourth day, baseline pre-exercise activity was assessed for 30 minutes using laser-sensor activity cages (AccuScan Instruments Inc.). Mice were then acclimatized to the treadmill for 5 minutes at 0m/min at 15° decline. Without the use of electrical shock, mice were then encouraged to walk on the treadmill for 5 min at 5m/min followed by 10 minutes at 15m/min. After exercise, activity was measured for 30 minutes. Total number of vertical episodes were counted and post-exercise activity reported as a percentage of the pre-exercise activity.

Eccentric contraction analysis

Mice were anesthetized with sodium pentobarbitoal and the extensor digitorum

longus (EDL) muscle dissected out. Silk suture was used to attach the proximal tendon to a static structure and the distal tendon to a force transducer (Model 300B-LR, Aurora Scientific). The EDL was suspended in Ringer's solution [120.5mM NaCl, 4.8mM KCl, 1.2mM $MgSO_4$ 1.2mM Na_2HPO_4, 20.4mM $NaHCO_3$, 10mM glucose, 10mM pyruvate, 1.5mM $CaCl_2$], while 95% O_2/5% CO_2 was bubbled in. Muscles were lengthened to an optimal tension and this set as the optimal length (L_0). Maximal twitch and tetanus were measured. Then EDL muscle was subjected to an eccentric contraction protocol consisting of 5 maximal tetanic stimulations (5.7ms pulses at 150Hz for 200 ms) while stretching from 95% to 105% of the L_0 at 0.5 lengths per second. Three minutes recovery was allowed between each eccentric contraction and maximum force recorded. Force production was plotted as percentage of the first contraction.

Statistics

All statistical calculation were performed with JMP® statistics software. Data are presented as mean ± standard error of the mean. To determine significance for all data with three or more groups, one-way ANOVA analysis was performed with $\alpha=0.05$. Upon significance of the ANOVA, the Tukey post hoc test was performed with all pairs of data at $\alpha=0.05$.

Results

Transgenes were engineered harboring either L54R or L172H mutations in full-length dystrophin under the human skeletal α-actin (HSA) promoter which expresses almost exclusively in skeletal muscle. These constructs were used to generate transgenic mice on a C57BL/6 background (Figure 4.1). Transgenic L54R or L172H mice were crossed onto the *mdx* dystrophin-null mouse line to generate mice that expressed only mutant dystrophin (mL54R and mL172H).

Tibialis anterior (T.A.), gastrocnemius, and heart were analyzed by RT-qPCR (Figure 4.2A,B). Amplification of endogenous dystrophin transcript (top panel) reveals that *mdx* and transgenic lines on the *mdx* background have decreased levels due to nonsense mediated decay similar to prior reports. As expected for transgenes driven by the HSA promoter, robust expression of mutant transcripts in both transgenic lines was only detected in skeletal muscle (middle panel). Amplification of an intragenic region of dystrophin transcript (bottom panel) detected both endogenous and transgenic dystrophin for a side-by-side comparison. Statistical analyses show that both of the transgenic lines express dystrophin transcript at a level that is similar to WT mice. Quantitative western blot analysis of skeletal muscle revealed that L54R and L172H mice expressed significantly less dystrophin compared to WT (Figure 4.2C-F). mL54R mice expressed dystrophin protein at 7-9% that of WT and mL172H mice at 44%, both of which are statistically different from WT, correspond very closely to values from the transgenic myoblast lines in Chapter 3, and most importantly are

inversely correlated with disease severity of the patients with these mutations.

Mouse lines mL54R and mL172H were then analyzed for quantity of several components of the dystrophin glycoprotein complex (DGC) compared to WT and *mdx* mice (Figure 4.3A,B). Dys1 and Dys2 antibodies, with affinity to the central rod domain and C-terminus of dystrophin respectively, showed similar results and corroborate data in Figure 4.2. Quantitiation reveals that utrophin levels in *mdx* were approximately 2-fold that of WT consistent with previous findings, and utrophin in the transgenic lines is similarly elevated. The DGC components α-dystroglycan, β-dystroglycan, dystrobrevin, and nNOS, were significantly decreased in *mdx*, mL54R, and mL172H compared to WT, indicating both new transgenic lines still exhibit dystrophic DGC phenotypes. The DGC component nNOS, however, shows an upward trend in abundance correlating to dystrophin protein levels in the mouse lines, and indeed mL172H expressed significantly more nNOS than *mdx*.

Localization of mutant dystrophin and members of the DGC were analyzed by immunofluorescence (Figure 4.3C). Dystrophin was visibly absent in *mdx* as expected. The mutant dystrophin that is present in the two transgenic lines appears to be localized correctly to the sarcolemma. Utrophin in WT animals is present only at the myotendinus and neuromuscular junctions, and in *mdx* mice it is seen up-regulated and at the sarcolemma. Transgenic lines also show utrophin present at the sarcolemma where it acts to mediate the loss of dystrophin. The components of the DGC which were shown to be decreased in

the transgenic lines (Figure 4.3A,B) are still localizing to the sarcolemma, similar to previous reports of immunofluorescent DGC analysis in BMD patients (Arechavala-Gomeza et al., 2010; Anthony et al., 2011). These results indicate that mutant dystrophin is present in the muscle at lower levels, but what is there is correctly localized to the membrane and is not forming aggregates within the cell. These data corroborate the data of Chapter 2, Figure 2.7D which showed full-length mutant dystrophin did not form aggregates *in vitro.* Similarly, components of the DGC are not involved in protein aggregation and are correctly localized.

Histological analyses of WT, *mdx*, mL54R, and mL172H revealed signs of muscular dystrophy for both transgenic lines (Figure 4.4). From representative images in Figure 4.4A, WT mice display uniform muscle fibers with nuclei localized at the periphery. *Mdx* mice have fibers that are not uniform in size or shape and many fibers have centralized nuclei as has been reported many times before. The mL54R line shows dystrophic features similar to *mdx*. The mL172H is also dystrophic, but possibly to a lesser degree. To quantify these observations, the fibers which are centrally-nucleated (CNF) were counted as a percentage of total fibers (Figure 4.4B). The data reveal that *mdx* has significantly more CNFs than WT, as expected. The mL54R and mL172H lines also had significantly increased CNFs over WT, but with lower average values than *mdx*. Indeed mL172H quadriceps had significantly lower CNFs than both *mdx* and mL54R. Across the four phenotypes, CNF values are proportional to

the quantity of dystrophin protein measured (Figure 4.2) and the severity of patient muscular dystrophy symptoms modeled by each line.

As an indicator of sarcolemmal integrity, creatine kinase (CK) activity was measured in the serum from each line of mice (Figure 4.4C) and it was found that WT mice had almost no activity as expected. *Mdx* had significantly elevated levels (11615 ± 1622) compared to WT. Both mL54R and mL172H, however, had lower levels of CK activity (7848 ± 1840 and 4764 ± 2177 respectively), both of which were not statistically different from WT nor different from *mdx*. The intermediate serum CK activity correlates inversely with dystrophin protein quantity and directly with disease severity.

We assessed our new transgenic mL5R and mL172H lines for several physiological impairments associated with muscular dystrophy in the *mdx* mouse, including grip strength, whole body tension, activity after exercise, and force loss during eccentric contraction (Figure 4.5). WT mice display an average grip strength of 32 mN/g (Figure 4.5A), while all three dystrophic lines (*mdx*, mL54R, mL172H) had significantly decreased grip strengths. Whole body tension measures the force of both the proximal and distal muscles in all four limbs at once, with a WT mouse showing approximately 140mN/g of tension (Figure 4.5B). The *mdx* line gave a large range of variability, but each of the transgenic lines mL54R and mL172H were significantly decreased compared to WT. The activity levels of mice were monitored before and after exercise (Figure 4.5C), and it was found that each of the dystrophic lines were significantly less active

than WT. As a final assessment of physiological performance, extensor digitorum longus muscle was analyzed *ex vivo* for force loss after eccentric contraction (Figure 4.5D). WT mice maintain the same level of force after 5 eccentric contractions, while *mdx*, mL54R, and mL172H all drop to approximately 20% of initial force by the 5th eccentric contraction. A summary of all the *ex vivo* parameters measured (Table 4.1) shows that all three of the dystrophic models are significantly different than WT for specific force, change in specific force after eccentric contractions, and total force drop during eccentric contraction. Together, the physiological assays indicate both missense mutant lines are mildly dystrophic similar to *mdx*.

To determine if the missense mutations in dystrophin were stimulating the heat shock pathway, the relative abundance of the major heat shock proteins was measured by western blot analysis, similar to analysis of the myoblast models in Chapter 3. Quantification from three separate sets of animals revealed no difference in the levels of Hsp40, Hsp70, Hsp90, or Hsp27P. Hsp90P levels were almost undetectable. While there was no significant increase, Hsp27P showed a upward trend for the mL54R line, indicating that there may be a slight perturbance to the heat shock pathway. Relative increases, however, are nothing like the response from an actual heat shock that misfolds a large percentage of the proteome. The lack of global heat shock response was similar to the missense myoblast model, and leaves the heat shock pathway as a possible therapeutic target for increasing dystrophin protein levels.

Discussion

Here we have reported on the generation of two transgenic mouse lines, representing severe DMD (L54R) and mild BMD (L172H) caused by missense mutations in dystrophin. The transgenic transcript for each line is expressed at a level that is not different than endogenous WT dystrophin transcript, but the transgenic protein levels are at steady state levels of 7-9% for L54R and 43% for L172H. Therefore dystrophin protein abundance inversely correlates with disease severity seen in the patients and we believe is the major mechanism of disease. Molecular analysis of the dystrophin glycoprotein complex (DGC) components demonstrate that they are correctly localized but decreased in abundance. Histological analysis of the two transgenic lines indicates that muscle degeneration and regeneration occurs in both L54R and L172H, with L54R being more severely affected and closer to *mdx* phenotype. Physiological analyses demonstrate that despite expression of some dystrophin protein, both of the missense mutant lines display symptoms of muscular dystrophy.

The original reports of missense mutations L54R and L172H were more than a decade apart from each other and therefore could not be compared side by side (Prior et al., 1993; Hamed et al., 2005). While the physiology of the patients was well reported the molecular analysis was minimal, with both groups estimating that the patient expressed 20% dystrophin levels. Here we have demonstrated in a side-by-side manner in our mouse models that dystrophin protein levels are much lower in the severely affected L54R mutation. These

results correlate with the level of protein seen in the cell culture models from Chapter 3, and these decreased levels can be ascribed to the degree of *in vitro* misfolding as seen by differential scanning fluorimetry in Chapter 2. It is important to note that there is thus far no evidence of aggregation, but rather only elimination of the mutant dystrophin protein. This evidence differentiates missense DMD/BMD from protein aggregation diseases such as Huntington's and Alzheimer's, and offers hope that upregulating the amount of dystrophin protein could alleviate symptoms of disease.

Several reports have examined the relationship between dystrophin protein expression levels and disease phenotype. Two separate studies of transgenic mice expressing either full-length or mini-dystrophin have shown that serum CK levels and CNF percentages inversely correlate with dystrophin protein levels, similar to our two transgenic lines (Wells et al., 1995; Phelps et al., 1995). Unlike our lines, however, both groups found that expression at or above 20% of controls was enough to ameliorate most dystrophic phenotypes. The mL172H line expresses dystrophin at approximately 40% that of control but is not rescued for any of the physiological assays, indicating the missense mutations may be affecting dystrophin functionality. Analysis of two non-transgenic mouse models, one harboring a splice-site mutation in dystrophin and the other with non-random X-inactivation, have led the authors to conclude that only 5% of WT dystrophin is enough to partially protect it from some dystrophic phenotypes (Li et al., 2008a; van Putten et al., 2012). Our mL54R line expresses >5% dystrophin

protein and shows no significant differences compared to *mdx*, again suggesting the amino acid change may decrease the functionality of the dystrophin protein present at steady-state levels. Indeed perturbations such as the 4-fold decrease in actin-binding affinity caused by L54R (Henderson et al., 2010) may have a large effect when <10% of normal protein levels are present. To determine whether missense mutations decrease the *in vivo* functionality of dystrophin, future studies will aim to increase mutant dystrophin levels with small molecule treatments. If an up-regulation of mutant dystrophin does not improve physiological performance then the missense mutations are likely impairing dystrophin function.

The two dystrophin low-expression mouse models described above have been crossed to mice lacking both utrophin and dystrophin (*mdx*/utr$^{-/-}$), which then showed even greater separation of phenotype based on percentage of dystrophin protein (Li et al., 2010b; van Putten et al., 2013). Given that the *mdx* model itself has mild physiological symptoms compared to DMD patients with the same type of mutation largely due to compensatory utrophin upregulation, it may be that subtle changes in phenotype of mL54R and mL172H lines compared to *mdx* are being masked. Therefore future studies will cross each line to the *mdx*/utr$^{-/-}$ mouse line. If a significant difference in physiological assays is seen between m/utr$^{-/-}$/L54R and m/utr$^{-/-}$/L172H compared to *mdx*/utr$^{-/-}$ then utrophin is likely masking subtle phenotypic differences caused by the missense mutations.

In summary, mouse lines mL54R and mL172H demonstrate that missense

mutations decrease dystrophin protein levels similar to values seen in myoblast cell models and proportional to disease severity seen in patients. It is our hope that these models will aid in the development of personalized therapeutics for DMD and BMD patients with missense mutations.

Figures

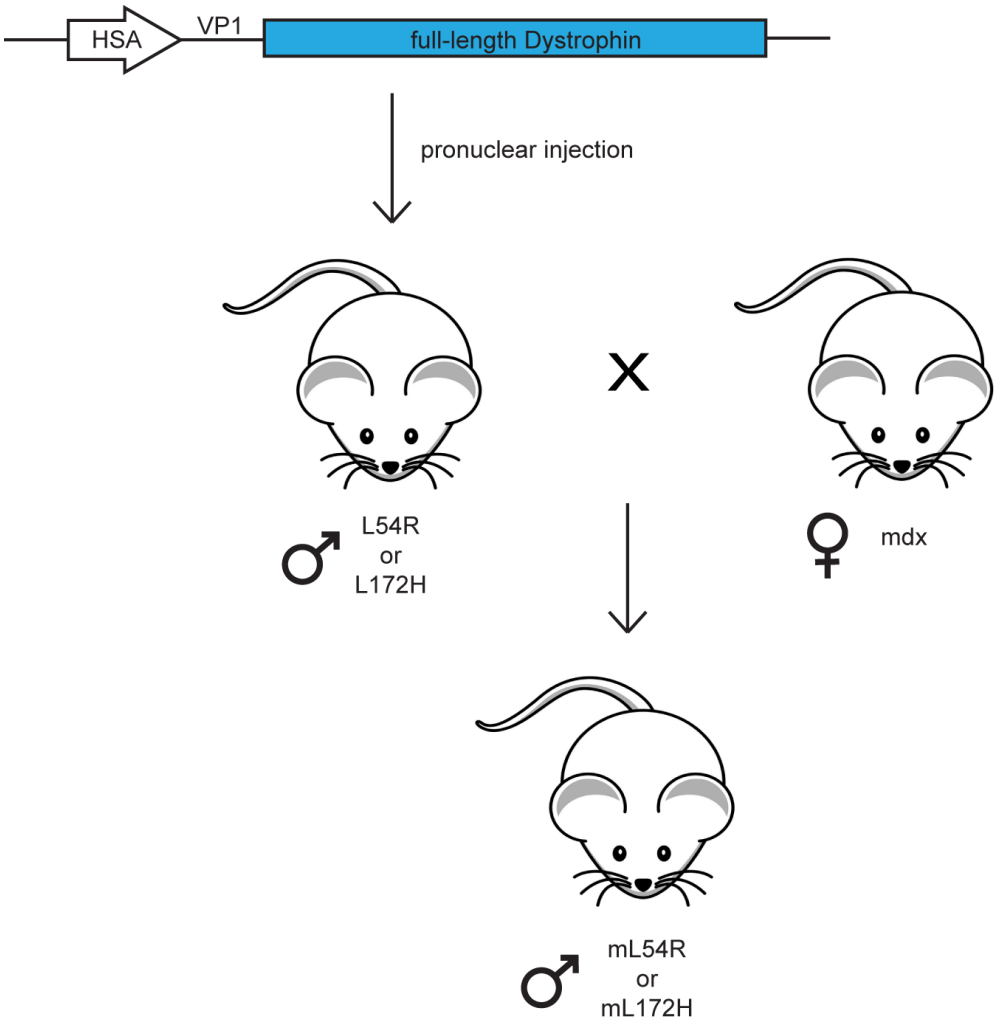

Figure 4.1: Expression construct and experimental concept. Full-length, mouse dystrophin cDNA was subcloned into a vector containing a human skeletal α-actin (HSA) promoter and Vp1 intron. The fragment was pronuclear injected into fertilized eggs and transplanted into a pseudopregnant mouse. Male founders (L54R and L172H) were crossed to female *mdx*. Male offspring express the transgene on an *mdx* background (mL54R and mL172H).

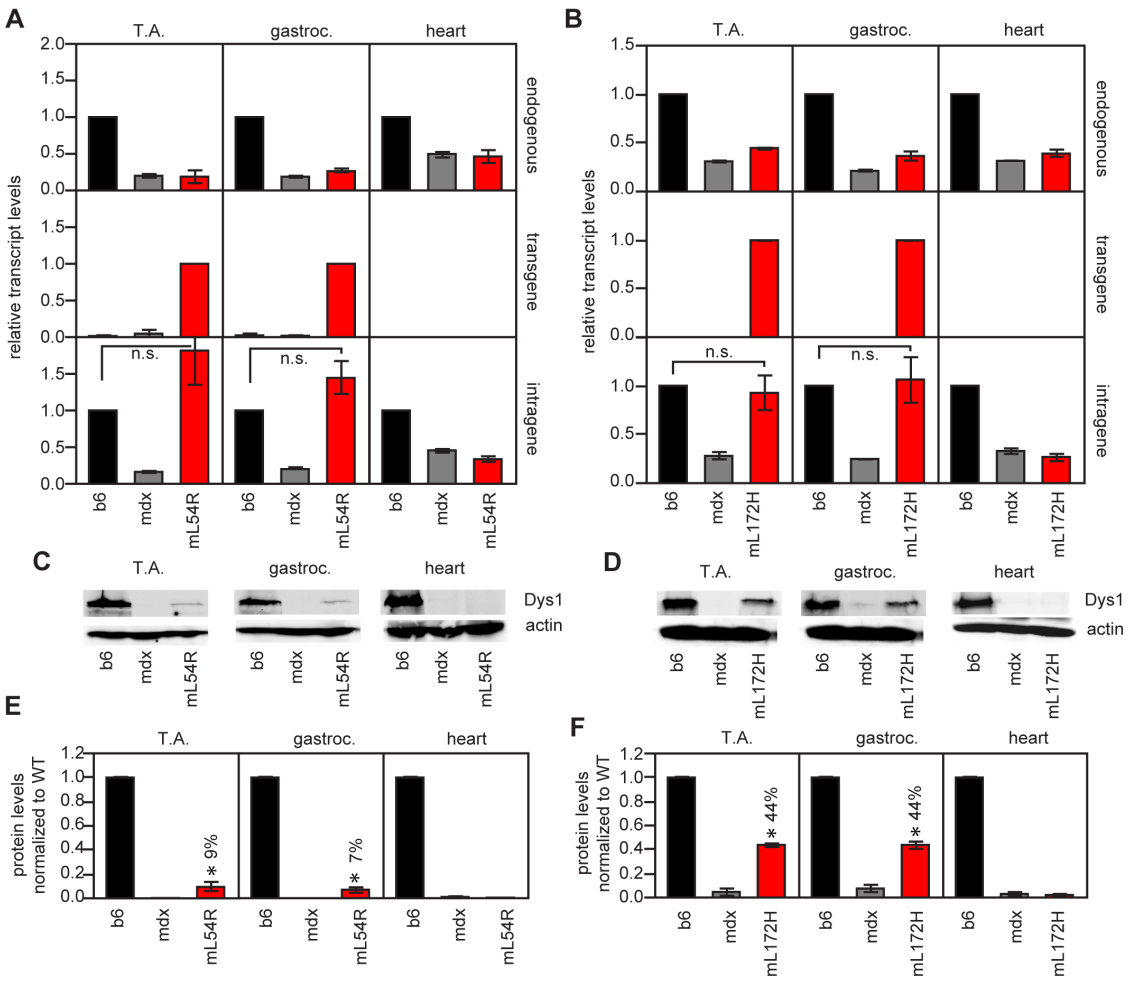

Figure 4.2: RNA and protein expression levels in transgenic mouse lines. (A) and (B) RT-qPCR analysis for mouse lines L54R and L172H respectively. Top panel shows amplification within the 3'UTR of endogenous mouse dystrophin. Middle panel shows amplification within the 3'UTR of the transgenic dystrophin. Bottom panel shows amplification within the coding region of dystrophin, amplifying both endogenous and transgenic dystrophin. ANOVA analysis of the intragene amplifications were $F<0.05$ for both lines. Post hoc analysis between WT and transgenic were n.s. (not significant). **(C) and (D)** Representative western blot analyses of mouse lines L54R and L172H respectively. **(E) and (F)** Quantification of western blots from n=3 separate sets of mice. ANOVA analysis for both lines gave $F<0.05$. Post hoc analysis $*p<0.05$ compared to WT.

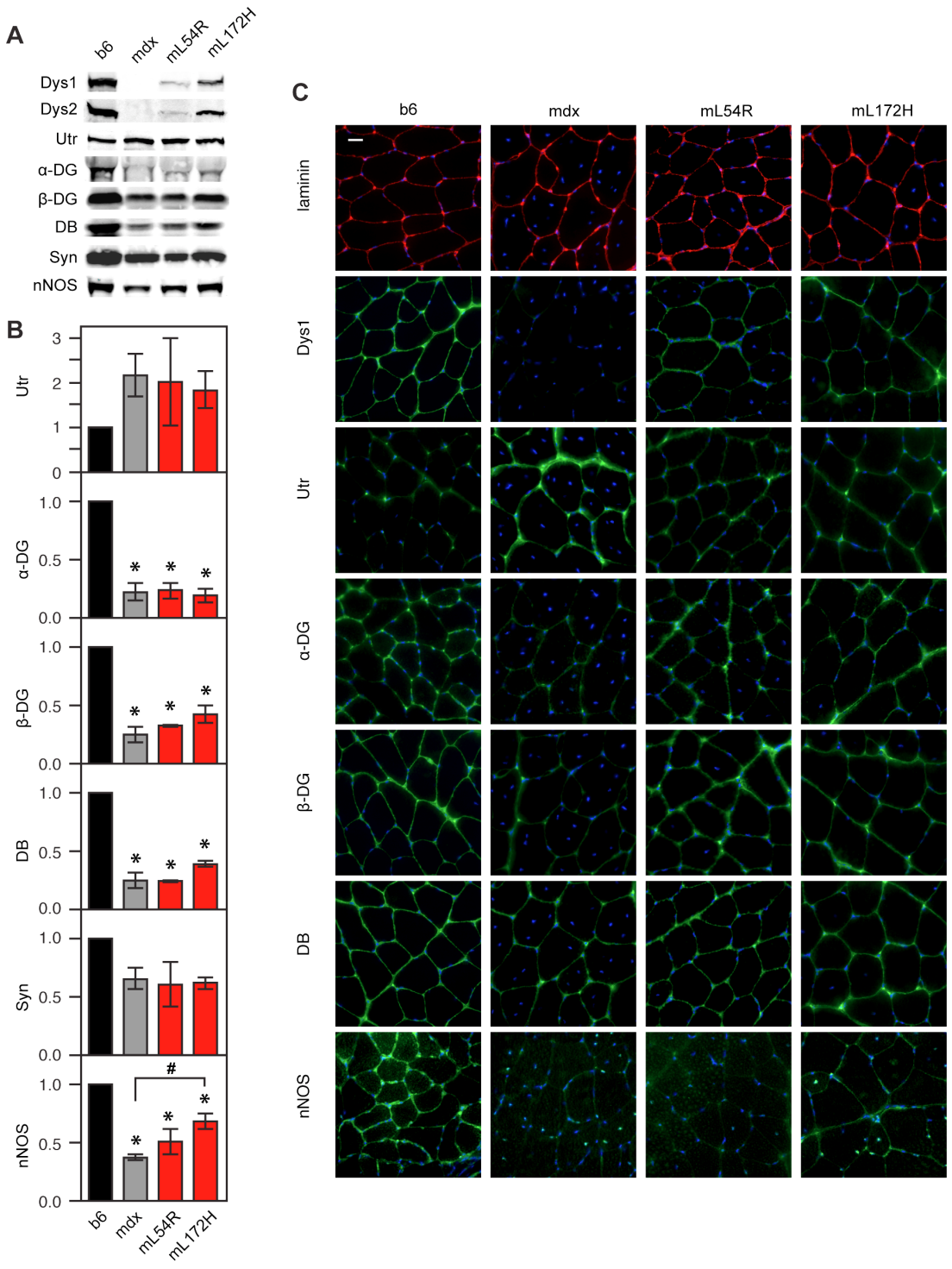

Figure 4.3: Expression levels and localization of components in the Dystrophin Glycoprotein Complex. **(A-C)** Utr = utrophin, α-DG = alpha-dystroglycan, β-DG = beta-dystroglycan, DB = dystrobrevin, Syn = syntrophin,

nNOS = neuronal nitric oxide synthase. **(A)** Representative western blot analyses for several components of the DGC in tibialis anterior muscle, including two different antibodies for dystrophin corroborating results found in Figure 4.2. **(B)** Quantification of western blots for n=3 separate sets of mice. Values are all normalized to WT for each blot. ANOVA with significance of $F<0.05$ were analyzed with post hoc statistics. ∗$p<0.05$ compared to WT. **#**$p<0.05$ between *mdx* and L172H. **(C)** Immunofluorescent analysis of components of the DGC in quadriceps muscle. Scale bar = 20μm.

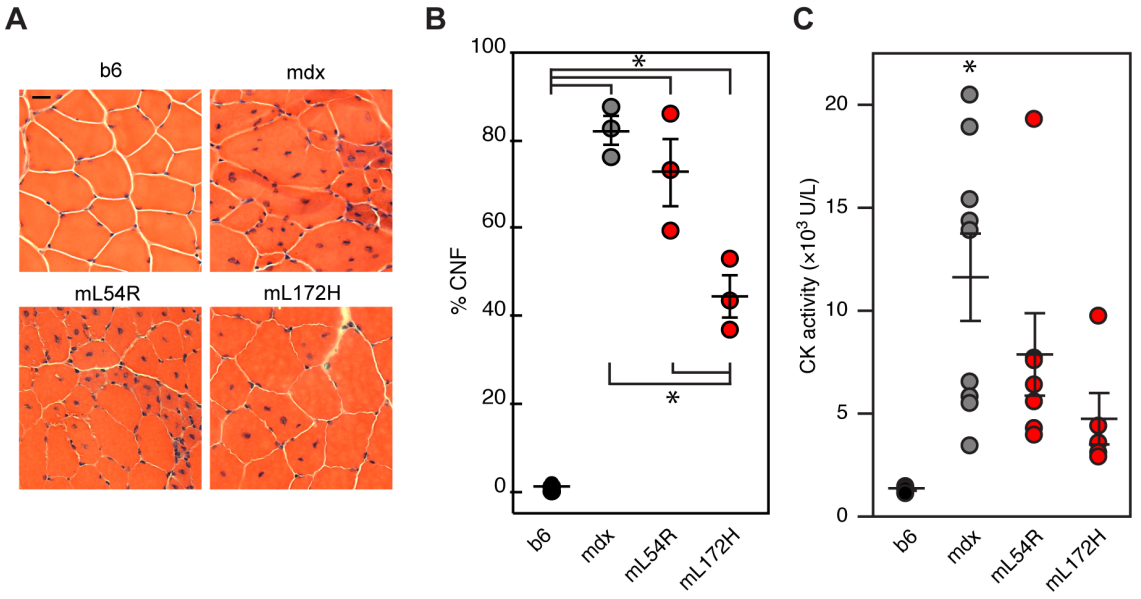

Figure 4.4: Fiber morphology and permeability. (A) Representative quadriceps muscle sections stained with H&E and imaged at 200x magnification. Scale bar = 20μm. **(B)** Quantification of centrally nucleated fibers (CNF) as a percentage of the total fibers. A minimum of 250 fibers were counted for each mouse. ANOVA analysis was significant at $F<0.0001$. Post hoc analysis gave ∗$p<0.05$ for WT versus all disease models, and for mL172H versus *mdx* and mL54R. **(C)** Serum creatine kinase (CK) activity from cheek bleeds of individual mice. ANOVA analysis was significant at $F<0.01$. Post-hoc analysis gave ∗$p<0.01$ for WT versus *mdx*. Both transgenics were not statistically different from WT.

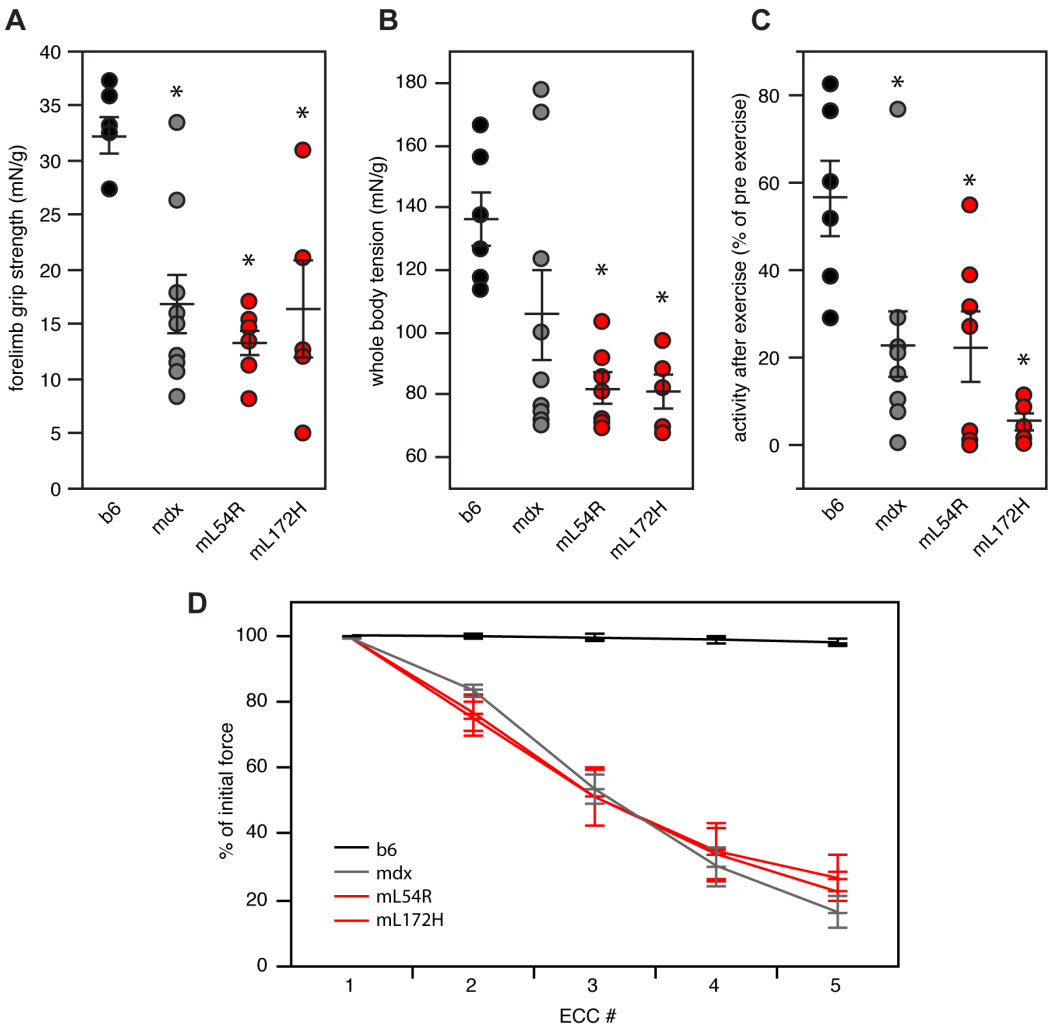

Figure 4.5: Physiology of transgenic mouse models. **(A)** Forelimb grip strength analysis. Individual points are an average of 5 trials for each mouse. ANOVA was significant at $F<0.001$. Post hoc analysis gave $*p<0.005$ compared to WT. **(B)** Whole body tension analysis. Individual points are an average of 5 trials for each mouse. ANOVA was significant at $F<0.01$. Post hoc analysis gave $*p<0.05$ compared to WT. **(C)** Activity after exercise analysis. ANOVA was significant at $F<0.005$. Post hoc analysis gave $*p<0.05$ compared to WT. **(D)** Ex vivo EDL force measurement during eccentric contraction. For ECC 2-5, all three dystrophic models were significantly different than WT.

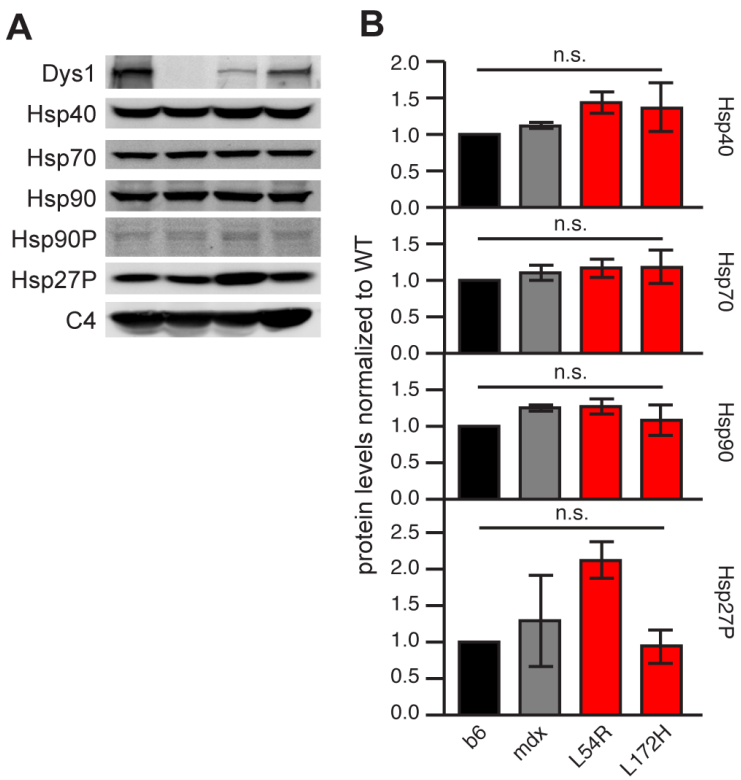

Figure 4.6: Effect of missense mutations on the heat shock pathway of the mice. **(A)** Representative western blots of heat shock proteins in each of the mouse lines from tibialis anterior muscle. Hsp90P was barely detectable. **(B)** Quantification of n=3 sets of mice. ANOVA analysis for each protein was not significant.

	WT	*mdx*	mL54R	mL172H
EDL mass (mg)	12.8 ± 0.4	16.3 ± 1.5	14.2 ± 0.8	13.5 ± 0.7
L_0 (mm)	13.3 ± 0.2	12.3 ± 0.1	12.4 ± 0.1	12.9 ± 0.1
CSA (cm^2)	0.021 ±0.001	0.029 ± 0.003	0.025 ± 0.001	0.022 ± 0.001
passive stiffness (N/m)	13.9 ± 0.9	16.8 ± 1.0	14.2 ± 0.6	15.8 ± 0.7
active stiffness (N/m)	755.7 ± 36.2	720.7 ± 31.8	695.4 ± 38.2	785.5 ± 20.6
P_0 (mN)	448.5 ± 8.8	416.8 ± 31.5	414.7 ± 29.5	393.2 ± 34.7
specific P_0 (N/cm^2)	21.8 ± 0.5	14.8 ± 0.8 **#**	16.9 ± 0.5 **#**	17.4 ± 0.9 **#**
ΔP_0 (%)	11.1 ± 3.1	82.8 ± 5.4 **#**	75.8 ± 5.8 **#**	73.6 ± 4.4 **#**
force drop (%)	2.1	75.1 ± 4.3 **#**	69.5 ± 5.5 **#**	65.7 ± 2.1 **#**

Table 4.1: Summary of *ex vivo* EDL parameters. For measurements of specific force, change in specific force, and force drop during eccentric contractions ANOVA was significant at $F<0.01$. Post hoc analysis gave #$p<0.05$ compared to WT.

Chapter 5

Conclusions and Discussion

Thesis Findings

Duchenne and Becker muscular dystrophy have been described clinically since the mid-1800's, and in the late 1980's it was discovered that the diseases were due to mutations in a 2.4Mb gene on the X-chromosome encoding the 427kDa protein dystrophin (Duchenne, 1861; Koenig et al., 1988, 1987). Causative mutations vary in type from exonic deletions and insertions to nonsense and splice-site mutations (Aartsma-Rus et al., 2006). A small, but growing number of patients harbor missense mutations in the *DMD* gene and experience a wide range of muscular dystrophy severity (Prior et al., 1993; Hamed et al., 2005). The aims of this thesis were to compare the *in vitro* effect of missense mutations in the various domains of dystrophin, determine the cellular consequences of missense mutant dystrophin, and to generate animal models of severe and mild forms of muscular dystrophy caused by missense mutations.

Several studies have examined the effect of missense mutations on peptide fragments of dystrophin *in vitro* (Singh et al., 2010; Legardinier et al., 2009; Ishikawa-Sakurai et al., 2004), and previous work in our lab has discovered that missense mutations in the N-terminal ABD1 cause thermal instability of full-length dystrophin protein *in vitro* (Henderson et al., 2010). In chapter 2, we reported that missense mutations in the spectrin-like repeats of the central rod domain cause no visible change in protein stability when expressed in Dp260 or full-length dystrophin *in vitro*. In contrast, several missense mutations

in the cysteine-rich and C-terminal domain caused decreased solubility and expression. Finally side-by-side comparison of mutations in the three major domains of dystrophin revealed that only mutations in the N-terminal domain perturbed the tertiary structure. The *in vitro* model of missense mutations in dystrophin provided understanding of the biochemical effects a mutation could have on the protein and lead to hypotheses about the fate of mutant dystrophin in the cell.

The study of transgenic dystrophin in a cell culture system has been limited to a few reports that expressed small fragment peptides, including a report of missense mutations in the β-dystroglycan binding domain, two of which decreased the levels of the dystrophin peptide and one which ablated dystroglycan binding (Vulin et al., 2014). In chapter 3, we have reported on the generation of four transgenic myoblast cell lines stably expressing full-length dystrophin. The two lines expressing disease-causing missense mutations, L54R and L172H, express protein at a steady-state level that is decreased relative to WT and inversely correlates with muscular dystrophy severity of the modeled patients. We demonstrated that mutant dystrophin protein could be increased with the use of small molecule osmolytes, heat shock activators, or proteasome inhibitors; indicating the mutant protein is unstable, targeted by the heat shock pathway, and degraded by the proteasome. The myoblast lines offer insight into the molecular mechanism of muscular dystrophy when caused by missense mutations and can serve as a platform for discovery of more

personalized medicine approaches.

The *mdx* mouse has served as a well-studied model of nonsense mutations in dystrophin (Sicinski et al., 1989), and recently a pig was reported as a model of missense mutations in dystrophin (Hollinger et al., 2013). In chapter 4 we reported the generation of two new mouse models, transgenically expressing full-length dystrophin with missense mutations L54R and L172H. Both mL54R and mL172H lines express dystrophin transcript at levels similar to endogenous WT dystrophin, yet have steady-state protein levels of ~10% and ~40% of WT respectively. Decreased protein levels suggest the missense mutations cause misfolding and/or instability which targets the dystrophin protein for degradation in the muscle to a degree that is proportional to disease severity seen in the modeled patients. Histological analyses of serum CK and CNF percentage also correlate with dystrophin levels. Interestingly, physiological assessment of mL54R and mL172H mice reveals no difference compared to *mdx* while other studies of low dystrophin expression show phenotypic improvements, which leads to the hypothesis that either the missense mutations are somehow perturbing the functionality of the dystrophin protein that is not degraded or the mild phenotype of the *mdx* mouse is masking subtly differences in phenotype. Mouse lines mL54R and mL172H corroborate the molecular mechanism of disease discovered in the myoblast cell lines and further characterization will hopefully lead to novel avenues of treatment for DMD and BMD caused by missense mutations.

Personalized Therapeutics for Missense Mutations in Dystrophin

While there are currently efforts to treat nonsense mutations with stop codon read-through drugs and insertion/deletions with exon skipping, there is currently no personalized therapeutic aimed at missense mutations in dystrophin. In chapter 3 we demonstrated that there are at least three categories of small molecules that were able to increase the steady-state level of missense mutant protein: osmolytes, heat shock activators, and proteasome inhibitors. The osmolyte betaine was found to stabilize mutant dystrophin at very high concentrations. Therefore it could not be used as a stand alone treatment, but has the potential to be used in combination with other therapies as a small contributor to dystrophin stability. The heat shock activator gedunin was found at moderate concentrations of less than 100μM to restore mutant dystrophin to WT levels. While 40-80μM is likely too high of a dosage to be used as a therapeutic, gedunin serves as a proof-of-principle for the use of heat shock activators. Future high-throughput screens may find one of sufficient efficacy to be given at a tolerated dose for the treatment of missense mutations.

The most successful category of small molecules for increasing mutant dystrophin levels was the proteasome inhibitors. Each of the tested proteasome inhibitors restored mutant dystrophin to WT levels at concentrations less than 10μM, which is a reasonable dosage for patient administration. Indeed, patients are currently receiving treatments of proteasome inhibitors such as bortezomib and epoxomicin-derivative carfilzomib for treatment of multiple myeloma and

other cancers (Kisselev et al., 2012). Cancer treatment is intended to be acute given that once the cancer is gone, treatment is terminated. If proteasome inhibitors were used to increase dystrophin protein levels in patients with missense mutations, however, treatment would need to be continued for the entire life of the patient. Further work is needed to determine if chronic proteasome inhibition could be tolerated, but it still offers a promising new route of therapy.

While inhibiting the proteasome is an effective way to block the degradation of dystrophin, it also inhibits the degradation of all other proteins in the cell thereby interfering with the normal cell metabolism. If, however, the upstream ubiquitination ligases specific to dystrophin were inhibited, the cell could maintain normal function. Similarly, the cancer biology field has been developing several proteasome inhibitors for treatment of multiple myeloma (Kumar et al., 2008), yet recently have begun to target the cancer specific E3 ligases responsible for ubiquitination of p53 and c-Myc (reviewed in Weathington & Mallampalli, 2014). Determining the specific E1-E2-E3 cascade for a given substrate is a difficult task given that there are approximately 40 E2 conjugating enzymes and over 600 E3 ligases (Deshaies and Joazeiro, 2009; Li et al., 2008b). The missense cell lines that we have generated are the first model system that could allow for the efficient identification of the E1, E2, and E3 enzymes responsible for ubiquitination and subsequent degradation of dystrophin. Small molecule inhibitors of the specific E3 ligase could then be

used as a highly targeted form of therapy for persons with missense mutations in dystrophin.

Whether heat shock activators, proteasome inhibitors, or ubiquitin ligase inhibitors, potential therapeutics will need to be researched extensively in pre-clinical studies. The two transgenic mouse lines expressing missense mutated dystrophin reported in chapter 4 can serve as models for such pre-clinical investigations. A candidate small molecule would be administered to the mice to determine proper dosage, dosing schedule, degree of phenotype improvement, side effects, etc. An ideal therapeutic would be well tolerated by the mice, cause large increases in dystrophin protein levels, and rescue the dystrophic phenotypes of the mice. Small molecules which show promise in the mouse models could then be pre-clinically studied in the pig model of missense mutations in dystrophin.

Applications to Other Mutations and Therapies

Missense mutations in dystrophin are rare, estimated to occur in less than 10% of DMD and BMD patients (Flanigan et al., 2009), yet the understanding gained from missense mutation models has the potential to aide in the treatment of patients with other types of mutations. BMD is often the result of in-frame deletions or insertions, resulting in internally-truncated dystrophin protein. In addition to potentially lacking functional domains, internally-truncated dystrophin has been shown to be thermally unstable *in vitro* (Henderson et al., 2011). Protein instability manifests as decreased protein expression seen in BMD patients (Anthony et al., 2011), similar to the results seen here for missense mutations. If a therapeutic is discovered that increases the levels of missense mutant dystrophin and phenotypic improvements are observed, the same therapy could potentially be applied to BMD insertion and deletion patients.

In addition to missense mutation therapies expanding to other types of mutations, they may be relevant as an “add-on” to other personalized treatments. Exon-skipping is a promising gene therapy aimed at DMD patients with out-of-frame deletions or insertions (Goemans et al., 2011), with effective treatment resulting in in-frame deletions of the transcript. The restored protein would therefore mimic BMD patient protein described above and potentially benefit from the same treatment that decreases degradation due to protein misfolding. Similarly, gene replacement strategies currently rely on internally-truncated dystrophin sequences that are small enough to be encoded within AAV

constructs, and would likely result in expression of dystrophin protein at levels below WT due to misfolding and degradation. Finally, stop codon read-through drugs are currently in clinical trials to treat DMD patients with nonsense mutations in dystrophin (Peltz et al., 2013). Successful read-through would result in the incorporation of a random amino acid effectively turning a nonsense mutation into a phenotypic missense mutation, making the work of this thesis and future missense mutation studies directly applicable.

Continuing Study

The evidence from the cell culture models of Chapter 3 suggest that mutant dystrophin is being degraded by the proteasome, and future studies will determine if proteasome degradation is also occurring in the mouse models in Chapter 4. Efforts are currently underway to treat mL54R and mL172H mice with proteasome inhibitors, which lead to several questions about the consequences of increasing the levels of these mutant dystrophins. For instance, does blocking their degradation by the proteasome now cause them to aggregate or do they function normally? And what percentage of WT dystrophin would be needed to ameliorate symptoms? If treatment increases dystrophin protein levels, we plan to assess the mice for improved physiological performance by eccentric contraction force drop measurements. An improvement in maximal force output after 5 serial eccentric contractions compared to *mdx* would indicate two things: 1) the main disease mechanism of missense mutations is decreasing the amount of dystrophin protein and 2) increasing mutant dystrophin is a viable treatment option to ameliorate phenotypes of disease. A lack of improvement may indicate the increased mutant dystrophin is aggregating, therefore muscle pathology and protein aggregation will be evaluated histologically in collaboration with Dr. Michael Lawlor using a panel of histochemical stains, including H&E, Gomori trichrome, NADH, and congo red stains. Patterns indicative of aggregation will include both visible aggregates of protein and/or evidence of organelle displacement as a result of abnormal protein localization.

In addition to proteasome inhibition, we plan to cross the mL54R and mL172H lines to the utrophin- and dystrophin-null mouse, *mdx*/utr$^{-/-}$ as discussed in chapter 4. If the molecular, histological, and physiological analyses of the resulting m/utr$^{-/-}$/L54R and m/utr$^{-/-}$/L172H mice show less dystrophic phenotypes compared to non-transgenic littermate controls then utrophin was likely masking subtle differences in phenotype caused by the missense mutations. These mice would be more accurate models of the original patients diagnosed with DMD (L54R) and BMD (L172H), just as the *mdx*/utr$^{-/-}$ mouse itself is a better phenotypic model of DMD patients with nonsense mutations. If, alternatively, physiological phenotypes are still comparable between transgenic and non-transgenic littermates, then the missense mutations are likely causing a decrease in the functionality of dystrophin in addition to causing a decrease in the steady-state levels of the protein.

As mentioned in the personalized therapeutics section, identification of the E2 and E3 ligases responsible for the ubiquitination of misfolded dystrophin would possibly allow for highly specific inhibition of dystrophin degradation without inhibiting the degradation of all other proteins in the cell. Efforts are currently underway to systematically knock-down E1, E2, and E3 ubiquitin ligases in L54R myoblasts with commercially available 96-well siRNA arrays. Initially the set of E1 activating enzymes and E2 conjugating enzymes will be assessed and then E3 ligases. Positive hits detected as increased GFP fluorescence by flow cytometry (Figure 3.6B) will be validated with larger scale

cell culture knock-down and western blot analysis for full-length dystrophin. If an E3 ligase is identified, the literature will be searched for an existing knockout mouse model or a knock-out will be generated. The E3-null mouse could then be crossed to the mL54R and mL172H mice and progeny assayed for mutant dystrophin protein abundance and muscular dystrophy phenotypes.

In summary, the models of missense mutations in dystrophin reported in this thesis will continue to be useful for further understanding the mechanism of disease and for developing personalized therapy options for patients with missense mutations.

References

Aartsma-Rus, A., J.C.T. Van Deutekom, I.F. Fokkema, G.J.B. Van Ommen, and J.T. Den Dunnen. 2006. Entries in the Leiden Duchenne muscular dystrophy mutation database: an overview of mutation types and paradoxical cases that confirm the reading-frame rule. *Muscle Nerve*. 34:135–44.

Acsadi, G., S.A. Moore, A. Chéron, O. Delalande, L. Bennett, W. Kupsky, M. El-Baba, E. Le Rumeur, and J.-F. Hubert. 2012. Novel mutation in spectrin-like repeat 1 of dystrophin central domain causes protein misfolding and mild Becker muscular dystrophy. *J. Biol. Chem.* 287:18153–62.

Ahn, A.H., and L.M. Kunkel. 1995. Syntrophin binds to an alternatively spliced exon of dystrophin. *J. Cell Biol.* 128:363–71.

Akerfelt, M., R.I. Morimoto, and L. Sistonen. 2010. Heat shock factors: integrators of cell stress, development and lifespan. *Nat. Rev. Mol. Cell Biol.* 11:545–55.

Alter, J., F. Lou, A. Rabinowitz, H. Yin, J. Rosenfeld, S.D. Wilton, T.A. Partridge, and Q.L. Lu. 2006. Systemic delivery of morpholino oligonucleotide restores dystrophin expression bodywide and improves dystrophic pathology. *Nat. Med.* 12:175–7.

Angelini, C. 2007. The role of corticosteroids in muscular dystrophy: a critical appraisal. *Muscle Nerve*. 36:424–35.

Anthony, K., S. Cirak, S. Torelli, G. Tasca, L. Feng, V. Arechavala-Gomeza, A. Armaroli, M. Guglieri, C.S. Straathof, J.J. Verschuuren, A. Aartsma-Rus, P. Helderman-van den Enden, K. Bushby, V. Straub, C. Sewry, A. Ferlini, E. Ricci, J.E. Morgan, and F. Muntoni. 2011. Dystrophin quantification and clinical correlations in Becker muscular dystrophy: implications for clinical trials. *Brain*. 134:3547–59.

Arakawa, T., D. Ejima, Y. Kita, and K. Tsumoto. 2006. Small molecule pharmacological chaperones: From thermodynamic stabilization to pharmaceutical drugs. *Biochim. Biophys. Acta*. 1764:1677–87.

Arechavala-Gomeza, V., M. Kinali, L. Feng, S.C. Brown, C. Sewry, J.E. Morgan, and F. Muntoni. 2010. Immunohistological intensity measurements as a tool to assess sarcolemma-associated protein expression. *Neuropathol. Appl. Neurobiol.* 36:265–74.

Ashburner, M., and J.J. Bonner. 1979. The induction of gene activity in drosophilia by heat shock. *Cell*. 17:241–54.

Azakir, B.A., B. Erne, S. Di Fulvio, G. Stirnimann, and M. Sinnreich. 2014. Proteasome inhibitors increase missense mutated dysferlin in patients with muscular dystrophy. *Sci. Transl. Med.* 6:250ra112–250ra112.

Bar, S., E. Barnea, Z. Levy, S. Neuman, D. Yaffe, and U. Nudel. 1990. A novel product of the Duchenne muscular dystrophy gene which greatly differs from the known isoforms in its structure and tissue distribution. *Biochem. J.* 272:557–60.

Barton-Davis, E.R., L. Cordier, D.I. Shoturma, S.E. Leland, and H.L. Sweeney. 1999. Aminoglycoside antibiotics restore dystrophin function to skeletal muscles of *mdx* mice. *J. Clin. Invest.* 104:375–81.

Basak, S., D. Pookot, E.J. Noonan, and R. Dahiya. 2008. Genistein down-regulates androgen receptor by modulating HDAC6-Hsp90 chaperone function. *Mol. Cancer Ther.* 7:3195–202.

Belanto, J.J., T.L. Mader, M.D. Eckhoff, D.M. Strandjord, G.B. Banks, M.K. Gardner, D.A. Lowe, and J.M. Ervasti. 2014. Microtubule binding distinguishes dystrophin from utrophin. *Proc. Natl. Acad. Sci. U. S. A.* 111:5723–8.

Bhosle, R.C., D.E. Michele, K.P. Campbell, Z. Li, and R.M. Robson. 2006. Interactions of intermediate filament protein synemin with dystrophin and utrophin. *Biochem. Biophys. Res. Commun.* 346:768–77.

Blake, D.J., A. Weir, S.E. Newey, and K.E. Davies. 2002. Function and genetics of dystrophin and dystrophin-related proteins in muscle. *Physiol. Rev.* 82:291–329.

Bork, P., and M. Sudol. 1994. The WW domain: a signalling site in dystrophin? *Trends Biochem. Sci.* 19:531–3.

Bovolenta, M., D. Erriquez, E. Valli, S. Brioschi, C. Scotton, M. Neri, M.S. Falzarano, S. Gherardi, M. Fabris, P. Rimessi, F. Gualandi, G. Perini, and A. Ferlini. 2012. The DMD locus harbours multiple long non-coding RNAs which orchestrate and control transcription of muscle dystrophin mRNA isoforms. *PLoS One*. 7:e45328.

Bozaykut, P., N.K. Ozer, and B. Karademir. 2014. Regulation of Protein Turnover by Heat Shock Proteins. *Free Radic. Biol. Med.* 1–15.

Brandt, G.E.L., M.D. Schmidt, T.E. Prisinzano, and B.S.J. Blagg. 2008. Gedunin, a novel hsp90 inhibitor: semisynthesis of derivatives and preliminary structure-activity relationships. *J. Med. Chem.* 51:6495–502.

Brenman, J.E., D.S. Chao, H. Xia, K. Aldape, and D.S. Bredt. 1995. Nitric oxide synthase complexed with dystrophin and absent from skeletal muscle sarcolemma in Duchenne muscular dystrophy. *Cell*. 82:743–52.

Briguet, A., I. Courdier-Fruh, M. Foster, T. Meier, and J.P. Magyar. 2004. Histological parameters for the quantitative assessment of muscular dystrophy in the *mdx*-mouse. *Neuromuscul. Disord.* 14:675–82.

Buchanan, C.C., E.S. Torstenson, W.S. Bush, and M.D. Ritchie. 2012. A comparison of cataloged variation between International HapMap Consortium and 1000 Genomes Project data. *J. Am. Med. Inform. Assoc.* 19:289–94.

Bulfield, G. 1984. X Chromosome-Linked Muscular Dystrophy (*mdx*) in the Mouse. *Proc. Natl. Acad. Sci.* 81:1189–1192.

Burg, M.B. 1995. Molecular basis of osmotic regulation. *Am. J. Physiol. - Ren. Physiol.* 268:F983–F996.

Buysse, K., M. Riemersma, G. Powell, J. van Reeuwijk, D. Chitayat, T. Roscioli, E.J. Kamsteeg, C. van den Elzen, E. van Beusekom, S. Blaser, R. Babul-Hirji, W. Halliday, G.J. Wright, D.L. Stemple, Y.Y. Lin, D.J. Lefeber, and H. van Bokhoven. 2013. Missense mutations in β-1,3-N-acetylglucosaminyltransferase 1 (B3GNT1) cause Walker-Warburg syndrome. *Hum. Mol. Genet.* 22:1746–54.

Byers, T.J., H.G. Lidov, and L.M. Kunkel. 1993. An alternative dystrophin transcript specific to peripheral nerve. *Nat. Genet.* 4:77–81.

Carlson, C.G., and R. V Makiejus. 1990. A noninvasive procedure to detect muscle weakness in the *mdx* mouse. *Muscle Nerve*. 13:480–4.

Casas-Delucchi, C.S., A. Brero, H.P. Rahn, I. Solovei, A. Wutz, T. Cremer, H. Leonhardt, and M.C. Cardoso. 2011. Histone acetylation controls the inactive X chromosome replication dynamics. *Nat. Commun.* 2:222.

Castillo, K., M. Nassif, V. Valenzuela, F. Rojas, S. Matus, G. Mercado, F.A. Court, B. van Zundert, and C. Hetz. 2013. Trehalose delays the progression of amyotrophic lateral sclerosis by enhancing autophagy in motoneurons. *Autophagy*. 9:1308–1320.

Chakkalakal, J. V, P. Miura, G. Bélanger, R.N. Michel, and B.J. Jasmin. 2008. Modulation of utrophin A mRNA stability in fast versus slow muscles via an AU-rich element and calcineurin signaling. *Nucleic Acids Res.* 36:826–38.

Chamberlain, J.S., J.A. Pearlman, D.M. Muzny, R.A. Gibbs, J.E. Ranier, C.T. Caskey, and A.A. Reeves. 1988. Expression of the murine Duchenne muscular dystrophy gene in muscle and brain. *Science*. 239:1416–8.

Chang, B.H., L. Smith, J. Huang, and M. Thayer. 2007. Chromosomes with delayed replication timing lead to checkpoint activation, delayed recruitment of Aurora B and chromosome instability. *Oncogene*. 26:1852–61.

Chung, J., A.K. Nguyen, D.C. Henstridge, A.G. Holmes, M.H.S. Chan, J.L. Mesa, G.I. Lancaster, R.J. Southgate, C.R. Bruce, S.J. Duffy, I. Horvath, R. Mestril, M.J. Watt, P.L. Hooper, B. a Kingwell, L. Vigh, A. Hevener, and M. a Febbraio. 2008. HSP72 protects against obesity-induced insulin resistance. *Proc. Natl. Acad. Sci. U. S. A.* 105:1739–44.

Connolly, A.M., R.M. Keeling, S. Mehta, A. Pestronk, and J.R. Sanes. 2001. Three mouse models of muscular dystrophy: the natural history of strength and fatigue in dystrophin-, dystrophin/utrophin-, and laminin α2-deficient mice. *Neuromuscul. Disord.* 11:703–712.

Cooper, B.J., N.J. Winand, H. Stedman, B.A. Valentine, E.P. Hoffman, L.M. Kunkel, M.O. Scott, K.H. Fischbeck, J.N. Kornegay, and R.J. Avery. 1988. The homologue of the Duchenne locus is defective in X-linked muscular dystrophy of dogs. *Nature*. 334:154–6.

Cox, G.A., N.M. Cole, K. Matsumura, S.F. Phelps, S.D. Hauschka, K.P. Campbell, J.A. Faulkner, and J.S. Chamberlain. 1993. Overexpression of dystrophin in transgenic *mdx* mice eliminates dystrophic symptoms without toxicity. *Nature*. 364:725–9.

D'Souza, V.N., T.M. Nguyen, G.E. Morris, W. Karges, D.A. Pillers, and P.N. Ray. 1995. A novel dystrophin isoform is required for normal retinal electrophysiology. *Hum. Mol. Genet.* 4:837–42.

Delgado, I., X. Huang, S. Jones, L. Zhang, R. Hatcher, B. Gao, and P. Zhang. 2003. Dynamic gene expression during the onset of myoblast differentiation in vitro. *Genomics*. 82:109–121.

Deshaies, R.J., and C.P. Joazeiro. 2009. RING domain E3 ubiquitin ligases. *Annu. Rev. Biochem.* 78:399–434.

DeWolf, C., P. McCauley, A.F. Sikorski, C.P. Winlove, A.I. Bailey, E. Kahana, J.C. Pinder, and W.B. Gratzer. 1997. Interaction of dystrophin fragments with model membranes. *Biophys. J.* 72:2599–604.

Djinovic-Carugo, K., M. Gautel, J. Ylänne, and P. Young. 2002. The spectrin repeat: a structural platform for cytoskeletal protein assemblies. *FEBS Lett.* 513:119–23.

Draviam, R.A., B. Wang, J. Li, X. Xiao, and S.C. Watkins. 2006. Mini-dystrophin efficiently incorporates into the dystrophin protein complex in living cells. *J. Muscle Res. Cell Motil.* 27:53–67.

Duchenne, G.B. 1861. De l'électrisation localisée et de son application a la pathologie et a la thérapeutique. J.-B. Baillière et Fils, Paris.

Ervasti, J.M. 2003. Costameres: the Achilles' heel of Herculean muscle. *J. Biol. Chem.* 278:13591–4.

Ervasti, J.M. 2007. Dystrophin, its interactions with other proteins, and implications for muscular dystrophy. *Biochim. Biophys. Acta*. 1772:108–17.

Ervasti, J.M., and K.P. Campbell. 1991. Membrane organization of the dystrophin-glycoprotein complex. *Cell*. 66:1121–31.

Ervasti, J.M., K. Ohlendieck, S.D. Kahl, M.G. Gaver, and K.P. Campbell. 1990. Deficiency of a glycoprotein component of the dystrophin complex in dystrophic muscle. *Nature*. 345:315–9.

Fabb, S.A., D.J. Wells, P. Serpente, and G. Dickson. 2002. Adeno-associated virus vector gene transfer and sarcolemmal expression of a 144 kDa micro-dystrophin effectively restores the dystrophin-associated protein complex and inhibits myofibre degeneration in nude/*mdx* mice. *Hum. Mol. Genet.* 11:733–41.

Flanigan, K.M., D.M. Dunn, A. von Niederhausern, P. Soltanzadeh, E. Gappmaier, M.T. Howard, J.B. Sampson, J.R. Mendell, C. Wall, W.M. King, A. Pestronk, J.M. Florence, A.M. Connolly, K.D. Mathews, C.M. Stephan, K.S. Laubenthal, B.L. Wong, P.J. Morehart, A. Meyer, R.S. Finkel, C.G. Bonnemann, L. Medne, J.W. Day, J.C. Dalton, M.K. Margolis, V.J. Hinton, and R.B. Weiss. 2009. Mutational spectrum of DMD mutations in dystrophinopathy patients: application of modern diagnostic techniques to a large cohort. *Hum. Mutat.* 30:1657–66.

Flanigan, K.M., A. von Niederhausern, D.M. Dunn, J. Alder, J.R. Mendell, and R.B. Weiss. 2003. Rapid direct sequence analysis of the dystrophin gene. *Am. J. Hum. Genet.* 72:931–9.

Gehrig, S.M., C. van der Poel, T.A. Sayer, J.D. Schertzer, D.C. Henstridge, J.E. Church, S. Lamon, A.P. Russell, K.E. Davies, M.A. Febbraio, and G.S. Lynch. 2012. Hsp72 preserves muscle function and slows progression of severe muscular dystrophy. *Nature*. 484:394–398.

Glickman, M.H., and A. Ciechanover. 2002. The ubiquitin-proteasome proteolytic pathway: destruction for the sake of construction. *Physiol. Rev.* 82:373–428.

Goemans, N.M., M. Tulinius, J.T. van den Akker, B.E. Burm, P.F. Ekhart, N. Heuvelmans, T. Holling, A.A. Janson, G.J. Platenburg, J.A. Sipkens, J.M.A. Sitsen, A. Aartsma-Rus, G.-J.B. van Ommen, G. Buyse, N. Darin, J.J. Verschuuren, G. V Campion, S.J. de Kimpe, and J.C. van Deutekom. 2011. Systemic administration of PRO051 in Duchenne's muscular dystrophy. *N. Engl. J. Med.* 364:1513–22.

Goldberg, L.R., I. Hausmanowa-Petrusewicz, A. Fidzianska, D.J. Duggan, L.S. Steinberg, and E.P. Hoffman. 1998. A dystrophin missense mutation showing persistence of dystrophin and dystrophin-associated proteins yet a severe phenotype. *Ann. Neurol.* 44:971–6.

González, E., C. Montañez, P.N. Ray, P.L. Howard, F. García-Sierra, D. Mornet, and B. Cisneros. 2000. Alternative splicing regulates the nuclear or cytoplasmic localization of dystrophin Dp71. *FEBS Lett.* 482:209–14.

Górecki, D.C., A.P. Monaco, J.M. Derry, A.P. Walker, E.A. Barnard, and P.J. Barnard. 1992. Expression of four alternative dystrophin transcripts in brain regions regulated by different promoters. *Hum. Mol. Genet.* 1:505–10.

Gowers, W.R. 1886. A Manual of Diseases of the Nervous System. American E. P. Blakiston, Son & Co., Philadelphia.

Grady, R.M., R.W. Grange, K.S. Lau, M.M. Maimone, M.C. Nichol, J.T. Stull, and J.R. Sanes. 1999. Role for alpha-dystrobrevin in the pathogenesis of dystrophin-dependent muscular dystrophies. *Nat. Cell Biol.* 1:215–20.

Gregorevic, P., M.J. Blankinship, J.M. Allen, R.W. Crawford, L. Meuse, D.G. Miller, D.W. Russell, and J.S. Chamberlain. 2004. Systemic delivery of genes to striated muscles using adeno-associated viral vectors. *Nat. Med.* 10:828–34.

Hamed, S., A. Sutherland-Smith, J. Gorospe, J. Kendrick-Jones, and E. Hoffman. 2005. DNA sequence analysis for structure/function and mutation studies in Becker muscular dystrophy. *Clin. Genet.* 68:69–79.

Hara, Y., B. Balci-Hayta, T. Yoshida-Moriguchi, M. Kanagawa, D. Beltrán-Valero de Bernabé, H. Gündeşli, T. Willer, J.S. Satz, R.W. Crawford, S.J. Burden, S. Kunz, M.B.A. Oldstone, A. Accardi, B. Talim, F. Muntoni, H. Topaloğlu, P. Dinçer, and K.P. Campbell. 2011. A dystroglycan mutation associated with limb-girdle muscular dystrophy. *N. Engl. J. Med.* 364:939–46.

Hartley, J.L. 2000. DNA cloning using in vitro site-specific recombination. *Genome Res.* 10:1788–1795.

Henderson, D.M., J.J. Belanto, B. Li, H. Heun-Johnson, and J.M. Ervasti. 2011. Internal deletion compromises the stability of dystrophin. *Hum. Mol. Genet.* 20:2955–63.

Henderson, D.M., A. Lee, and J.M. Ervasti. 2010. Disease-causing missense mutations in actin binding domain 1 of dystrophin induce thermodynamic instability and protein aggregation. *Proc. Natl. Acad. Sci. U. S. A.* 107:9632–7.

Hnia, K., D. Zouiten, S. Cantel, D. Chazalette, G. Hugon, J.A. Fehrentz, A. Masmoudi, A. Diment, J. Bramham, D. Mornet, and S.J. Winder. 2007. ZZ domain of dystrophin and utrophin: topology and mapping of a beta-dystroglycan interaction site. *Biochem. J.* 401:667–77.

Hoffman, E.P., R.H. Brown, and L.M. Kunkel. 1987a. Dystrophin: the protein product of the Duchenne muscular dystrophy locus. *Cell*. 51:919–28.

Hoffman, E.P., R.H. Brown, and L.M. Kunkel. 1987b. Dystrophin: the protein product of the Duchenne muscular dystrophy locus. *Cell*. 51:919–28.

Hollinger, K., C.X. Yang, R.E. Montz, D. Nonneman, J.W. Ross, and J.T. Selsby. 2013. Dystrophin insufficiency causes selective muscle histopathology and loss of dystrophin-glycoprotein complex assembly in pig skeletal muscle. *FASEB J.* 1–10.

Huang, X., F. Poy, R. Zhang, A. Joachimiak, M. Sudol, and M.J. Eck. 2000. Structure of a WW domain containing fragment of dystrophin in complex with beta-dystroglycan. *Nat. Struct. Biol.* 7:634–8.

Ishikawa-Sakurai, M., M. Yoshida, M. Imamura, K.E. Davies, and E. Ozawa. 2004. ZZ domain is essentially required for the physiological binding of dystrophin and utrophin to beta-dystroglycan. *Hum. Mol. Genet.* 13:693–702.

Juan-Mateu, J., L. González-Quereda, M.J. Rodríguez, E. Verdura, K. Lázaro, C. Jou, A. Nascimento, C. Jiménez-Mallebrera, J. Colomer, S. Monges, F. Lubieniecki, M.E. Foncuberta, S.I. Pascual-Pascual, J. Molano, M. Baiget, and P. Gallano. 2013. Interplay between DMD point mutations and splicing signals in dystrophinopathy phenotypes. *PLoS One*. 8:e59916.

Kisselev, A.F., T.N. Akopian, and A.L. Goldberg. 1998. Range of sizes of peptide products generated during degradation of different proteins by archaeal proteasomes. *J. Biol. Chem.* 273:1982–1989.

Kisselev, A.F., W.A. van der Linden, and H.S. Overkleeft. 2012. Proteasome inhibitors: an expanding army attacking a unique target. *Chem. Biol.* 19:99–115.

Koenig, M., A. Beggs, M. Moyer, S. Scherpf, K. Heindrich, T. Bettecken, G. Meng, C.R. Müller, M. Lindlöf, and H. Kaariainen. 1989. The molecular basis for Duchenne versus Becker muscular dystrophy: correlation of severity with type of deletion. *Am. J. Hum. Genet.* 45:498–506.

Koenig, M., E.P. Hoffman, C.J. Bertelson, A.P. Monaco, C. Feener, and L.M. Kunkel. 1987. Complete cloning of the Duchenne muscular dystrophy (DMD) cDNA and preliminary genomic organization of the DMD gene in normal and affected individuals. *Cell*. 50:509–17.

Koenig, M., and L.M. Kunkel. 1990. Detailed analysis of the repeat domain of dystrophin reveals four potential hinge segments that may confer flexibility. *J. Biol. Chem.* 265:4560–6.

Koenig, M., A.P. Monaco, and L.M. Kunkel. 1988. The complete sequence of dystrophin predicts a rod-shaped cytoskeletal protein. *Cell*. 53:219–28.

Kornegay, J.N., J.R. Bogan, D.J. Bogan, M.K. Childers, J. Li, P. Nghiem, D.A. Detwiler, C.A. Larsen, R.W. Grange, R.K. Bhavaraju-Sanka, S. Tou, B.P. Keene, J.F. Howard, J. Wang, Z. Fan, S.J. Schatzberg, M.A. Styner, K.M. Flanigan, X. Xiao, and E.P. Hoffman. 2012. Canine models of Duchenne muscular dystrophy and their use in therapeutic strategies. *Mamm. Genome*. 23:85–108.

Kramer, G., D. Boehringer, N. Ban, and B. Bukau. 2009. The ribosome as a platform for co-translational processing, folding and targeting of newly synthesized proteins. *Nat. Struct. Mol. Biol.* 16:589–97.

Kumar, R. 2009. Role of naturally occurring osmolytes in protein folding and stability. *Arch. Biochem. Biophys.* 491:1–6.

Kumar, S.K., S.V. Rajkumar, A. Dispenzieri, M.Q. Lacy, S.R. Hayman, F.K. Buadi, S.R. Zeldenrust, D. Dingli, S.J. Russell, J.A. Lust, P.R. Greipp, R.A. Kyle, and M.A. Gertz. 2008. Improved survival in multiple myeloma and the impact of novel therapies. *Blood*. 111:2516–20.

Lanneau, D., G. Wettstein, P. Bonniaud, and C. Garrido. 2010. Heat shock proteins: cell protection through protein triage. *ScientificWorldJournal.* 10:1543–52.

Lederfein, D., Z. Levy, N. Augier, D. Mornet, G. Morris, O. Fuchs, D. Yaffe, and U. Nudel. 1992. A 71-kilodalton protein is a major product of the Duchenne muscular dystrophy gene in brain and other nonmuscle tissues. *Proc. Natl. Acad. Sci. U. S. A.* 89:5346–50.

Lee, S.M., J.A. Olzmann, L.S. Chin, and L. Li. 2011. Mutations associated with Charcot-Marie-Tooth disease cause SIMPLE protein mislocalization and degradation by the proteasome and aggresome-autophagy pathways. *J. Cell Sci.*

Legardinier, S., J.F. Hubert, O. Le Bihan, C. Tascon, C. Rocher, C. Raguénès-Nicol, A. Bondon, S. Hardy, and E. Le Rumeur. 2008. Sub-domains of the dystrophin rod domain display contrasting lipid-binding and stability properties. *Biochim. Biophys. Acta*. 1784:672–82.

Legardinier, S., B. Legrand, C. Raguénès-Nicol, A. Bondon, S. Hardy, C. Tascon, E. Le Rumeur, and J.F. Hubert. 2009. A two-amino acid mutation encountered in Duchenne Muscular Dystrophy decreases stability of the rod domain 23 (R23) spectrin-like repeat of dystrophin. *J. Biol. Chem.* 284:8822–32.

Lenk, U., K. Oexle, T. Voit, U. Ancker, K. Hellner, A. Speer, and C. Hübner. 1996. A cysteine 3340 substitution in the dystroglycan-binding domain of dystrophin associated with Duchenne muscular dystrophy, mental retardation and absence of the ERG b-wave. *Hum. Mol. Genet.* 5:973–5.

Li, D., A. Bareja, L. Judge, Y. Yue, Y. Lai, R. Fairclough, K.E. Davies, J.S. Chamberlain, and D. Duan. 2010a. Sarcolemmal nNOS anchoring reveals a

qualitative difference between dystrophin and utrophin. *J. Cell Sci.* 123:2008–13.

Li, D., Y. Yue, and D. Duan. 2008a. Preservation of muscle force in *Mdx*3cv mice correlates with low-level expression of a near full-length dystrophin protein. *Am. J. Pathol.* 172:1332–41.

Li, D., Y. Yue, and D. Duan. 2010b. Marginal level dystrophin expression improves clinical outcome in a strain of dystrophin/utrophin double knockout mice. *PLoS One*. 5:e15286.

Li, W., M.H. Bengtson, A. Ulbrich, A. Matsuda, V. Reddy, A. Orth, S.K. Chanda, S. Batalov, and C.A.P. Joazeiro. 2008b. Genome-wide and functional annotation of human E3 ubiquitin ligases identifies MULAN, a mitochondrial E3 that regulates the organelle's dynamics and signaling. *PLoS One*. 3:e1487.

Lidov, H.G., S. Selig, and L.M. Kunkel. 1995. Dp140: a novel 140 kDa CNS transcript from the dystrophin locus. *Hum. Mol. Genet.* 4:329–35.

Liu, Y., Y. Wang, C. Wu, Y. Liu, and P. Zheng. 2009. Deletions and missense mutations of EPM2A exacerbate unfolded protein response and apoptosis of neuronal cells induced by endoplasm reticulum stress. *Hum. Mol. Genet.* 18:2622–31.

López-Bigas, N., B. Audit, C. Ouzounis, G. Parra, and R. Guigó. 2005. Are splicing mutations the most frequent cause of hereditary disease? *FEBS Lett.* 579:1900–3.

Malik, V., L.R. Rodino-Klapac, L. Viollet, C. Wall, W. King, R. Al-Dahhak, S. Lewis, C.J. Shilling, J. Kota, C. Serrano-Munuera, J. Hayes, J.D. Mahan, K.J. Campbell, B. Banwell, M. Dasouki, V. Watts, K. Sivakumar, R. Bien-Willner, K.M. Flanigan, Z. Sahenk, R.J. Barohn, C.M. Walker, and J.R. Mendell. 2010. Gentamicin-induced readthrough of stop codons in Duchenne muscular dystrophy. *Ann. Neurol.* 67:771–80.

Mayer, M.P., and B. Bukau. 2005. Hsp70 chaperones: cellular functions and molecular mechanism. *Cell. Mol. Life Sci.* 62:670–84.

McGeachie, J.K., M.D. Grounds, T.A. Partridge, and J.E. Morgan. 1993. Age-related changes in replication of myogenic cells in *mdx* mice: quantitative autoradiographic studies. *J. Neurol. Sci.* 119:169–79.

Mendell, J.R., K. Campbell, L. Rodino-Klapac, Z. Sahenk, C. Shilling, S. Lewis, D. Bowles, S. Gray, C. Li, G. Galloway, V. Malik, B. Coley, K.R. Clark, J. Li, X. Xiao, J. Samulski, S.W. McPhee, R.J. Samulski, and C.M. Walker. 2010. Dystrophin immunity in Duchenne's muscular dystrophy. *N. Engl. J. Med.* 363:1429–37.

Mendell, J.R., C. Shilling, N.D. Leslie, K.M. Flanigan, R. al-Dahhak, J. Gastier-Foster, K. Kneile, D.M. Dunn, B. Duval, A. Aoyagi, C. Hamil, M. Mahmoud, K. Roush, L. Bird, C. Rankin, H. Lilly, N. Street, R. Chandrasekar, and R.B. Weiss. 2012. Evidence-based path to newborn screening for Duchenne muscular dystrophy. *Ann. Neurol.* 71:304–13.

Michele, D.E., R. Barresi, M. Kanagawa, F. Saito, R.D. Cohn, J.S. Satz, J. Dollar, I. Nishino, R.I. Kelley, H. Somer, V. Straub, K.D. Mathews, S.A. Moore, and K.P. Campbell. 2002. Post-translational disruption of dystroglycan-ligand interactions in congenital muscular dystrophies. *Nature*. 418:417–22.

Mirza, A., M. Sagathevan, N. Sahni, L. Choi, and N. Menhart. 2010. A biophysical map of the dystrophin rod. *Biochim. Biophys. Acta*. 1804:1796–809.

Miura, P., and B.J. Jasmin. 2006. Utrophin upregulation for treating Duchenne or Becker muscular dystrophy: how close are we? *Trends Mol. Med.* 12:122–9.

Moens, P., P.H. Baatsen, and G. Maréchal. 1993. Increased susceptibility of EDL muscles from *mdx* mice to damage induced by contractions with stretch. *J. Muscle Res. Cell Motil.* 14:446–51.

Monaco, A.P., C.J. Bertelson, S. Liechti-Gallati, H. Moser, and L.M. Kunkel. 1988. An explanation for the phenotypic differences between patients bearing partial deletions of the DMD locus. *Genomics*. 2:90–5.

Moorwood, C., N. Soni, G. Patel, S.D. Wilton, and T.S. Khurana. 2013. A cell-based high-throughput screening assay for posttranscriptional utrophin upregulation. *J. Biomol. Screen.* 18:400–6.

Muthu, M., K.A. Richardson, and A.J. Sutherland-Smith. 2012. The crystal structures of dystrophin and utrophin spectrin repeats: implications for domain boundaries. *PLoS One*. 7:e40066.

Neef, D.W., A.M. Jaeger, and D.J. Thiele. 2011. Heat shock transcription factor 1 as a therapeutic target in neurodegenerative diseases. *Nat. Rev. Drug Discov.* 10:930–44.

Nguyen, F., Y. Cherel, L. Guigand, I. Goubault-Leroux, and M. Wyers. 2002. Muscle lesions associated with dystrophin deficiency in neonatal golden retriever puppies. *J. Comp. Pathol.* 126:100–8.

Niesen, F.H., H. Berglund, and M. Vedadi. 2007. The use of differential scanning fluorimetry to detect ligand interactions that promote protein stability. *Nat. Protoc.* 2:2212–21.

Norwood, F.L., A.J. Sutherland-Smith, N.H. Keep, and J. Kendrick-Jones. 2000. The structure of the N-terminal actin-binding domain of human dystrophin and how mutations in this domain may cause Duchenne or Becker muscular dystrophy. *Structure*. 8:481–91.

Nudel, U., D. Zuk, P. Einat, E. Zeelon, Z. Levy, S. Neuman, and D. Yaffe. 1989. Duchenne muscular dystrophy gene product is not identical in muscle and brain. *Nature*. 337:76–8.

Ozawa, E., Y. Mizuno, Y. Hagiwara, T. Sasaoka, and M. Yoshida. 2005. Molecular and cell biology of the sarcoglycan complex. *Muscle Nerve*. 32:563–76.

Palmer, E., J.M. Wilhelm, and F. Sherman. 1979. Phenotypic suppression of nonsense mutants in yeast by aminoglycoside antibiotics. *Nature*. 277:148–50.

Pascual, J., J. Castresana, and M. Saraste. 1997. Evolution of the spectrin repeat. *Bioessays*. 19:811–7.

Peltz, S.W., M. Morsy, E.M. Welch, and A. Jacobson. 2013. Ataluren as an agent for therapeutic nonsense suppression. *Annu. Rev. Med.* 64:407–25.

Pennisi, E. 2010. 1000 Genomes Project gives new map of genetic diversity. *Science*. 330:574–5.

Phelps, S.F., M.A. Hauser, N.M. Cole, J.A. Rafael, R.T. Hinkle, J.A. Faulkner, and J.S. Chamberlain. 1995. Expression of full-length and truncated dystrophin mini-genes in transgenic *mdx* mice. *Hum. Mol. Genet.* 4:1251–8.

Pillers, D.A., D.E. Bulman, R.G. Weleber, D.A. Sigesmund, M.A. Musarella, B.R. Powell, W.H. Murphey, C. Westall, C. Panton, and L.E. Becker. 1993. Dystrophin expression in the human retina is required for normal function as defined by electroretinography. *Nat. Genet.* 4:82–6.

Ponting, C.P., D.J. Blake, K.E. Davies, J. Kendrick-Jones, and S.J. Winder. 1996. ZZ and TAZ: new putative zinc fingers in dystrophin and other proteins. *Trends Biochem. Sci.* 21:11–13.

Prins, K.W., J.L. Humston, A. Mehta, V. Tate, E. Ralston, and J.M. Ervasti. 2009. Dystrophin is a microtubule-associated protein. *J. Cell Biol.* 186:363–9.

Prior, T.W., A.C. Papp, P.J. Snyder, A.H.M. Burghes, C. Bartolo, M.S. Sedra, L.M. Western, and J.R. Mendell. 1993. A missense mutation in the dystrophin gene in a Duchenne muscular dystrophy patient. *Nat. Genet.* 4:357–360.

Punnoose, A.R., A.E. Burke, and R.M. Golub. 2011. JAMA patient page. Muscular dystrophy. *JAMA*. 306:2526.

Van Putten, M., M. Hulsker, V.D. Nadarajah, S.H. van Heiningen, E. van Huizen, M. van Iterson, P. Admiraal, T. Messemaker, J.T. den Dunnen, P.A.C. 't Hoen, and A. Aartsma-Rus. 2012. The effects of low levels of dystrophin on mouse muscle function and pathology. *PLoS One*. 7:e31937.

Van Putten, M., M. Hulsker, C. Young, V.D. Nadarajah, H. Heemskerk, L. van der Weerd, P.A.C. 't Hoen, G.J.B. van Ommen, and A.M. Aartsma-Rus. 2013. Low dystrophin levels increase survival and improve muscle pathology and function in dystrophin/utrophin double-knockout mice. *FASEB J.* 27:2484–95.

Rahimov, F., and L.M. Kunkel. 2013. The cell biology of disease: Cellular and molecular mechanisms underlying muscular dystrophy. *J. Cell Biol.* 201:499–510.

Rall, S., and T. Grimm. 2012. Survival in Duchenne muscular dystrophy. *Acta Myol.* 31:117–20.

Ritossa, F. 1962. A new puffing pattern induced by temperature shock and DNP in drosophila. *Experientia*. 18:571–573.

Roberts, R.G., A.J. Coffey, M. Bobrow, and D.R. Bentley. 1993. Exon structure of the human dystrophin gene. *Genomics*. 16:536–8.

Rybakova, I.N., K.J. Amann, and J.M. Ervasti. 1996. A new model for the interaction of dystrophin with F-actin. *J. Cell Biol.* 135:661–72.

Sadoulet-Puccio, H.M., M. Rajala, and L.M. Kunkel. 1997. Dystrobrevin and dystrophin: an interaction through coiled-coil motifs. *Proc. Natl. Acad. Sci. U. S. A.* 94:12413–8.

Sakharkar, M.K., V.T.K. Chow, and P. Kangueane. 2004. Distributions of exons and introns in the human genome. *In Silico Biol.* 4:387–93.

Schulman, B.A., and J.W. Harper. 2009. Ubiquitin-like protein activation by E1 enzymes: the apex for downstream signalling pathways. *Nat. Rev. Mol. Cell Biol.* 10:319–31.

Sharp, N.J., J.N. Kornegay, S.D. Van Camp, M.H. Herbstreith, S.L. Secore, S. Kettle, W.Y. Hung, C.D. Constantinou, M.J. Dykstra, and A.D. Roses. 1992. An error in dystrophin mRNA processing in golden retriever muscular dystrophy, an animal homologue of Duchenne muscular dystrophy. *Genomics*. 13:115–21.

Shiber, A., and T. Ravid. 2014. Chaperoning Proteins for Destruction: Diverse Roles of Hsp70 Chaperones and their Co-Chaperones in Targeting Misfolded Proteins to the Proteasome. *Biomolecules*. 4:704–24.

Sicinski, P., Y. Geng, A.S. Ryder-Cook, E.A. Barnard, M.G. Darlison, and P.J. Barnard. 1989. The molecular basis of muscular dystrophy in the *mdx* mouse: a point mutation. *Science*. 244:1578–80.

Singh, S.M., N. Kongari, J. Cabello-Villegas, and K.M.G. Mallela. 2010. Missense mutations in dystrophin that trigger muscular dystrophy decrease protein stability and lead to cross-beta aggregates. *Proc. Natl. Acad. Sci. U. S. A.* 107:15069–74.

Sonnemann, K.J., H. Heun-Johnson, A.J. Turner, K.A. Baltgalvis, D.A. Lowe, and J.M. Ervasti. 2009. Functional substitution by TAT-utrophin in dystrophin-deficient mice. *PLoS Med.* 6:e1000083.

Stone, M.R., A. O'Neill, D. Catino, and R.J. Bloch. 2005. Specific interaction of the actin-binding domain of dystrophin with intermediate filaments containing keratin 19. *Mol. Biol. Cell*. 16:4280–93.

Summers, D.W., P.M. Douglas, C.H.I. Ramos, and D.M. Cyr. 2009. Polypeptide transfer from Hsp40 to Hsp70 molecular chaperones. *Trends Biochem. Sci.* 34:230–3.

Suzuki, A., M. Yoshida, K. Hayashi, Y. Mizuno, Y. Hagiwara, and E. Ozawa. 1994. Molecular organization at the glycoprotein-complex-binding site of

dystrophin. Three dystrophin-associated proteins bind directly to the carboxy-terminal portion of dystrophin. *Eur. J. Biochem.* 220:283–92.

Tanaka, M., Y. Machida, S. Niu, T. Ikeda, N.R. Jana, H. Doi, M. Kurosawa, M. Nekooki, and N. Nukina. 2004. Trehalose alleviates polyglutamine-mediated pathology in a mouse model of Huntington disease. *Nat. Med.* 10:148–54.

Taylor, P.J., S. Maroulis, G.L. Mullan, R.L. Pedersen, A. Baumli, G. Elakis, S. Piras, C. Walsh, B. Prósper-Gutiérrez, F. De La Puente-Alonso, C.G. Bell, D.R. Mowat, H.M. Johnston, and M.F. Buckley. 2007. Measurement of the clinical utility of a combined mutation detection protocol in carriers of Duchenne and Becker muscular dystrophy. *J. Med. Genet.* 44:368–72.

Tennyson, C.N., H.J. Klamut, and R.G. Worton. 1995. The human dystrophin gene requires 16 hours to be transcribed and is cotranscriptionally spliced. *Nat. Genet.* 9:184–90.

Tennyson, C.N., Q. Shi, and R.G. Worton. 1996. Stability of the human dystrophin transcript in muscle. *Nucleic Acids Res.* 24:3059–64.

Thrower, J.S., L. Hoffman, M. Rechsteiner, and C.M. Pickart. 2000. Recognition of the polyubiquitin proteolytic signal. *EMBO J.* 19:94–102.

Trott, A., J.D. West, L. Klaic, S.D. Westerheide, R.B. Silverman, R.I. Morimoto, and K.A. Morano. 2008. Activation of Heat Shock and Antioxidant Responses by the Natural Product Celastrol : Transcriptional Signatures of a Thiol-targeted Molecule. *Mol. Biol. Cell*. 19:1104–1112.

Valentine, B.A., B.J. Cooper, A. de Lahunta, R. O'Quinn, and J.T. Blue. 1988. Canine X-linked muscular dystrophy. An animal model of Duchenne muscular dystrophy: clinical studies. *J. Neurol. Sci.* 88:69–81.

Vulin, A., N. Wein, D.M. Strandjord, E.K. Johnson, A.R. Findlay, B. Maiti, M.T. Howard, Y.J. Kaminoh, L.E. Taylor, T.R. Simmons, W.C. Ray, F. Montanaro, J.M. Ervasti, and K.M. Flanigan. 2014. The ZZ Domain of Dystrophin in DMD: Making Sense of Missense Mutations. *Hum. Mutat.* 35:257–64.

Wang, F., L.A. Durfee, and J.M. Huibregtse. 2013. A Cotranslational Ubiquitination Pathway for Quality Control of Misfolded Proteins. *Mol. Cell*. 50:368–378.

Watchko, J., T. O'Day, B. Wang, L. Zhou, Y. Tang, J. Li, and X. Xiao. 2002. Adeno-associated virus vector-mediated minidystrophin gene therapy

improves dystrophic muscle contractile function in *mdx* mice. *Hum. Gene Ther.* 13:1451–60.

Weathington, N.M., and R.K. Mallampalli. 2014. Emerging therapies targeting the ubiquitin proteasome system in cancer. *J. Clin. Invest.* 124:6–12.

Wells, D.J., K.E. Wells, E.A. Asante, G. Turner, Y. Sunada, K.P. Campbell, F.S. Walsh, and G. Dickson. 1995. Expression of human full-length and minidystrophin in transgenic *mdx* mice: implications for gene therapy of Duchenne muscular dystrophy. *Hum. Mol. Genet.* 4:1245–50.

Westerheide, S.D., J.D. Bosman, B.N.A. Mbadugha, T.L.A. Kawahara, G. Matsumoto, S. Kim, W. Gu, J.P. Devlin, R.B. Silverman, and R.I. Morimoto. 2004. Celastrols as inducers of the heat shock response and cytoprotection. *J. Biol. Chem.* 279:56053–60.

White, M.B., M. Carvalho, D. Derse, S.J. O'Brien, and M. Dean. 1992. Detecting single base substitutions as heteroduplex polymorphisms. *Genomics*. 12:301–6.

White, S.J., A. Aartsma-Rus, K.M. Flanigan, R.B. Weiss, A.L.J. Kneppers, T. Lalic, A.A.M. Janson, H.B. Ginjaar, M.H. Breuning, and J.T. den Dunnen. 2006. Duplications in the DMD gene. *Hum. Mutat.* 27:938–45.

Xing, Y., and C. Lee. 2006. Alternative splicing and RNA selection pressure--evolutionary consequences for eukaryotic genomes. *Nat. Rev. Genet.* 7:499–509.

Yaffe, D., and O. Saxel. 1977. Serial passaging and differentiation of myogenic cells isolated from dystrophic mouse muscle. *Nature*. 270:725–7.

Yancey, P.H., M.E. Clark, S.C. Hand, R.D. Bowlus, and G.N. Somero. 1982. Living with water stress: evolution of osmolyte systems. *Science*. 217:1214–22.

Ye, Y., and M. Rape. 2009. Building ubiquitin chains: E2 enzymes at work. *Nat. Rev. Mol. Cell Biol.* 10:755–64.

Zhang, G., and Z. Ignatova. 2011. Folding at the birth of the nascent chain: coordinating translation with co-translational folding. *Curr. Opin. Struct. Biol.* 21:25–31.

Zubrzycka-Gaarn, E.E., D.E. Bulman, G. Karpati, A.H.M. Burghes, B. Belfall, H.J. Klamut, J. Talbot, R.S. Hodges, P.N. Ray, and R.G. Worton. 1988. The

Duchenne muscular dystrophy gene product is localized in sarcolemma of human skeletal muscle. *Nature*. 333:466–469.